

Holographic Sensing for Control of Flexible Structures

by

Michael Frederick Barsky

Dissertation submitted to the Faculty of the

Virginia Polytechnic Institute and State University

in partial fulfillment of the requirements for the degree of

Doctor of Philosophy

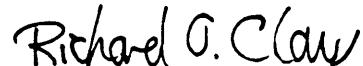
in

Electrical Engineering

APPROVED:



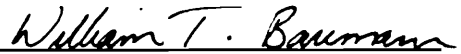
Douglas K. Lindner, Chairman



Richard O. Claus



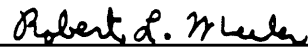
Stanoje Bingulac



William T. Baumann



Ting-Chung Poon



Robert L. Wheeler

January, 1990

Blacksburg, Virginia

Holographic Sensing for Control of Flexible Structures

by

Michael Frederick Barsky

Douglas K. Lindner, Chairman

Electrical Engineering

(ABSTRACT)

A state feedback control system for flexible structures implemented using a holographic sensor and optical processor is presented. Real-time holography provides a mechanism for sensing the distributed shape of a broad class of one and two-dimensional flexible structures in a form that can be processed using fixed optics. The optical processing solves the spillover problem in the theory of the control of flexible structures. The optical processing also simplifies the computation allowing the state feedback control of a large number of vibrational without a digital computer. The combination of holographic sensing and optical processing provides a potential solution to both the spillover and computation problems in the control of flexible structures.

Dedication

In memory of my Grandmother Celia Barsky

Acknowledgements

I have had the good fortune to work with many talented people over the past decade. One of the most farsighted was Dr. D. K. Lindner who has encouraged me to develop my unusual approach to control theory. His guidance, support and friendship were invaluable during my graduate career.

I have had the pleasure of working with Dr. R. O. Claus since my sophomore year as an undergraduate. Despite the fact that he is one of the busiest professors on campus, he always seemed to find the time to discuss a new idea and offer suggestions. I would especially like to thank him, his research associates, and his other graduate students for their generosity in providing laboratory space and assistance for experiments.

I have taken several courses from Dr. S. Bingulac and appreciated his heuristic methods for understanding algorithms. I believe I have learned much more from him than the content covered in his courses. It has been a comfort to have such an accessible expert on my committee.

I have greatly enjoyed working with Dr. W. T. Baumann. The seeds of many of the ideas in this thesis were planted through conversations in his office. In particular, his insight into the nature of spatial functions has been instructive.

I would like to thank Dr. T. C. Poon for his assistance in optical signal processing. His optical engineering course has opened many doors for me.

I am grateful to Dr. R. L. Wheeler for reading my thesis and serving as a member of my committee. His interest and assistance were appreciated.

In addition to my official committee, I would like to acknowledge my advisor Dr. R. C. Montgomery and Mrs. S. S. Welch at NASA Langley Research Center for the idea of holographic sensing for control of flexible structures, and for offering me the opportunity to make a contribution to the effort. While at NASA, I also had the good fortune to work with Dr. J. S. Gibson of UCLA on his visits to ICASE. His insight into the important computational role for optics in the control of flexible structures was inspiring.

Finally, I would like to thank my parent for their guidance, support and love.

Table of Contents

- 1.0 Introduction 1
- 2.0 Distributed Sensing 6
 - 2.1 Introduction 6
 - 2.2 Preliminaries 9
 - 2.3 The Imaging Method 12
 - 2.4 The Interference Method 15
 - 2.5 The Desensitized Interference Method 19
 - 2.6 The Holographic Method 23
 - 2.7 Multifrequency Holography 27
 - 2.8 Real-Time Holography 29
 - 2.9 Discrete-Time Holography 32
 - 2.10 Summary 34
- 3.0 Modelling and Design 36
 - 3.1 Introduction 36
 - 3.2 Modelling 36

3.3	Control System Design	50
3.3.1	The Continuous Time Control System	51
3.3.2	Spillover Analysis	54
3.3.3	Simplification of the Continuous-Time Design	57
3.3.4	The Discrete-Time Control System	60
3.3.5	Extension to Plate Structures	66
3.3.6	Design Summary	70
3.4	Summary	70
4.0	Example	72
4.1	Introduction	72
4.2	The Simulations	73
4.3	Summary	83
5.0	Implementation	88
5.1	Introduction	88
5.2	Mixed Processor	89
5.3	The All-Optical Processor	97
5.4	Extensions to Two-Dimensional Structures	100
5.5	Summary	106
6.0	Summary and Recommendations	108
6.1	Summary	108
6.2	Recommendations for Future Work	109
6.2.1	Experiments	110
6.2.2	Control Theory	115
References		118

Appendix A. Functional Estimator 121

Vita 125

List of Illustrations

Figure 1. Flexible Structure with State Feedback Control System 2

Figure 2. Cantilevered Beam with Tip-Actuator 7

Figure 3. Optical Signal 10

Figure 4. Intensity Function 13

Figure 5. Imaging System 14

Figure 6. Michelson Interferometer 16

Figure 7. Holographic Sensing System 24

Figure 8. Real-Time Holographic Sensor 31

Figure 9. Discrete-Time Holographic Sensor 33

Figure 10. Closed-loop Poles for 4-mode Design 74

Figure 11. 4-mode Distributed Sensor Design Controlling a 12-mode Beam 75

Figure 12. 4-mode Point Sensor Design Controlling a 12-mode Beam 77

Figure 13. Closed-loop Poles with 2% Parameter Perturbations 78

Figure 14. Closed-loop Poles with 5% Parameter Perturbations 79

Figure 15. 2% and 5% Perterbations in 4th Mode Shape 81

Figure 16. Integrating Kernels for Functional Estimator 82

Figure 17. Closed-loop Poles for Functional Estimator 84

Figure 18. Time Response 85

Figure 19. Time Response of Functional Observer 86

Figure 20. Squared Error in Time Responses 87

Figure 21. Pointwise Multiplication by Absorption Transparency 90

Figure 22. Full Spatial Processor 92

Figure 23. Sum of Modes for Cantilevered Beam 94

Figure 24. Bipolar Spatial Processor 96

Figure 25. Functional Estimator 98

Figure 26. Block Diagram of an All-Optical Processor 101

Figure 27. Integrator with one-dimensional kernel 102

Figure 28. Integrator with two-dimensional kernel 103

Figure 29. Beam Splitter for Addition 104

Figure 30. Control Modulator 105

Figure 31. Slide Projector-type Sensor Output Simulator 113

1.0 Introduction

In this dissertation, we present a control system for flexible structures implemented by a new sensing and processing method. The control system is shown in Figure 1, where the dashed line encloses the area of new results. The control system utilizes a form of real-time holography to sense the shape of the flexible structure as a function of time and space. The optical output of the sensor is processed optically to generate an electrical control signal. Hence, we are sensing and processing distributed functions to calculate a scalar function. The control signal is followed by a point actuator on the structure. The actuator damps the structural vibrations. We discuss the design and implementation of the processor, and demonstrate how the control system addresses to major problems in the control of flexible structures: The problems of spillover and computation.

The problem of controlling vibrations in flexible structures has received a great deal of attention in recent years. In theory, flexible structures are described by an infinite number of elastic modes. Generally, it is not necessary to actively control all of the modes to reduce the vibrations to a tolerable level [1]. This is because the higher modes tend to be outside the bandwidth of excitation, and the higher modes require a large

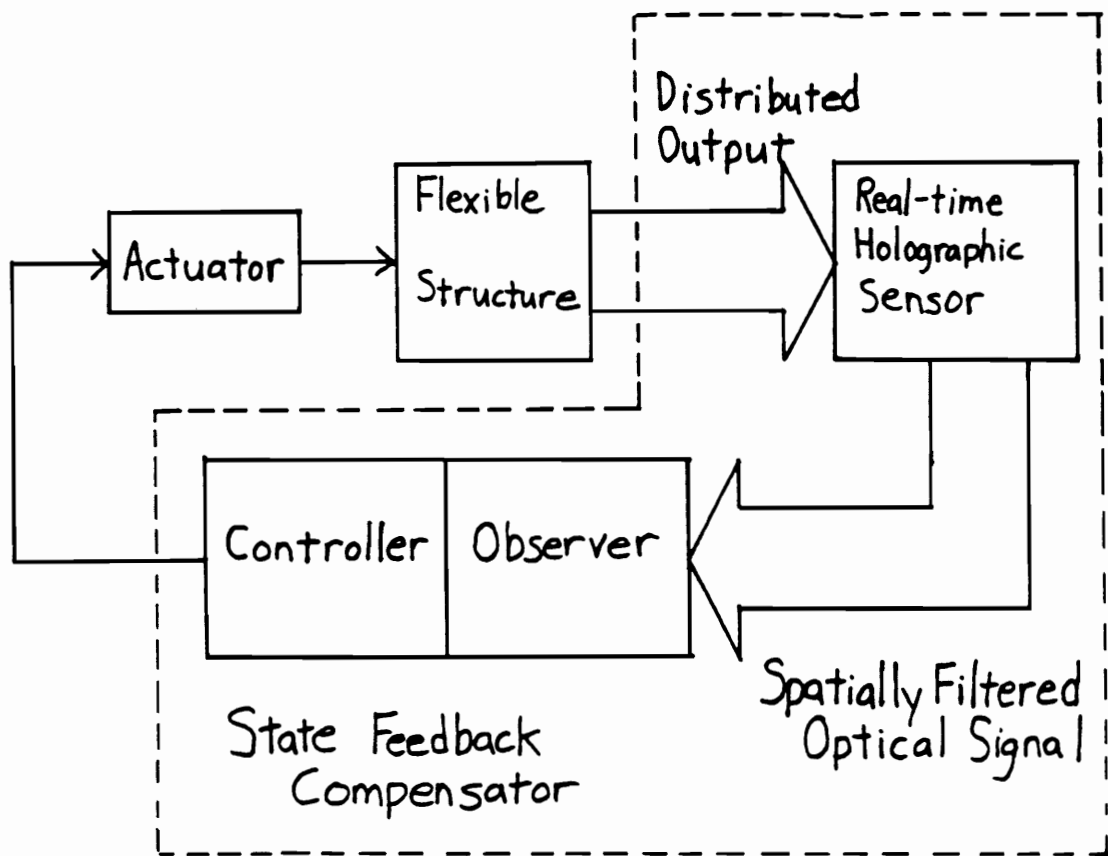


Figure 1. Flexible Structure with State Feedback Control System: The parts enclosed in the dashed line constitute the novel concepts. In a conventional state feedback control system, the output would be a vector rather than the distributed output function shown. The compensator converts the filtered optical signal into an electrical control signal.

amount of energy to excite. However, tens to hundreds of low frequency modes are expected to exist on typical appendages attached to satellites planned for the near future [2].

Two major problems have been identified when state feedback methods are applied to the control of flexible structures [1]. First, if only a finite number of modes are controlled, then the controller must not destabilize any of the remaining modes. The destabilization of the remaining modes is known as the spillover problem. Secondly, the control system design must account for the hardware used in the implementation. For example, it may be impractical to expect a powerful computer on-board a space-borne satellite to be dedicated to vibration suppression in the flexible appendages. We solve both problems by considering the theory and the implementation simultaneously.

In the context of state feedback, Balas [3] defines the spillover problem by dividing the compensator into a controller and an observer. If the finite dimensional state estimates from the observer are contaminated by sensor outputs containing all of the modes, then observation spillover exists. If the controller excites the remaining modes, then control spillover exists. If both control and observation spillover exist, the closed-loop control system is potentially unstable. Balas demonstrated that if either the control spillover or observation spillover is eliminated, then there is no instability problem.

Early methods for solving the spillover problem used the fact that each elastic mode oscillates at a particular temporal frequency. By prefiltering the sensor measurements in the temporal frequency domain, all but the frequencies under control may be rejected [3]. The prefilter is implemented using a bank of bandpass filters tuned to pass the controlled mode frequencies while rejecting all of the remaining modes. Hence, the time domain prefilter attempts to solve the spillover problem by eliminating the observation spillover. The method requires the controlled modes to be observable and controllable

from a finite number of point sensors and actuators. The placement of the sensors and actuators is otherwise arbitrary. This method does not address the problem of implementing the control system using limited computation.

Other approaches use the orthogonality of the modes [4] in the space domain. For instance, the independent modal-space control method in [1] uses space domain filters to prefilter the measurements from a distributed sensor in the space domain. If a distributed sensor or actuator is not available, the theory can be applied with some success if a large number of point sensors and actuators are available. If point sensors and actuators are used, the spillover can be eliminated in as many modes as sensor and actuator pairs. Each mode is controlled independently, greatly reducing the computational requirements. However, the spillover problem is completely solved only in the case where the sensor or actuator is distributed, and the computational burden increases linearly as the number of modes increases [1].

Efforts have been made to develop distributed sensing and actuating methods. For example, distributed piezoelectric sensors and actuators were recently demonstrated in a limited capacity [5]. The piezoelectric effect in PVDF film can be weighted as a function of space. If the PVDF film is attached to a structure exhibiting one-dimensional vibrations, then the sensor response weighting can be chosen to filter all but the first and second modes in the sensing operation, and control only the first and second modes in the actuation operation.

Another approach to distributed sensing is to use optical methods. This approach has been demonstrated in the context of the shape control of a segmented reflector [6]. The segmented reflector is composed of several rigid segments. The segments tend to move out of alignment over time, and must be realigned with submicron accuracy. An optical interferometer is used to measure the topography of the reflector. The sensor is processed by a video system which interprets the fringes to calculate the topology of the

reflector dish at a large number of points. The points are fit to a set of mode shape polynomials. The coefficients of the polynomial fit are compared to a set of coefficients representing the desired shape, and the control signal is issued accordingly to actuators attached to each segment. Since the structure is not continuously flexible, no spillover problems exist, but computational requirements are significant.

Our approach is to use real-time holography [7] to sense the shape of a flexible structure as a continuous optical function. The output of the sensor is in a form that can be filtered using optical methods allowing us to extract the modal content of the controlled modes exclusive of the remaining modes. Several implementations are given which allow the control to either be computed entirely by optical means, or by mixing temporal and spatial processing to various degrees. Thus, a powerful computer for processing is not necessary. The optical sensing and processing offer a potential solution to both the spillover and computation problems.

Chapter 2 describes several optical sensing methods leading up to the recommended holographic method. Chapter 3 presents the control system design methods. Chapter 4 presents an example of the effects of model order truncation in the design of a control system for a cantilevered beam. Chapter 5 presents some concepts for optically processing the signal from the optical sensor to implement the design of the Chapter 3. Chapter 6 presents a summary of the results and a detailed discussion of future work.

2.0 Distributed Sensing

2.1 Introduction

In this section, we introduce the concept of distributed sensing using a heuristic description of the sight process. Consider the flexible cantilevered beam shown in Figure 2 with an actuator attached to the free end. When we look at the cantilevered beam, we are performing a distributed sensing operation. The operation consists of properly illuminating the structure so that our eyes can detect the reflected radiation, and the focussing of the image of the structure onto our retinas. After the light is focussed onto the retina, the light is sampled by our rods and cones. The sampled image is processed in our minds, and we see the shape of the structure. The division of an optical sensor and processor is not precise. For example, the retina represents the boundary between the optical sensor and processor in our example. Everything before the retina is clearly part of the sensor, and everything after the retina is processing. The retina itself could either be considered part of the sensor or processor. In this dissertation, we will consider the devices which convert optical images into electrical

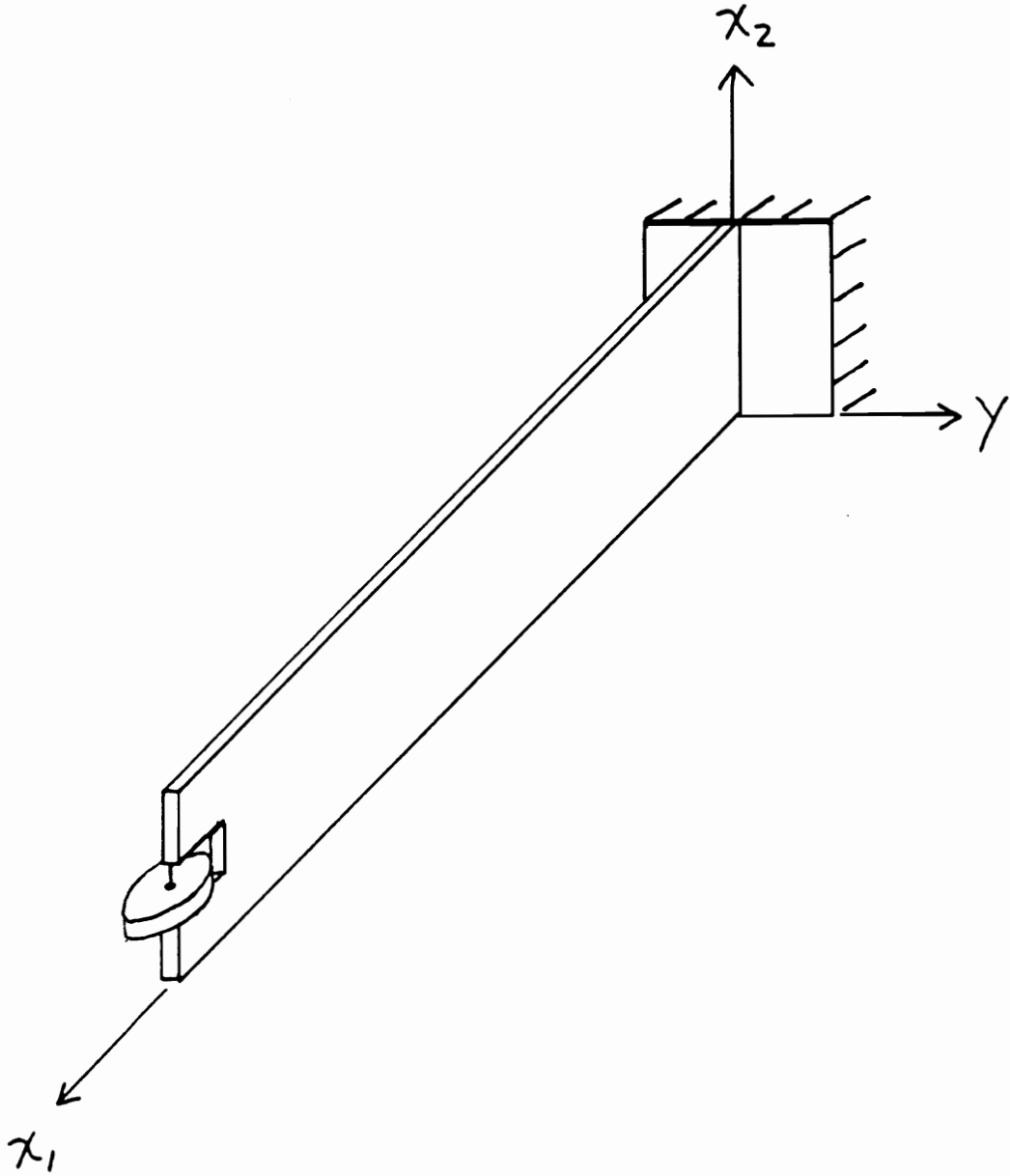


Figure 2. Cantilevered Beam with Tip-Actuator: The cantilevered beam is an example of a flexible structure. The beam is fixed at $x_1 = 0$. An actuator is attached to the free end where it can act to damp vibrations.

signals part of the processor by convention. Hence, in the example, we consider the retina part of the processor.

Before we extricate ourselves from the processing, let us consider more closely how we see the shape of a cantilevered beam by looking at it. If we were to look at the beam with one eye, then we could see the deflection along the x_1 -axis most clearly if we viewed the structure from above along the x_2 -axis. This is because an eye samples the image focussed on the retina to determine the coordinates of the image in a plane, but the eye is not sensitive to the depth of the image. Therefore, if we viewed the cantilevered beam from the y -axis, we could not determine the size of small deflections along the x_1 -axis, because the coordinates of the structure do not change from this perspective. However, if an eye could sense depth as well as position, the view from the y -axis would have several advantages. Imagine, for example, that the brightness of the image on the retina changed linearly as a function of the distance from the structure to the retina. Then view from along the y -axis would allow us to see deflections in both the x_1 and x_2 directions simultaneously. But even more significantly, we could determine the shape without following the image through space. The image would remain stationary in space, and the brightness at a point would vary as a function of time only. This property could be called spatial stationarity.

In optical signal processing, spatial stationarity allows us to process the sensed image using spatially fixed optics. In particular, we will show that spatial sampling (performed by eyes and digital cameras) will not be required in our processor to compute the control signal for the actuator.

We shall consider several optical sensing methods which build up to a real-time holographic sensing method. In the Section 2.2 we present notation and establish some preliminaries on optics. In Section 2.3 we consider a imaging sensor similar to the photography or vision. In Section 2.4 we augment the imaging sensor with a reference

light to create an interferometer highly sensitive depth and linear in the response. In Section 2.5 we present a multifrequency interferometer tuned to beat at a frequency to control the degree of sensitivity. In Section 2.6 we introduce holography as an alternate spatial approach at desensitizing the interferometer. In Section 2.7 we combine the multifrequency interferometric methods with holography. In Section 2.8 we show how the holographic methods can be implemented in real-time. In Section 2.9 we present a discrete-time version of the holographic sensor which may be useful in distributed processing. Finally, in Section 2.10 we summarize the methods.

2.2 Preliminaries

In this section, we state the optical terminology used in the development of the distributed sensor. We define an optical signal as a collimated beam of light propagating through space, as shown in Figure 3. In general, an optical signal is given by

$$U(x,t) = E(x,t) e^{j\omega(x,t)}, \quad (2.2.1)$$

where $E(x,t)$ is the amplitude of the signal, and $\omega(x,t)$ is the spectrum of the signal. If $E(x,t) = E$, then the amplitude is uniform. The instantaneous intensity function for an optical signal is defined as

$$I(x,t) \equiv U(x,t) U^*(x,t), \quad (2.2.2)$$

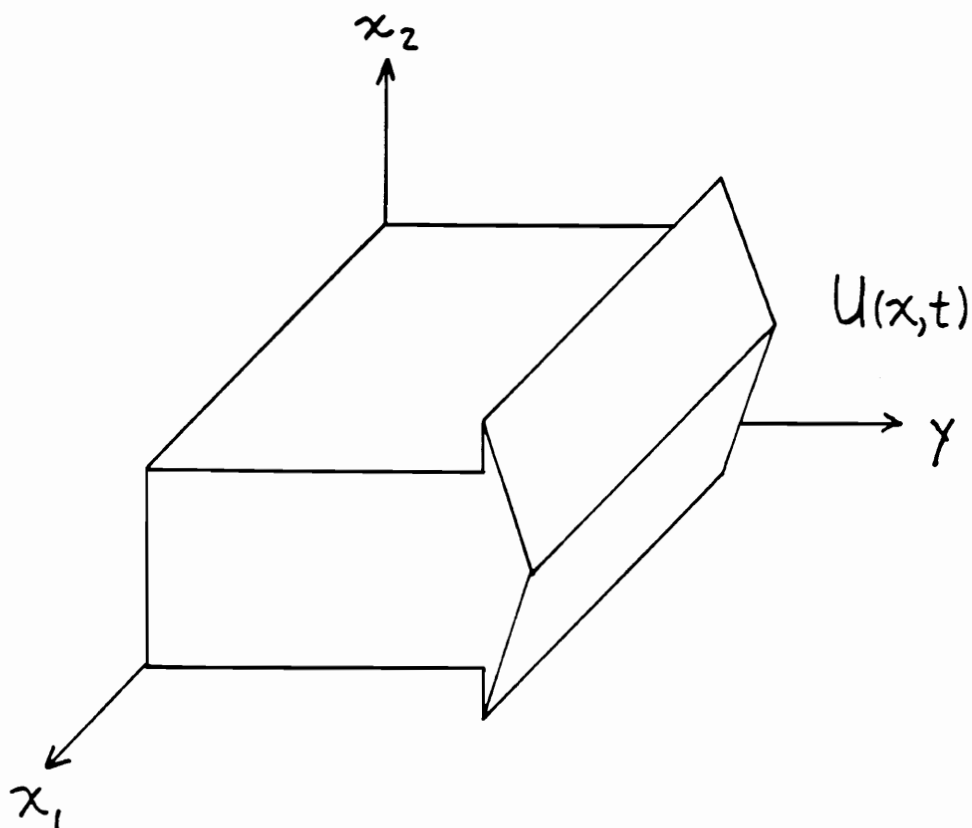


Figure 3. Optical Signal: An optical signal is a collimated beam of light propagating through space in the y direction.

where the asterix indicates the complex conjugate. All intensity function detectors measure the average intensity function. The average intensity function (or intensity function) at t_0 is given by

$$I(x, t_0) \equiv \{U(x, t) U^*(x, t)\} = \int_{t_0}^{t_0 + \tau} U(x, t) U^*(x, t) dt, \quad (2.2.3)$$

where τ is the time constant of the detector.

If the signal is monochromatic, then the spectrum consists of a single frequency.

That is,

$$\omega(x, t) = \omega_0 t + \phi(x, t), \quad (2.2.4)$$

where ω_0 is constant, and $\phi(x, t)$ is the phase of the monochromatic signal. The phase term characterizes the coherence of the signal [9] [10]. The signal is temporally coherent if $\phi(x, t_0)$ implies $\phi(x, t_1)$. For example, if $\phi(x, t) = \phi(x)$, then the signal is temporally coherent. Similarly, the signal is spatially coherent if $\phi(x_0, t)$ implies the phase at $\phi(x_1, t)$. For example, $\phi(x, t) = \phi(t)$ is spatially coherent. If the phase is constant, then the signal is both spatially and temporally coherent.

Several of the sensing methods involve imaging (or focussing) an optical signal onto an image plane. This is usually accomplished using a lens or a system of lenses. We will consider a signal well focussed if each point over the cross section of the signal is mapped in a one-to-one fashion onto an image plane. If the optical signal represents the deflection of a flexible structure, the structure is well focussed if each point on the structure is mapped one-to-one onto the image plane. A structure is diffusely reflecting if incident light is reflected in all directions with equal intensity. Hence, if a beam of light is incident on a diffusely reflecting structure, then the intensity of the light reflected onto

a detector will be independent of the angle of incidence. A structure is retroreflecting if it reflects all incident light back in the direction of origin. Our goal in the following sections is to sense the deflection as an intensity function over a spatial domain, as shown in Figure 4.

2.3 *The Imaging Method*

The imaging method is the technique used in photography. An image of a diffusely reflecting flexible structure is focussed on an image plane, as shown in Figure 5. The light is reflected in all directions. Therefore, intensity averaged over any area will decrease as an inverse square proportion [11]. The intensity function in the image plane will be

$$I(x) \propto \frac{1}{y_o^2(x)}, \quad (2.3.1)$$

where $y_o(x)$ is the distance from the undeflected or equilibrium position of the structure to the image plane. If the beam is deflected away from equilibrium by $y(x,t)$, then the intensity would change to yeild,

$$I(x,t) \propto \frac{1}{(y_o(x) + y(x,t))^2}. \quad (2.3.2)$$

Several problems become apparent if we wish to calculate the amount of deflection away from equilibrium by measuring the intensity function $I(x,t)$. First, if the beam is in focus in its equilibrium position $\sigma(x)$, then it will not be in focus (the mapping will not be

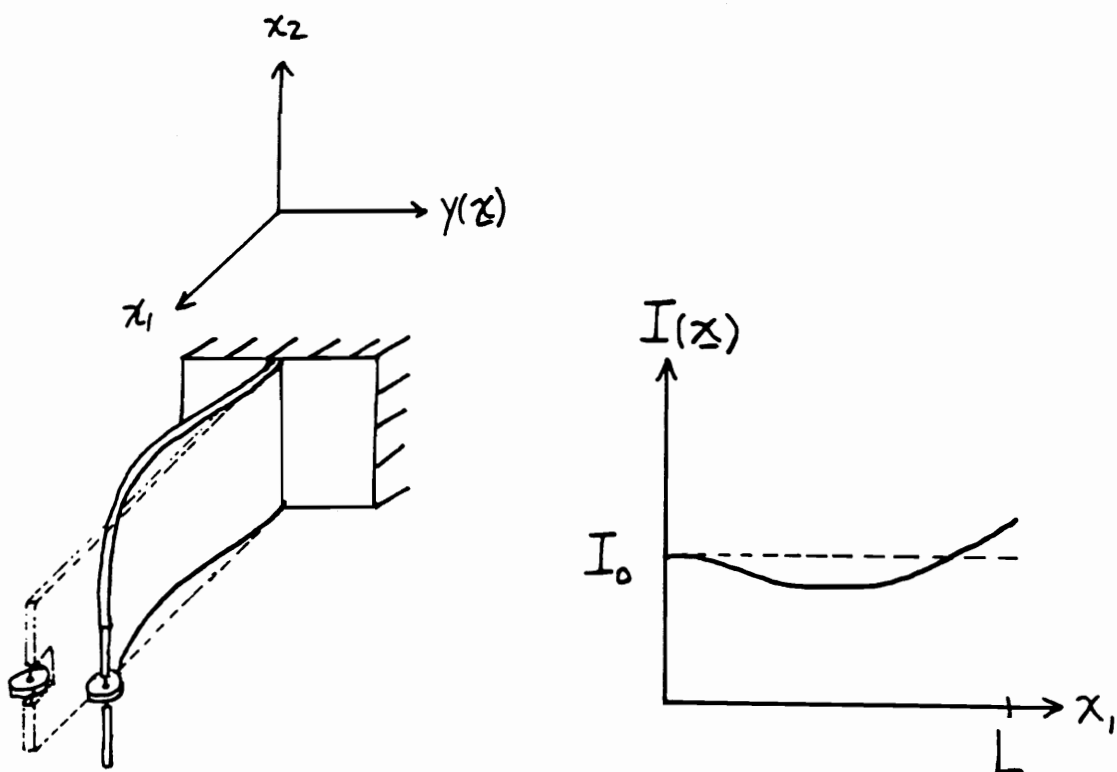


Figure 4. Intensity Function: The figure on the left is a beam that is undergoing deflection from equilibrium. The figure on the right is the corresponding intensity function. The constant bias should be small for a high signal to noise ratio.

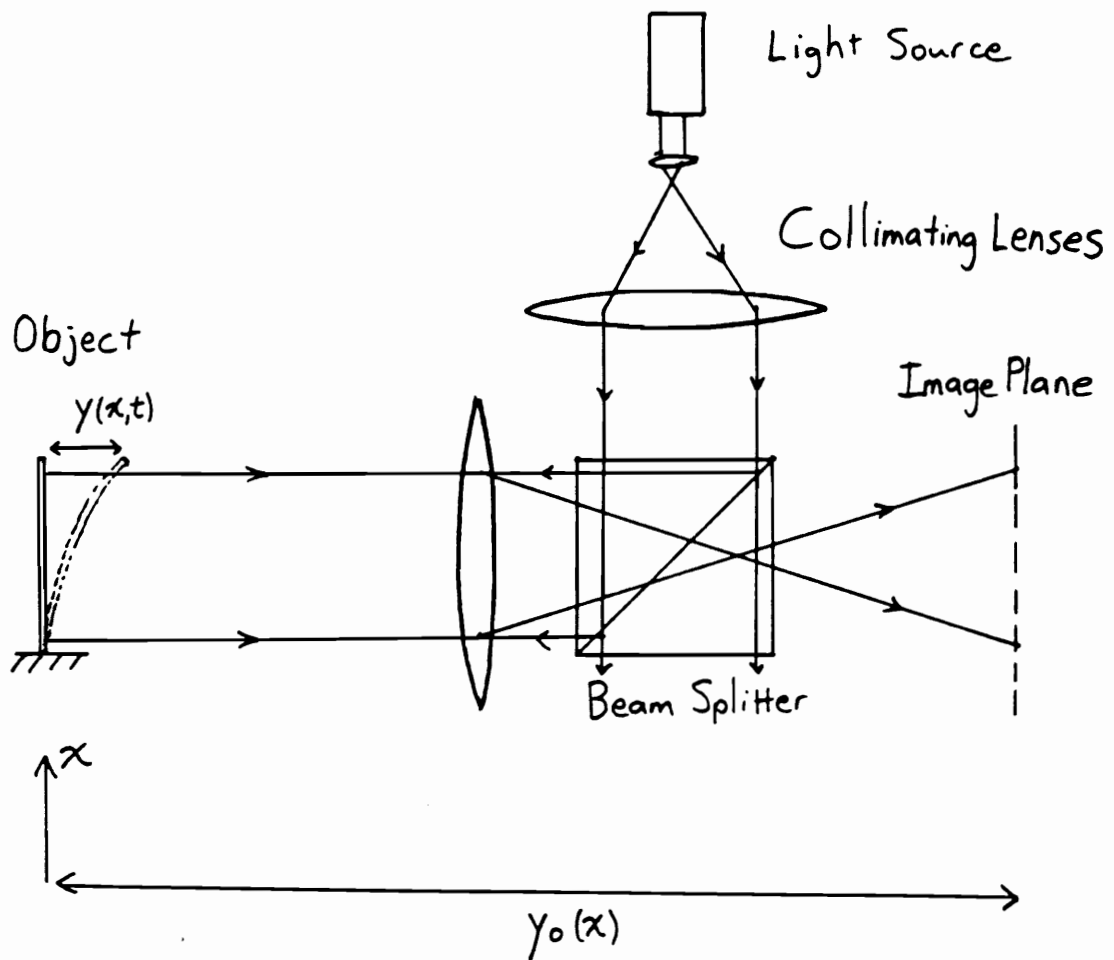


Figure 5. Imaging System: The imaging system uses a lens to focus an image of the beam onto a plane. If the beam is uniformly lit, then the intensity in the image plane is inversely proportional to the square of the distance from the beam to the image plane.

one-to-one) if $y(x,t)$ is large. Therefore, we must enforce the constraint $y_s(x) \gg y(x,t)$ over the surface of the structure. Secondly, it is apparent from Equation (2.3.2) that if $y_s(x)$ is much greater than $y(x,t)$, then the variations in the intensity due to $y(x,t)$ will be insignificant. Direct intensity methods such as the imaging method tend to be highly sensitive to disturbances or variations in the source intensity or beam surface diffusivity, further exasperating the situation.

If an acceptable compromise could be found in the above contradiction, the method would still require square root detection and inversion to recover $y(x,t)$. In the next section, we modify the imaging system to greatly increase its sensitivity, and create an intensity function which is in a form suitable for optical processing.

2.4 *The Interference Method*

The interference method uses a Michelson interferometer [11]. The Michelson interferometer system is similar to the imaging system with two exceptions. First, the illuminating source must be a laser. In the imaging system, the only requirement on the source was uniform intensity. Secondly, the source must be divided to create two beams for interference. The system for dividing and combining beams is shown in Figure 6. These two changes resolve many of the problems in the simple imaging system. This method is most effective on retroreflecting structures because light energy is not lost in the illumination.

In the interferometric system, a laser is required because the source must be monochromatic and spatially coherent. These changes allow us to refer to the light source as a wavefront, because adjacent light rays are travelling in phase forming a

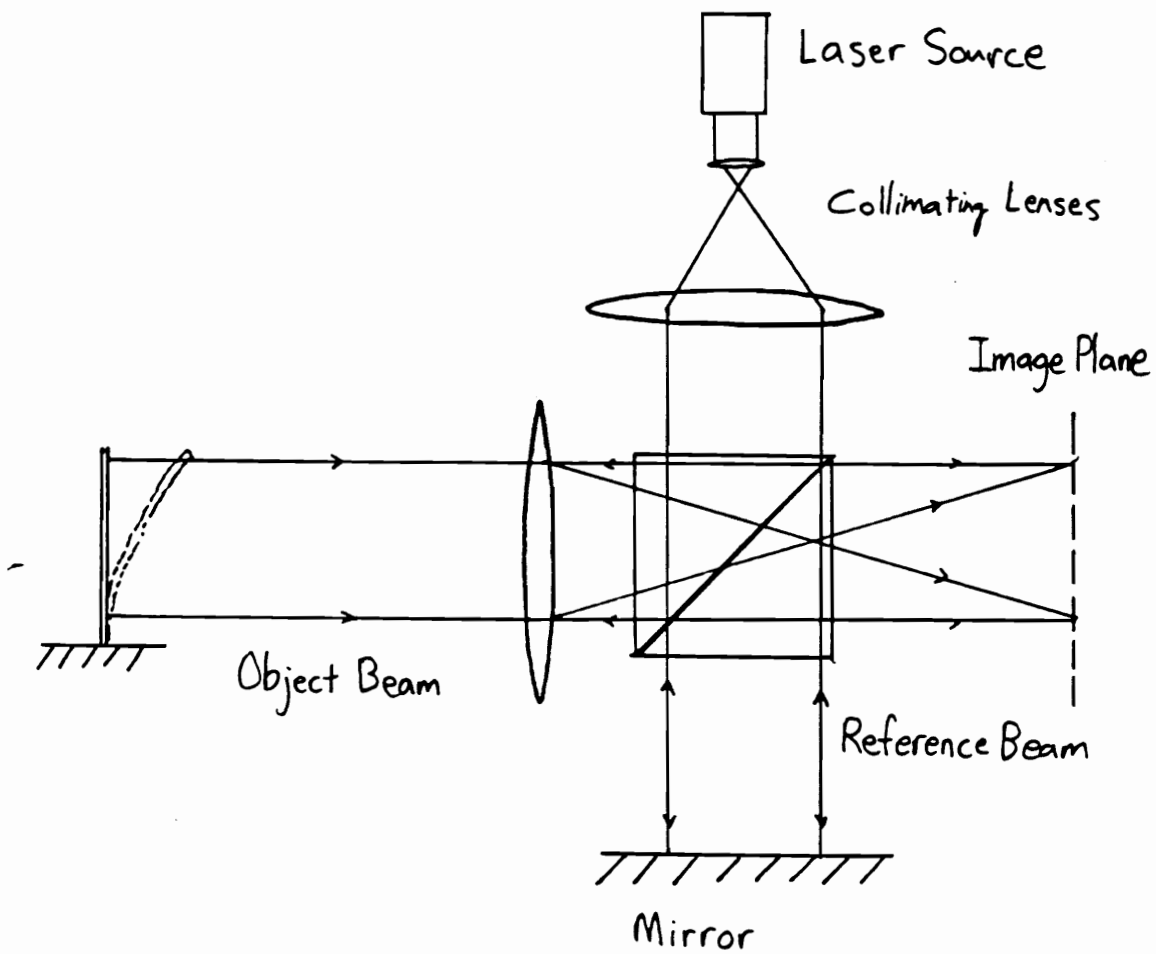


Figure 6. Michelson Interferometer: This system is similar to the imaging system, but the source must be a laser and an additional mirror is required for the reference. An interference pattern is formed in the image plane.

parallel lines of maximum amplitude orthogonal to the direction of propagation. A good laser can generate nearly monochromatic and spatially coherent wavefronts.

The source is both divided and joined by a beam splitter; a half silvered mirror which splits a single beam into two equally intense beams. The beam propagating toward the flexible structure is called the object beam. The beam propagating toward the mirror is called the reference beam. Upon reflection, the reference and object beams return to the beam splitter where they sum to form an image beam. In terms of complex exponentials, the reference beam is

$$U_r(x,t) = E_r e^{j(\omega t + \phi_r(x))}, \quad (2.4.1)$$

and the object beam is

$$U_o(x,t) = E_o e^{j(\omega t + \phi_o(x,t))}. \quad (2.4.2)$$

The source phase is an arbitrary constant, and is set to zero. The object and reference beams are assumed to have constant amplitudes over x . This assumption is valid if the deflections of the structure are small compared to the distance from the structure to the beam splitter, and the structure is retroreflecting. In the image plane, the object and reference beams add to create the image beam. Using (2.4.1) and (2.4.2), we can express the image as,

$$\begin{aligned} U(x,t) &= U_r(x,t) + U_o(x,t) \\ &= E_r e^{j(\omega t + \phi_r(x))} + E_o e^{j(\omega t + \phi_o(x,t))}. \\ &= e^{j\omega t} (E_r e^{j\phi_r(x)} + E_o e^{j\phi_o(x,t)}) \end{aligned} \quad (2.4.3)$$

Using the definition of intensity (2.1.3), we may calculate the intensity in the image plane [10],

$$\begin{aligned}
I(x,t) &= \{U(x,t)U^*(x,t)\} \\
&= \{e^{j\omega t}(E_r e^{j\phi_r(x)} + E_o e^{j\phi_o(x,t)})e^{-j\omega t}(E_r e^{-j\phi_r(x)} + E_o e^{-j\phi_o(x,t)})\} \\
&= E_r^2 + E_o^2 + E_r E_o e^{j(\phi_o(x,t) - \phi_r(x))} + E_r E_o e^{j(\phi_r(x) - \phi_o(x,t))} \\
&= E_r^2 + E_o^2 + 2E_r E_o \cos(\phi_o(x,t) - \phi_r(x)),
\end{aligned} \tag{2.4.4}$$

where, again, the braces indicate time averaging. The first two terms in (2.4.4) are constant bias intensities. The third term depends on the difference in path length of the reference and object beams. Assume the mirror is orthogonal to the object beam, so the reference phase $\phi_r(x)$ is a constant over x . Let $y_o(x,t)$ and $y_r(x)$ be the distance from the object and reference, respectively, to the image plane. Then,

$$\begin{aligned}
\phi_o(x) &= \frac{4\pi y_o(x,t)}{\lambda} \\
\phi_r(x) &= \frac{4\pi y_r(x)}{\lambda}
\end{aligned} \tag{2.4.5}$$

or, if $y(x,t) = y_o(x,t) - y_r(x)$, then

$$\begin{aligned}
\phi_o(x) - \phi_r(x) &= \frac{4\pi y(x,t)}{\lambda} \\
&\equiv \phi(x,t)
\end{aligned} \tag{2.4.6}$$

where λ is the wavelength of the source beam. If we pick $\phi(x,t)$ to be $-\frac{\pi}{2}$ when no vibrations are present, then

$$\cos(\phi(x,t)) \simeq y_o(x,t), \text{ for } -\frac{3\pi}{4} < \phi(x,t) < -\frac{\pi}{4}. \tag{2.4.7}$$

Hence, the intensity in (2.4.4) is proportional to the the deflection of the structure (plus bias terms). This appears to solve the problems in the imaging system. There are no conflicting requirements, the signal to bias levels are small, and the sensitivity is high.

Unfortunately, for many applications, the sensitivity is in fact too high. The range for a linear response in (2.4.7) implies that

$$y(x,t) < \frac{\lambda}{2}. \quad (2.4.8)$$

Typically, the wavelength λ is a fraction of a micron; much smaller than the maximum amplitude of vibrations one might expect in flexible structures.

The interferometric method solves many of the problems encountered in the imaging system at the expense of some complication. In particular, a laser source is required, and a reference beam must be supplied for interference. The result is a system that is sensitive to the shape of the structure regardless of the distance of the structure from the sensor. Unfortunately, the system is often too sensitive for practical purposes. One notable exception is in the shape control of segmented mirrors [6] where interferometric methods have been used with success. In the next section, a method of desensitizing the interferometric method is discussed.

2.5 The Desensitized Interference Method

This method is similar to the interferometric method presented in the previous section, except a multifrequency laser is used instead of the monochromatic source. We will consider the special case of a two frequency laser as an example; generalization to any number of frequencies, or even continuous frequency distributions, is straightforward [12] [10]. The basic idea is to take advantage of the beat frequency phenomena. Two waves differing slightly in frequency will tend to interfere at a

frequency proportional their difference. The beat wavelength corresponding to distance between maxima of interference is much longer than the wavelengths of the light source [11]. Since the range of the interferometer is on the order of the wavelength of the source, an effective long wavelength source may be synthesized. The principle limitation of the approach is the necessity for spatial envelope detection, as is discussed.

We may use the notation developed in the previous section to define the source beam. Assume the source emits at frequencies ω_1 and ω_2 , creating two collinear beams,

$$\begin{aligned} U_1(x,t) &= E_1 e^{j\omega_1 t} \\ U_2(x,t) &= E_2 e^{j\omega_2 t}. \end{aligned} \quad (2.5.1)$$

These beams create the reference beams,

$$\begin{aligned} U_{r_1}(x,t) &= E_{r_1} e^{j(\omega_1 t + \phi_{r_1}(x))} \\ U_{r_2}(x,t) &= E_{r_2} e^{j(\omega_2 t + \phi_{r_2}(x))}, \end{aligned} \quad (2.5.2)$$

and the object beams,

$$\begin{aligned} U_{o_1}(x,t) &= E_{o_1} e^{j(\omega_1 t + \phi_{o_1}(x,t))} \\ U_{o_2}(x,t) &= E_{o_2} e^{j(\omega_2 t + \phi_{o_2}(x,t))}. \end{aligned} \quad (2.5.3)$$

The resulting image field is the sum of the object and reference beams,

$$U(x,t) = U_{r_1}(x,t) + U_{r_2}(x,t) + U_{o_1}(x,t) + U_{o_2}(x,t). \quad (2.5.4)$$

The intensity of the image is given by,

$$\begin{aligned}
I(x,t) &= \{U_l(x,t)U_l^*(x,t)\} \\
&= E_{r_1}^2 + E_{r_2}^2 + E_{o_1}^2 + E_{o_2}^2 \\
&\quad + 2E_{o_1}E_{r_1} \cos(\phi_{o_1}(x,t) - \phi_{r_1}(x)) \\
&\quad + 2E_{o_2}E_{r_2} \cos(\phi_{o_2}(x,t) - \phi_{r_2}(x)),
\end{aligned} \tag{2.5.5}$$

where the cross terms average to zero. (It is assumed that all cross terms oscillate at a frequency much faster than the cut-off frequency in the time average of the intensity detectors. The intensity detectors may have a cut-off frequencies as high as several kHz, while the zero-mean oscillations of the cross terms are not likely to be less than a GHz.) If the intensities of the object and reference beams are equal, then we may combine the last two terms in (2.5.5) to yield

$$\begin{aligned}
I(x,t) &= E_{r_1}^2 + E_{r_2}^2 + E_{o_1}^2 + E_{o_2}^2 \\
&\quad + 4E_{o_1}E_{r_1} \cos\left(\frac{(\phi_{o_1}(x,t) - \phi_{r_1}(x))}{2} + \frac{(\phi_{o_2}(x,t) - \phi_{r_2}(x))}{2}\right) \times \\
&\quad \cos\left(\frac{(\phi_{o_1}(x,t) - \phi_{r_1}(x))}{2} - \frac{(\phi_{o_2}(x,t) - \phi_{r_2}(x))}{2}\right).
\end{aligned} \tag{2.5.6}$$

The first four terms of (2.5.6) are constant intensities, as in the first two terms of (2.4.4). The last term in (2.4.4) is a function of the beam deflection. The last term of (2.5.6) is also a function of the deflection, but (2.5.6) consists of a fast cosine,

$$c_f(x,t) = \cos\left(\frac{(\phi_{o_1}(x,t) + \phi_{o_2}(x,t))}{2} - \frac{(\phi_{r_1}(x) + \phi_{r_2}(x))}{2}\right), \tag{2.5.7}$$

and a slow cosine,

$$c_s(x,t) = \cos\left(\frac{(\phi_{o_1}(x) - \phi_{o_2}(x))}{2} + \frac{(\phi_{r_1}(x) - \phi_{r_2}(x))}{2}\right). \quad (2.5.8)$$

If

$$\lambda_c = \left(\frac{1}{\lambda_1} + \frac{1}{\lambda_2}\right)^{-1}, \quad (2.5.9)$$

and

$$\lambda_m = \left(\frac{1}{\lambda_1} - \frac{1}{\lambda_2}\right)^{-1}, \quad (2.5.10)$$

then by (2.4.8), the linear range of the deflection calculated using the slow cosine term $c_s(x,t)$ is

$$y(x,t) < \frac{\lambda_m}{2}, \quad (2.5.11)$$

while the deflection calculated using the fast cosine must be limited to

$$y(x,t) < \frac{\lambda_c}{2}. \quad (2.5.12)$$

Since $\lambda_m \gg \lambda_c$, if the deflections of the structure are large, the fast cosine $c_f(x)$ will superimpose fringes on top of the intensity function of the slow cosine $c_s(x)$.

The intensity function contains the product of a slow cosine and a fast cosine. The slow cosine modulates the fast cosine “carrier” frequency in the fashion of an amplitude modulation (AM) communication system. In a communications system, an envelope detector is required to demodulate the signal from the carrier. While the desensitized

interferometer may not be directly applicable, it is the key to utilizing the holographic methods explained in the remainder of this chapter.

2.6 The Holographic Method

The holographic method is similar in many ways to the interferometric method in Section 2.4, but there are two major differences. First, in holography the reference and object beams intersect at an angle in the image plane, rather than being joined by the beam splitter into a single beam. Second, the resulting interference pattern is not used directly. Instead, the interference pattern must be recorded and read. Hence, holography is a two step process. Holography on film is impractical for real-time processing. Holographic recording media which can be written and read simultaneously is the subject of Section 2.8. In this section, we assume the object is fixed for all time, so any suitable recording medium may be assumed. Our purpose is to show how holographic methods are used to address the sensing problem. The reader is referred to the references [13] [14] for standard texts on the subject.

A system for holographic sensing is shown in Figure 7. The idea is to give the interference pattern a constant spatial frequency about which deflections are modulated. This is why the beams meet at an angle. Unfortunately, if the beams are angled, the output is not a single beam, so spatial frequency methods cannot be used directly in demodulation. We will show that holographic methods offer some unexpected benefits. As in the interferometric system, the source is assumed to be monochromatic and spatially coherent. Using the development from Section 2.4, the object beam is given by

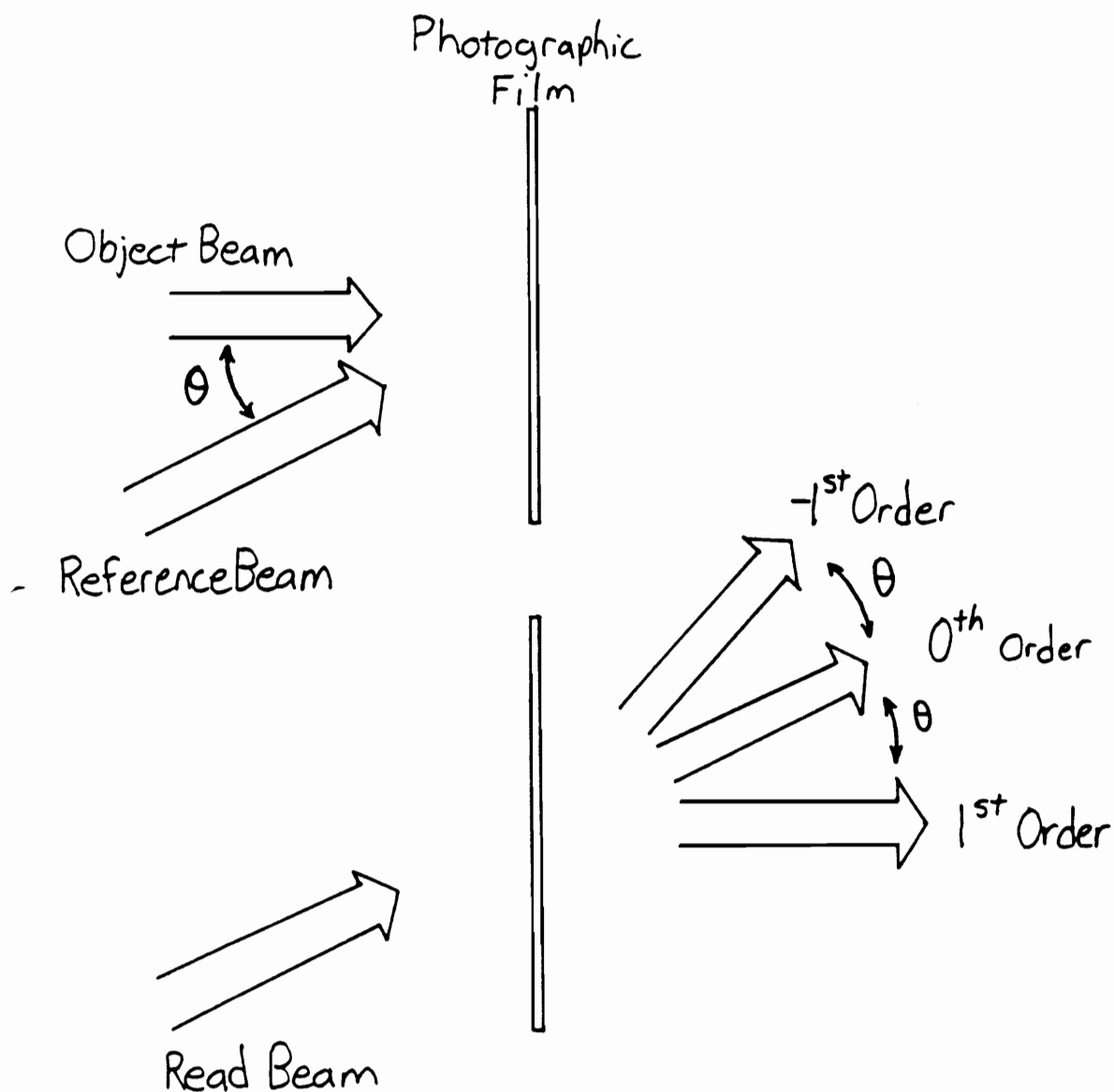


Figure 7. Holographic Sensing System: This system is similar to the interferometric system, but the object and reference beams intersect at the angle θ . The hologram is read by a beam counter propagating to the reference beam.

$$U_o(x,t) = E_o e^{j(\omega t + \phi_o(x))}, \quad (2.6.1)$$

and the reference beam is given by

$$U_r(x,t) = E_r e^{j(\omega t + \phi_r(x))}. \quad (2.6.2)$$

We assume the object beam wavefront is parallel to the film, and the reference beam is incident on the film at an angle θ such that

$$\phi_r(x) = \alpha x, \quad \text{where } \alpha = \frac{\sin \theta}{2\pi\lambda}, \quad (2.6.3)$$

and

$$\phi_o(x) = \frac{1}{2\pi\lambda} y(x), \quad (2.6.4)$$

where $y(x) = 0$ in equilibrium. From (2.4.4), the intensity of the interference pattern formed in the plane of intersection between the object and reference beams is given by

$$I(x) = E_r^2 + E_o^2 + 2E_r E_o \cos(\phi_o(x) - \phi_r(x)). \quad (2.6.5)$$

From our definition of $\phi_r(x)$ in (2.6.3), we can see that if the structure is undeflected, ($\phi_o(x) = 0$), then the spatial frequency of the fringes in $I(x)$ will be centered at α .

The transmission function for a hologram is a function used to describe the output when the hologram is read. After the film on which the hologram is recorded is developed, the transmittance function of the resulting transparency is given by

$$\begin{aligned} t_f(x) &= t_b + \beta(U_o(x)U_o^*(x) + U_r(x)U_r^*(x) + U_r^*(x)U_o(x) + U_r(x)U_o^*(x)) \\ &= t_b + \beta(E_o^2 + E_r^2 + E_r E_o e^{j(\phi_o(x) - \phi_r(x))} + E_r E_o e^{j(\phi_r(x) - \phi_o(x))}), \end{aligned} \quad (2.6.6)$$

where β is related to the properties of the film and exposure, and t_b is a constant background attenuating factor. If the transparency is illuminated by a beam counter propagating to the reference beam, the output beam is given by

$$\begin{aligned} E_r e^{j\phi_r(x)} t_f(x) = & t_b E_r e^{j\phi_r(x)} + \beta(E_o^2 E_r e^{j\phi_r(x)} + E_r^3 e^{j\phi_r(x)}) \\ & + \beta E_r e^{-j\phi_r(x)} E_r e^{j\phi_r(x)} E_o e^{j\phi_o(x)} \\ & + \beta E_r e^{j\phi_r(x)} E_r e^{j\phi_r(x)} E_o e^{-j\phi_o(x)}. \end{aligned} \quad (2.6.7)$$

The phase terms indicate the direction of propagation. The terms in the first row of (2.6.7)

$$U_o(x) = (t_b + \beta(E_o^2 + E_r^2)) E_r e^{j\phi_r(x)} \quad (2.6.8)$$

propagate in the direction of the reference beam, $\phi_r(x)$, and are called the zero order of the hologram output. The terms in the second row

$$U_1(x) = \beta E_r^2 E_o e^{j\phi_o(x)} \quad (2.6.9)$$

propagate in direction of the object beam with the phase of the object, and are called the first order. The last term

$$U_{-1}(x) = \beta E_r^2 E_o e^{j(2\phi_r(x) - \phi_o(x))} \quad (2.6.10)$$

propagates at twice the angle of the reference beam with the conjugate phase of the object, and are called the -1st order. Hence, each row of (2.6.7) is spatially separated, and may be detected separately. In particular, we may recognize that the first order $U_1(x)$ is proportional to the object beam in amplitude and phase. The carrier frequency α has been removed from the interference pattern. The recovery of the amplitude and phase differentiates holography from photography. We have assumed that the

amplitude is constant over the surface of the structure, so all information about the orientation of the structure is contained in the phase.

Unfortunately, this output signal contains the deflection information in the phase. Therefore, the phase associated with deflections larger than the wavelength of the light are ambiguous. However, the holographic method does successfully demodulate the spatial frequency offset induced by angling the intersection of the beams. In the next section we show that if the desensitizing method for the interferometer is used in holography, then the output beam is automatically demodulated.

2.7 Multifrequency Holography

In this section, the results from Sections 2.5 and 2.6 are combined to solve their respective modulation and sensitivity problems [13] [15] [16]. The monochromatic laser source in Section 2.6 is replaced by the two frequency source from Section 2.5, and the resulting hologram is read by a light source with only one of the frequencies.

If the reference is given by (2.5.2) and the object beam is given by (2.5.3), then the intensity at the intersection of the beams is given by (2.5.5). That is,

$$I_t = \{U_{o_1}U_{o_1}^* + U_{o_2}U_{o_2}^* + U_{r_1}U_{r_1}^* + U_{r_2}U_{r_2}^* + U_{o_1}U_{r_1}^* + U_{o_1}^*U_{r_1} + U_{o_2}U_{r_2}^* + U_{o_2}^*U_{r_2}\}. \quad (2.7.1)$$

If the hologram is read by the reference beams U_{r_1} , the output may be calculated as

$$\begin{aligned} U_{r_1}t_f(x) = & t_b U_{r_1} + \beta(E_{o_1}^2 U_{r_1} + E_{o_2}^2 U_{r_1} + E_{r_1}^2 U_{r_1} + E_{r_2}^2 U_{r_2}) \\ & + \beta(U_{r_1}U_{r_1}^*U_{o_1} + U_{r_1}U_{r_2}^*U_{o_2}) \\ & + \beta(U_{r_1}U_{r_1}U_{o_1}^* + U_{r_1}U_{r_2}U_{o_2}^*). \end{aligned} \quad (2.7.2)$$

The terms in the first row of (2.7.2) are the zero order, and propagate in the direction of the reference beams. The terms in the second row are the first order, and travel in the direction of the object beam. The last row is the -1st order, and is directed at an angle of twice the reference minus the object angle. We analyze the first order,

$$E_1(x) = E_{r_1}^2 E_{o_1} e^{j\phi_{o_1}(x)} + E_{r_2} E_{r_1} E_{o_2} e^{-j(\phi_{r_2}(x) - \phi_{r_1}(x) - \phi_{o_2}(x))}. \quad (2.7.3)$$

If $E_{r_1} = E_{r_2} = E_{o_1} = E_{o_2} \equiv E$, then the intensity of the first order is given by,

$$\begin{aligned} I_1(x) &= \{E_1 E_1^*\} \\ &= 2E^6 \left(1 + \cos \left(\frac{(\phi_{o_1}(x) - \phi_{o_2}(x))}{2} + \frac{(\phi_{r_1}(x) - \phi_{r_2}(x))}{2} \right) \right) \\ &= I_o \left(1 + \cos \left(\frac{(\phi_{o_1}(x) - \phi_{o_2}(x))}{2} + \frac{(\phi_{r_1}(x) - \phi_{r_2}(x))}{2} \right) \right). \end{aligned} \quad (2.7.4)$$

Hence, the output is similar to the output of the multifrequency interferometer (2.5.6), except the fast "carrier" frequency is not present. The output intensity cosine will vary at the beat frequency (2.5.10), and will be sensitive to deflections the size of the beat wavelength.

Multifrequency holography allows us to effectively detect the envelope of the fringe pattern generated by the multifrequency interferometer. The cost is in the holographic processing. Holography on film is impractical because the sequential nature of the process excludes real-time processing. In the next section we discuss a real-time method of holography that removes the film from the sensing process.

2.8 *Real-Time Holography*

Real-time holography is often called four wave mixing in literature, because all four waves are present simultaneously: read, write (or reference), object and output. It is also referred to more generally as nonlinear optical mixing; the nonlinearity being in the coupling between the waves. All four waves may be present simultaneously because the hologram is not formed in a photographic emulsion. Instead, the waves are mixed in photorefractive crystals.

Many materials exhibit some change in their index of refraction when exposed to high intensity levels. In fact, the nonlinear phenomena was first considered "optical damage" due to high power lasers [17]. A smaller class of materials such as BSO and BaTiO₃ are now known as photorefractive materials because they exhibit nonlinear responses at relatively low intensity levels. Free electrons doped into the crystals tend to drift away from areas in the crystal exposed to optical radiation. This exerts tensions inside the crystal which locally change the index of refraction. Hence, if an interference grating is exposed on the crystal, it will cause a corresponding refractive grating or phase grating to form. The analogy between the conventional holography discussed in this dissertation and real-time holography was first clearly defined in [18].

In [18], the equivalence is established in detail by solving the nonlinear coupled equations of four wave mixing. For our purposes it is sufficient to note that the principles of holography on film and holography in crystals are exactly analogous. However, we have ignored up to this point two practical considerations in our discussion of holography which cannot be neglected in real-time holography. These are the thickness of the recording medium and the mode of response.

If the medium in which the hologram is formed is thicker than the spacing between the fringes, then the resulting hologram is called a volume hologram. A detailed analysis of the effects of thickness may be found in [13]. A qualitative review of the effects is summarized here. If the recording medium is thick, then only one of the output orders will appear in the reading process, and the order that appears will depend on the angle of the read beam. Recall from Section 2.6 that the reading operation generated three terms separated in space (3 orders). In a volume hologram, a Bragg diffraction condition [14] exists which states that the order reconstructed depends on the direction of the read beam. In particular, a read beam counter propagating to the original write beam (reference beam) will only generate the phase conjugate beam. The original reference beam and the original object beams are not reconstructed. We will see that this is in fact the beam which we will want to reconstruct. The read beam must be precisely oriented, but the extraneous beams are eliminated. In addition, we will show that a problem caused by the mode of response is solved by the thickness of the medium.

Photographic film responds by altering the absorption characteristics of the resulting transparency, but the mode of response of the crystal is an index of refraction change. In the planar case, the consequence of the non-sinusoidal nature of the phase changes is the creation of orders beyond the three discussed above. This could make the reconstruction process difficult. However, if the phase hologram is formed in a thick medium, only one order will be reconstructed for a particular read angle. Hence, phase and absorption holograms are functionally identical in thick media.

A system for realizing a real-time holographic sensor is shown in Figure 8. The hologram is formed as in Section 2.7. The object and reference beams each contain two closely spaced optical frequencies. Simultaneously, a read beam consisting of only one of the frequencies is counter propagating to the reference beam. This creates the output beam which is removed using a beam splitter, as shown in Figure 8. From the analysis

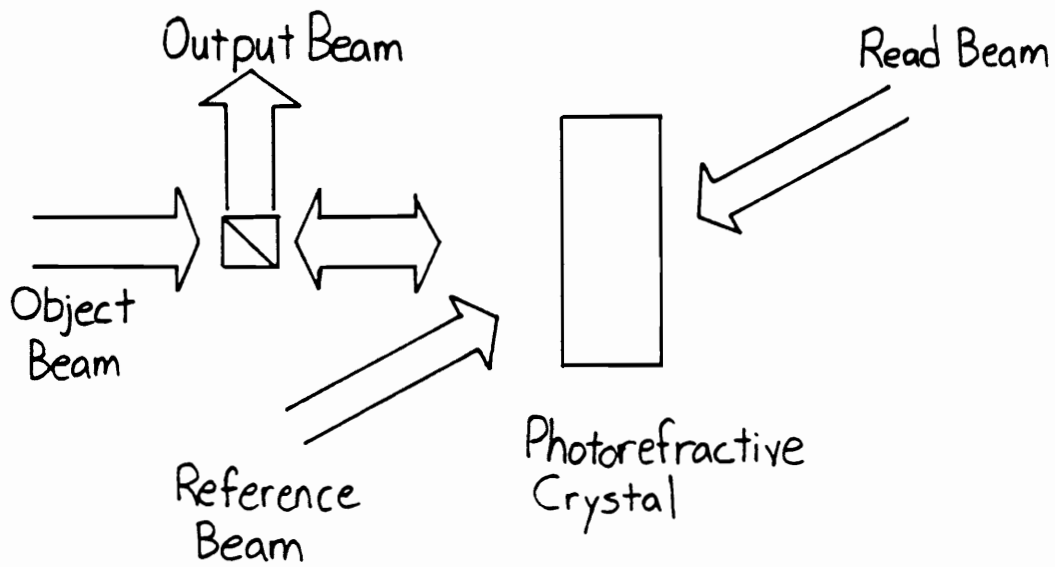


Figure 8. Real-Time Holographic Sensor: The multifrequency object and reference beams form an interference grating in the material. Simultaneously, the single frequency read beam forms the output beam counter propagating to the original object beam. The output is formed as a separate beam using a beam splitter.

in Section 2.7, the intensity of the output beam is proportional to the deflection of the beam. Therefore, we have found a suitable distributed sensor.

2.9 Discrete-Time Holography

Hardware for integrating a spatially distributed signal in time does not presently exist. This limits the processing of the continuous time holographic sensor to the space domain. However, a discrete-time holographic sensor is under development which could function as a delay or temporary storage device in a discrete-time processor. In such a system, temporary storage replaces distributed integration in time. The concept for discrete-time holography proposed in [8] uses two photorefractive crystals, as shown in Figure 9. The hologram is written into one of the crystals whose output becomes the object beam for the second crystal. The output of the second crystal is then fed back to the first, completing the oscillator loop. Once the oscillation is established, the original object beam may be removed, and the output held constant for reading. If the oscillation is established quickly, the unit functions as a distributed delay.

The practical application of this technology is limited to slow moving structures due to the relatively long response time of presently available crystals. Regardless of the present technical obstacles, we may consider the concept in our designs and implementations to analyze the advantages and limitations in discrete-time processing.

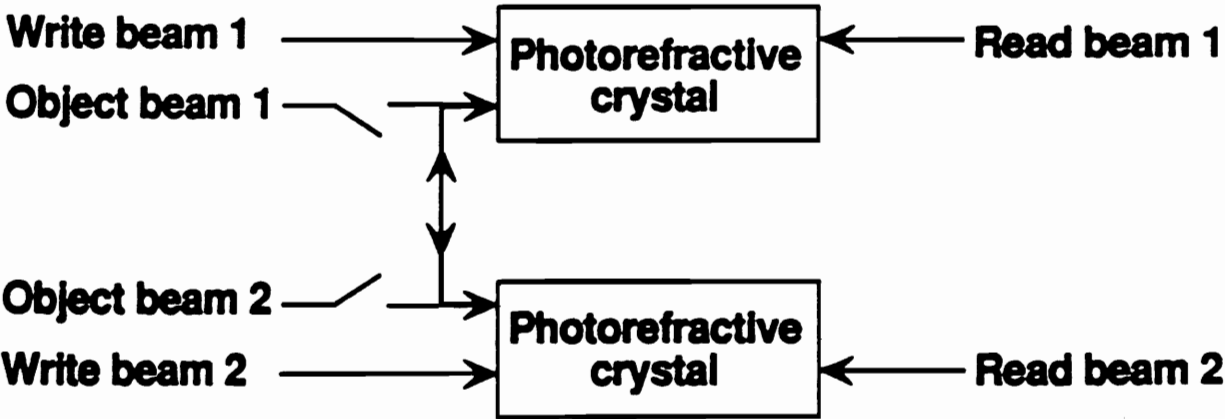


Figure 9. Discrete-Time Holographic Sensor: Two crystals form an oscillator to temporarily store a distributed image.

2.10 Summary

The purpose of this chapter has been to present and justify the real-time multifrequency holographic sensing method for distributed sensing. We began by discussing the imaging system used in photography. Then we augmented the imaging system with a reference signal to form an interferometer to improve the sensitivity and put the output into the desired form. Next we considered a desensitized interferometer system using a multifrequency laser. The multifrequency interferometer allows us to control (modulate) the amplitude of the fringes in the interferometer to superimpose large deflections on top of the fringe pattern. Holography was introduced and shown to be a successful means of demodulating the desensitized interferometer. Real-time holography in photorefractive crystals was presented to remove the unrealistic film development stage in sequential holography. Finally, we considered discrete-time holographic sensing because it offers the possibility of combining temporal and spatial processing into a single processor.

To summarize, in the imaging method, $y_o(x)$ is the equilibrium distance from the point x on the structure to the corresponding image point in the image plane, $y(x,t)$ is the distance of the point x on the structure at time t from its equilibrium position, and the sensor output is the intensity function

$$I(x,t) = \frac{I_o}{(y_o(x) + y(x,t))^2}, \quad (2.10.1)$$

where I_o is a proportionality constant. In the interferometric sensing method,

$$I(x,t) = I_o + y(x,t), \quad y(x,t) < \frac{\lambda}{2}, \quad (2.10.2)$$

where I_o is another constant. In the desensitized interferometric method,

$$I(x,t) = I_o + y(x,t) \cos\left(\frac{4\pi y(x,t)}{\lambda_m}\right), \quad (2.10.3)$$

for $y(x,t) < \frac{\lambda_m}{2}$. In the holographic sensing method, the output from the first order is not an intensity function but a complex amplitude given by

$$E(x) = E_o e^{j \frac{y(x)}{2\pi\lambda}}, \quad (2.10.4)$$

where E_o is a constant. In the multifrequency holographic method, the output corresponding to the first order is the intensity function

$$I(x) = I_o + y(x), \quad y(x) < \frac{\lambda_m}{2}, \quad (2.10.5)$$

where λ_m is the beat wavelength. In the real-time holographic sensor, the output intensity function is a time-varying version of the multifrequency holographic sensor given in (2.7.5). That is,

$$I(x,t) = I_o + y(x,t), \quad y(x,t) < \frac{\lambda_m}{2}. \quad (2.10.6)$$

The discrete-time holographic sensor has the same output as the real time holographic sensor, but the output is held fixed for a period T between samples. That is,

$$I(x,k) = I_o + y(x,k), \quad y(x,k) < \frac{\lambda_m}{2}, \quad (2.10.7)$$

where $k = nT$ $n = 1, 2, \dots$

3.0 Modelling and Design

3.1 Introduction

In the previous chapter, sensing technology was presented for measuring the distributed deflection of a flexible structure. Our goal is to apply the distributed sensing technology to control the structural vibrations. In this chapter we present models and control design methods for a uniform cantilevered beam, and extend the results to simply supported plates.

3.2 Modelling

While many models exist for flexible structures, we will consider an analytical method derived from the partial differential equation. The fixed-free cantilevered beam is used as an example. We begin by stating the partial differential equation. Next, we

solve the partial differential equation as an infinite series. The infinite series solution is truncated and put into state space form. We close the section with an extension to the modelling of plate structures.

Let the deflection of the cantilevered beam be given by $y(x,t)$, a function of both time and space. Furthermore, assume the beam is undamped, has uniform unit mass per unit length, and length L . Then the partial differential equation is given by [4],

$$\frac{\partial^2 y(x,t)}{\partial t^2} + \frac{\partial^4 y(x,t)}{\partial x^4} = b(x) u(t), \quad (3.2.1)$$

subject to the boundary conditions,

$$y(0,t) = \frac{\partial y(0,t)}{\partial x} = \frac{\partial^2 y(L,t)}{\partial x^2} = \frac{\partial^3 y(L,t)}{\partial x^3} = 0, \quad (3.2.2)$$

where $b(x)$ is the control influence function, and $u(t)$ is the control signal.

The partial differential equation (3.2.1) may be solved directly by the separation of variables method. We begin by assuming the solution to the homogeneous equation,

$$\frac{\partial^2}{\partial t^2} y(x,t) + \frac{\partial^4}{\partial x^4} y(x,t) = 0 \quad (3.2.3)$$

is in the form,

$$y(x,t) = \sum_{i=1}^{\infty} p_i(x) \xi_i(t), \quad (3.2.4)$$

where $p_i(x)$ are scaled such that

$$\int_0^L p_i(x)p_j(x)dx = \delta_{ij} \quad (3.2.5)$$

where

$$\delta_{ij} = \begin{cases} 1 & \text{if } i=j \\ 0 & \text{if } i \neq j. \end{cases} \quad (3.2.6)$$

Thus, the space domain functions are orthonormal. We shall call any set of functions satisfying (3.2.4) and (3.2.5) mode shapes. The corresponding time domain components $\xi_i(t)$ will be called modal amplitudes.

For each i ,

$$\frac{\partial^2}{\partial t^2} (p_i(x)\xi_i(t)) + \frac{\partial^4}{\partial x^4} (p_i(x)\xi_i(t)) = 0, \quad (3.2.7)$$

or

$$-\frac{1}{\xi_i(t)} \frac{\partial^2}{\partial t^2} (\xi_i(t)) = \frac{1}{p_i(x)} \frac{\partial^4}{\partial x^4} (p_i(x)). \quad (3.2.8)$$

Since x and t are independent variables, (3.2.8) is equal to a constant λ_i . Therefore,

$$\frac{d^4}{dx^4} p_i(x) = p_i(x)\lambda_i \quad (3.2.9)$$

and

$$\frac{d^2}{dt^2} \xi_i(t) = -\xi_i(t)\lambda_i. \quad (3.2.10)$$

The ordinary differential equation (3.2.9) with the boundary equations (3.2.2) may be solved to find λ_i implicitly, and $p_i(x)$ explicitly as:

$$\cos \lambda_i^{1/4} L \cosh \lambda_i^{1/4} L = -1, \quad (3.2.11)$$

$$p_i(x) = \sin \lambda_i^{1/4} x - \sinh \lambda_i^{1/4} x + a_i (\cos \lambda_i^{1/4} x - \cosh \lambda_i^{1/4} x), \quad (3.2.12)$$

where

$$a_i = \frac{\cos \lambda_i^{1/4} L + \cosh \lambda_i^{1/4} L}{\sin \lambda_i^{1/4} L - \sinh \lambda_i^{1/4} L}. \quad (3.2.13)$$

The mode shapes, $p_i(x)$, are orthonormal. Using the orthonormality property (3.2.5), we have

$$\int_0^L p_i(x) p_i''''(x) dx = \int_0^L p_i(x) \lambda_i p_i(x) dx = \lambda_i, \quad (3.2.14)$$

where the primes indicate partial differentiation with respect to x . Also, since

$$p_i''(x) = \lambda_i^{1/2} p_i(x), \quad (3.2.15)$$

we have

$$\int_0^L p_i(x) p_i''(x) dx = \int_0^L p_i(x) \lambda_i^{1/2} p_i(x) dx = \lambda_i^{1/2}. \quad (3.2.16)$$

The i th element of (3.2.4) is given by

$$y_l(x,t) = p_l(x)\xi_l(t). \quad (3.2.17)$$

Plugging (3.2.17) into the partial differential equation (3.2.1) yeilds

$$\ddot{\xi}_l(t)p_l(x) + \xi_l(t)p_l''''(x) = b(x) u(t), \quad (3.2.18)$$

where dots indicate differentiation with respect to time. Multiplying (3.2.18) by $p_j(x)$, integrating in space, and using (3.2.14) and (3.2.eqn) yeilds

$$\int_0^L p_j(x)\ddot{\xi}_l(t)p_l(x)dx + \int_0^L p_j(x)p_l''''(x)\xi_l(t)dx = \int_0^L p_j(x)b_l(x) u(t)dx \quad (3.2.19)$$

or

$$\ddot{\xi}_l(t) + \lambda_l\xi_l(t) = b_l u(t) \quad (3.2.20)$$

where

$$b_l = p_l(x)\delta(L)b_l(x) \quad (3.2.21)$$

for a point force actuator on the tip. Equation (3.2.20) describes the undamped dynamics of each mode.

The ordinary differential equations (3.2.20) may be solved (using appropriate initial conditions) by standard methods. Combining the solutions of (3.2.20) with the mode shapes (3.2.12) constitutes a solution of (3.2.1) as

$$y(x,t) = \sum_{l=1}^{\infty} y_l(x,t) = \sum_{l=1}^{\infty} p_l(x)\xi_l(t). \quad (3.2.22)$$

If (3.2.22) is examined on physical grounds, it becomes apparent that only a finite number of terms in the series are required to approximate the solution $y(x,t)$ beyond any level of uncertainty. To facilitate the design, we truncate the series to $N \in \mathbb{N}$ terms,

$$\bar{y}(x,t) = \sum_{l=1}^N p_l(x) \xi_l(t), \quad (3.2.23)$$

where N may be taken arbitrarily large. For the remainder of this dissertation, we assume that the truth model contains exactly N modes, and N is taken large enough so that for all practical purposes the unmodelled terms are zero. For example, N may be taken such that all higher modes would exceed the speed of light if the modal amplitude were anything but zero. Therefore, to simplify notation, the bar in (3.2.23) is dropped.

In reality, all structures contain some natural damping. If we assume all of the modes in our truth model have the damping ratio ζ , then (3.2.20) can be modified to include the damping dynamics as

$$\ddot{\xi}_i(t) + 2\zeta\lambda_i^{1/2}\dot{\xi}_i(t) + \lambda_i\xi_i(t) = b_i u(t), \quad \text{for } i = 1, 2, \dots, N. \quad (3.2.24)$$

Our model may be completed by converting to state space form. The state space form is simply a transformation from the second order form in (3.2.24) into a first order form. We begin by defining the states in terms of vectors corresponding to the distributed position and velocity. Let the position vector be the modal amplitudes describing the shape of the beam,

$$\xi(t) = [\xi_1(t) \ \xi_2(t) \ \dots \ \xi_N(t)]^T. \quad (3.2.25)$$

The velocity vector is given by the vector of time derivative of the modal amplitudes,

$$\dot{\xi}(t) = [\dot{\xi}_1(t) \ \dot{\xi}_2(t) \ \dots \ \dot{\xi}_N(t)]^T. \quad (3.2.26)$$

If we combine (3.2. 25) and (3.2.26) into a single vector,

$$\eta(t) = \begin{bmatrix} \xi(t) \\ \dot{\xi}(t) \end{bmatrix}, \quad (3.2.27)$$

then (3.2.24) may be written as,

$$\dot{\eta}(t) = A \eta(t) + B u(t), \quad (3.2.28)$$

where

$$A = \begin{bmatrix} 0_N & I_N \\ -\Lambda_N & 2\zeta\Lambda_N^{1/2} \end{bmatrix} \quad (3.2.29)$$

$$\Lambda_N = \text{diag}(\lambda_1, \lambda_2, \dots, \lambda_N) \quad (3.2.30)$$

$$\Lambda_N^{1/2} = \text{diag}(\lambda_1^{1/2}, \lambda_2^{1/2}, \dots, \lambda_N^{1/2}). \quad (3.2.31)$$

In the state space form, the sensor measurement of the distributed position is given by

$$y(x,t) = C(x) \eta(t) \quad (3.2.32)$$

where

$$C(x) = [p(x) \ 0], \quad (3.2.33)$$

and

$$p(x) = [p_1(x) \ p_2(x) \ \dots \ p_N(x)]. \quad (3.2.34)$$

We will find it useful to divide the N modes of the truth model into N_1 design modes and N_2 remaining modes, $N_1 + N_2 = N$. We begin by defining the $(N_1 \times 1)$ vector $\Xi_1(t)$ and the $(N_2 \times 1)$ vector $\Xi_2(t)$ such that

$$\xi(t) \equiv \begin{bmatrix} \Xi_1(t) \\ \Xi_2(t) \end{bmatrix}. \quad (3.2.35)$$

Similarly,

$$\dot{\xi}(t) \equiv \begin{bmatrix} \dot{\Xi}_1(t) \\ \dot{\Xi}_2(t) \end{bmatrix}. \quad (3.2.36)$$

Then the state vector for the truth system is

$$\eta(t) = \begin{bmatrix} \Xi_1(t) \\ \dot{\Xi}_1(t) \\ \Xi_2(t) \\ \dot{\Xi}_2(t) \end{bmatrix}, \quad (3.2.37)$$

where the state vector of the design subsystem is given by

$$\eta_1(t) \equiv \begin{bmatrix} \Xi_1(t) \\ \dot{\Xi}_1(t) \end{bmatrix}, \quad (3.2.38)$$

and the state vector of the remaining subsystem is given by

$$\eta_2(t) \equiv \begin{bmatrix} \Xi_2(t) \\ \dot{\Xi}_2(t) \end{bmatrix}. \quad (3.2.39)$$

Using (3.2.28) with $N = N_1$, we may define A_1 and B_1 such that

$$\dot{\eta}_1(t) = A_1 \eta_1(t) + B_1 u(t). \quad (3.2.40)$$

If the vector of mode shapes (3.2.34) is divided into the $(1 \times N_1)$ vector $P_1(x)$ and the $(1 \times N_2)$ vector $P_2(x)$ such that

$$p(x) = [P_1(x) \ P_2(x)], \quad (3.2.41)$$

then the output of the design system is given by

$$y_1(x, t) = C_1(x) \eta_1(t) \quad (3.2.42)$$

where

$$C_1(x) = [P_1(x) \ 0]. \quad (3.2.43)$$

The remaining system may be defined similarly as

$$\begin{aligned} \dot{\eta}_2(t) &= A_2 \eta_2(t) + B_2 u(t) \\ y_2(x, t) &= C_2(x) \eta_2(t), \end{aligned} \quad (3.2.44)$$

where A_2 and B_2 are calculated using (3.2.28) with only the remaining modes, and

$$C_2(x) = [P_2(x) \ 0]. \quad (3.2.45)$$

The continuous time state equations may be approximated in discrete time by assuming the input is constant over the sample interval. Using this assumption, the discrete time design model is given by

$$q(k+1) = A q(k) + B u(k), \quad (3.2.46)$$

where

$$q(k) = \begin{bmatrix} \xi(k) \\ \dot{\xi}(k) \end{bmatrix},$$

$$A = e^{A_1 T}$$

$$B = [A - I]A_1^{-1}B_1,$$

T is the sample period, and k is an integer [27]. We will not use the remaining modes in the discrete-time case, so there is no need to establish additional notation. Note that the system matrix A and the input vector B use the same notation as the truth model in the continuous case; no confusion should result.

The previous discussion on the modelling of a cantilevered beam may be extended to two dimensional flexible structures such as normalized uniform thin rectangular plates. We begin by replacing the spatial variable x by the vector in \mathbb{R}^2 . Let

$$\mathbf{x} = \begin{bmatrix} x_1 \\ x_2 \end{bmatrix}. \quad (3.2.47)$$

Next, the spatial partial derivative in (3.2.1) must be replaced with the Laplacian operator [4],

$$\nabla^2 = \frac{\partial^2}{\partial x_1^2} + \frac{\partial^2}{\partial x_2^2}, \quad (3.2.48)$$

and

$$\nabla^4 = \frac{\partial^4}{\partial x_1^4} + 2 \frac{\partial^4}{\partial x_1^2 \partial x_2^2} + \frac{\partial^4}{\partial x_2^4}. \quad (3.2.49)$$

Hence, the partial differential equation for two-dimensional structures is given by

$$\frac{\partial^2}{\partial t^2} y(\mathbf{x}, t) + \nabla^4 y(\mathbf{x}, t) = B(\mathbf{x})u(t). \quad (3.2.50)$$

We can solve (3.2.50) using the same method recommended for the one-dimensional problem. We first solve the undamped homogeneous system to solve for the mode shapes to form a spatial basis. Then we solve for the dynamics using the orthogonality property of the basis functions.

The undamped homogeneous two-dimensional partial differential equation is

$$\frac{\partial^2}{\partial t^2} y(\mathbf{x}, t) + \nabla^4 y(\mathbf{x}, t) = 0. \quad (3.2.51)$$

We make the separation of variables assumption

$$y(\mathbf{x}, t) = \sum_{i=1}^{\infty} p_i(\mathbf{x}) \xi_i(t), \quad (3.2.52)$$

where modes shapes $p_i(\mathbf{x})$ and modal amplitudes $\xi_i(t)$ are different from the functions in the one-dimensional case. For each i , substitute (3.2.52) into (3.2.51) to yield

$$p_i(\mathbf{x}) \frac{\partial^2}{\partial t^2} \xi_i(t) + \xi_i(t) (\nabla^4 p_i(\mathbf{x})) = 0, \quad (3.2.53)$$

or,

$$-\frac{1}{\xi_i(t)} \frac{\partial^2}{\partial t^2} \xi_i(t) = \frac{1}{p_i(\mathbf{x})} \nabla^4 p_i(\mathbf{x}). \quad (3.2.54)$$

This implies

$$-\frac{1}{\xi_i(t)} \frac{\partial^2}{\partial t^2} \xi_i(t) = \lambda_i \quad (3.2.55)$$

and,

$$\frac{1}{p_i(\mathbf{x})} \nabla^4 p_i(\mathbf{x}) = \lambda_i \quad (3.2.56)$$

Equations (3.2.55) and (3.2.56) are ordinary differential equations which may be solved given appropriate boundary conditions. The general solution of (3.2.56) is [4]

$$\begin{aligned} p(x_1, x_2) = & W_1 \sin(\alpha x_1) \sin(\gamma x_2) + W_2 \sin(\alpha x_1) \cos(\gamma x_2) \\ & + W_3 \cos(\alpha x_1) \sin(\gamma x_2) + W_4 \cos(\alpha x_1) \cos(\gamma x_2) \\ & + W_5 \sinh(\alpha_1 x_1) \sinh(\gamma_1 x_2) + W_6 \sinh(\alpha_1 x_1) \cosh(\gamma_1 x_2) \\ & + W_7 \cosh(\alpha_1 x_1) \sinh(\gamma_1 x_2) + W_8 \cosh(\alpha_1 x_1) \cosh(\gamma_1 x_2), \end{aligned} \quad (3.2.57)$$

where

$$\alpha^4 + \gamma^4 = \alpha_1^4 + \gamma_1^4 = \lambda. \quad (3.2.58)$$

We can solve (3.2.57) for $p(x_1, x_2)$ and λ once the boundary conditions are specified. For example, if the plate is simply supported, then the boundary conditions are given by

$$p(0, x_2, t) = p(x_1, 0, t) = \frac{\partial^2}{\partial x_1^2} p(L_1, x_2, t) = \frac{\partial^2}{\partial x_2^2} p(x_1, L_2, t) = 0 \quad (3.2.59)$$

where L_1 is the length of the plate in the x_1 direction, and L_2 is the length of the plate in the x_2 direction. The boundary conditions allow us to simplify (3.2.57) to two frequency equations,

$$\sin(\alpha L_1) = 0 \quad \text{and} \quad \sin(\gamma L_2) = 0, \quad (3.2.60)$$

implying that the natural frequencies for the simply supported plate are given by

$$\omega_{mn} = \pi^2 \left[\left(\frac{m}{L_1} \right)^2 + \left(\frac{n}{L_2} \right)^2 \right] \quad m, n = 1, 2, \dots \quad (3.2.61)$$

The eigenvalues may be ordered (arbitrarily) as

$$\lambda_1 = \omega_{11}^2, \lambda_2 = \omega_{12}^2, \lambda_3 = \omega_{21}^2, \lambda_4 = \omega_{22}^2, \dots \quad (3.2.62)$$

Then the mode shapes are given by

$$w_{mn}(x_1, x_2) = A_{mn} \sin \frac{m\pi x_1}{L_1} \sin \frac{n\pi x_2}{L_2} \quad m, n = 1, 2, \dots \quad (3.2.63)$$

Before defining A_{mn} , order the mode shapes as

$$p_1(\mathbf{x}) = w_{11}(\mathbf{x}), p_2(\mathbf{x}) = w_{12}(\mathbf{x}), p_3(\mathbf{x}) = w_{21}(\mathbf{x}), p_4(\mathbf{x}) = w_{22}(\mathbf{x}), \dots \quad (3.2.64)$$

Then A_{mn} are selected such that

$$\int_0^{L_2} \int_0^{L_1} p_i(x_1, x_2) p_j(x_1, x_2) dx_1 dx_2 = \begin{cases} 1 & \text{if } i = j \\ 0 & \text{if } i \neq j. \end{cases} \quad (3.2.65)$$

Hence, the mode shapes are orthonormal. We proceed to solve the partial differential equation as in the one dimensional case. Using (3.2.56) and orthonormality property (3.2.65), we have

$$\int_0^{L_2} \int_0^{L_1} p_i(x_1, x_2) \nabla^4 p_i(x_1, x_2) dx_1 dx_2 = \int_0^{L_2} \int_0^{L_1} p_i(x_1, x_2) \lambda_i p_i(x_1, x_2) dx_1 dx_2 = \lambda_i. \quad (3.2.66)$$

Also, since

$$\nabla^2 p_l(\mathbf{x}) = \lambda_l^{1/2} p_l(\mathbf{x}), \quad (3.2.67)$$

we have

$$\begin{aligned} \int_0^{L_2} \int_0^{L_1} p_l(x_1, x_2) \nabla^2 p_l(x_1, x_2) dx_1 dx_2 &= \int_0^{L_2} \int_0^{L_1} p_l(x_1, x_2) \lambda_l^{1/2} p_l(x_1, x_2) dx_1 dx_2 \\ &= \lambda_l^{1/2}. \end{aligned} \quad (3.2.68)$$

Plugging the element $y(\mathbf{x}, t) = p_l(\mathbf{x}) \xi_l(t)$ into (3.2.50) yields

$$\ddot{\xi}_l(t) p_l(\mathbf{x}) + \xi_l(t) \nabla^4 p_l(\mathbf{x}) = b_l(\mathbf{x}) u(t). \quad (3.2.69)$$

Multiplying by $p_l(\mathbf{x})$, integrating, and using (3.2.66) and (3.2.68), we conclude that

$$\ddot{\xi}_l(t) + \lambda_l \xi_l(t) = b_l u(t) \quad (3.2.70)$$

where

$$b_l = p_l(\mathbf{x}) \delta(L/2) b_l(\mathbf{x}) \quad (3.2.71)$$

for a point force actuator in the center of the plate. We may include a damping factor ζ as in the one dimensional case such that

$$\ddot{\xi}_l(t) + 2\zeta \lambda_l^{1/2} \dot{\xi}_l(t) + \lambda_l \xi_l(t) = b_l u(t). \quad (3.2.72)$$

We truncate the infinite sequence (3.2.72) to a finite sequence which can be put in state space form, as in the one-dimensional case, where the eigenvalues and mode shapes for the plate replace those for the beam. Hence, except for the change in the spatial domain to two-dimensional mode shapes, the model for the dynamics for plates is similar to the

model found in the previous sections for beams. The modes may be divided into design and remaining modes exactly the same manner as the development for the cantilevered beam. Similarly, the design may be converted to discrete time.

We have derived a finite dimensional state space model approximating the solution of the partial differential equation governing the dynamics of a flexible beam. We extended those results to the partial differential equation governing a flexible plate. We found the models for the plate and beam to be similar in that the shape of the flexible structure in each case can be defined by the weighted sum of mode shapes. The spatial dimensions of the mode shapes correspond to the spatial dimensions of the structure.

3.3 Control System Design

In this section, we present design methods for control systems based on both the continuous and discrete-time sensors. The idea in each case is to control the modes that lie well within response time of the sensor (and actuator) and our knowledge of the system. The designs developed here will form the architectures implemented in the remaining chapters.

The first part presents a state space plus observer, or deterministic Linear Quadratic Gaussian, design based on the continuous time sensor. To maintain compatibility with the implementation hardware, the continuous time control system operates on the spatially distributed measurements in the space domain only. In the second part we perform a spillover analysis. In the third part we simplify the estimator and consider a functional estimator design. The fourth part uses the results for the continuous time sensor to derive a similar control system for the discrete time sensor,

but delay operation is used to operate on the distributed measurements in both time and space. The fifth part extends the continuous and discrete-time designs for the control of a plate structure. The designs are summarized in the last part.

3.3.1 The Continuous Time Control System

In this part we use the model developed in the previous section and the continuous time distributed sensor developed in Chapter 2 to design a control system to damp vibrations in a beam. The design method is similar to the usual deterministic Linear Quadratic Gaussian approach. The design will be based on the design model (3.2.40). The only difficulty involved in applying the Linear Quadratic Quassian design method is in the accomodation of the distributed measurement (3.2.42). The method must be generalized to include the continuum of outputs corresponding to each point along the length of the beam.

We choose the control to be given by a linear combination of the states,

$$u(t) \equiv F \eta_1(t). \quad (3.3.1)$$

In the Linear Quadratic Gaussian design method, a control vector F is found to minimize the cost functional

$$J = \int_0^{\infty} \eta_1^T(t) Q_c \eta_1(t) + u^T(t) R_c u(t) dt, \quad (3.3.2)$$

where $Q_c \geq 0$ is the weight placed on the states, and $R_c > 0$ is the weight places on the control. It has been shown [19] that (3.3.2) is minimized by

$$F = R_c^{-1} B_1^T S, \quad (3.3.3)$$

where S is found by solving the Riccoti equation

$$0 = SA_1 + A_1^T S - SB_1 R_c^{-1} B_1^T S + Q_c. \quad (3.3.4)$$

Hence, the control vector F is designed using doublet (A_1, B_1) and the design parameter doublet (R_c, Q_c) .

Unfortunately, our sensor does not measure $\eta_1(t)$ directly. The measurement in the design system is given by

$$y_1(x, t) = \sum_{l=1}^{N_1} p_l(x) \xi_l(t) = P_1(x) \Xi_1(t). \quad (3.3.5)$$

Therefore, an observer (or estimator) must be designed to extract $\Xi_1(t)$ from (3.3.5), and to estimate the derivatives $\dot{\Xi}_1(t)$ to fully estimate $\eta_1(t) = \hat{\eta}_1(t)$. The state feedback control (3.3.1) can be rewritten as,

$$u(t) \equiv F \hat{\eta}_1(t), \quad (3.3.6)$$

where

$$\frac{d}{dt} \hat{\eta}_1(t) = A_1 \hat{\eta}_1(t) + B_1 u(t) + \int_0^L K(x) (y(x, t) - C_1(x) \hat{\eta}_1(t)) dx. \quad (3.3.7)$$

In the Linear Quadratic Gaussian method the observer (3.3.7) is designed by duality using the doublet $(A_1, C_1(x))$, where the components of the remaining modes are ignored. Unlike the controller design, the observer design is based on the vector function $C_1(x)$. Standard design methods are accommodated by discretizing each element of $C_1(x)$ in space and interpolating between the elements in the rows of the resulting observer matrix to generate an observer vector function. Hence, finite dimensional methods may be used to design an infinite dimensional observer.

The design of the observer begins by spatially sampling the measurement function $y_1(x, t)$ at M uniformly spaced points over the length of the beam. This is analogous to assuming M point sensors are located at the points

$$x_i = L \left(\frac{i}{M-1} \right), \quad i = 0, 1, \dots, M-1. \quad (3.3.8)$$

Let the sampled measurement be

$$\tilde{y}(t) = \bar{C}_1 \eta_1(t) \quad (3.3.9)$$

where \bar{C}_1 is the $(M \times 2N_1)$ matrix equal to (3.2.33) evaluated at the points in (3.3.8).

The spatially sampled version of the observer (3.3.7) is of the form

$$\frac{d}{dt} \hat{\eta}_1(t) = A_1 \hat{\eta}_1(t) + B_1 u(t) + \bar{K} (\tilde{y}(t) - \bar{C}_1 \hat{\eta}_1(t)), \quad (3.3.10)$$

where the estimator matrix \bar{K} must be determined. The estimator matrix can be found to minimize noises, but we shall use a deterministic approach. In the deterministic Linear Quadratic Gaussian estimator, the pair (A_1, B_1) and (R_e, Q_e) is replaced by (A_1^T, \bar{C}_1^T) and (R_e, Q_e) in the Riccati equation (3.3.4). Then by duality [19], the estimator matrix is given by

$$\bar{K} = S \bar{C}_1^T R_o^{-1} \quad (3.3.11)$$

where S is the solution of a Riccati equation. We will take

$$R_o = r I_{2M_1}, \text{ where } r \in \mathbb{R} > 0. \quad (3.3.12)$$

In this way, \bar{K} may be expressed in the form

$$\bar{K} = \bar{S} \bar{C}_1^T, \text{ where } \bar{S} = \left(\frac{1}{r} \right) S. \quad (3.3.13)$$

After solving the system (3.3.13) for \bar{S} , $K(x)$ may be calculated as

$$K(x) = \bar{S} C_1^T(x). \quad (3.3.14)$$

Hence, finite dimensional techniques may be used to generate an infinite dimensional observer. This completes the design. In the next part, we show that the design solves the spillover problem.

3.3.2 Spillover Analysis

The designs presented in Section 3.3.1 assumed that a model of the beam consists of exactly N_1 . In this part we analyze the effects of the truth model on the design model. The interaction between the design model and truth model is often called spillover [3]. Methods have been devised to evaluate the system order required for convergence to an infinite dimensional Linear Quadratic Gaussian design [20] [21] [22], but often practical consideration such as computational limitations, sensor bandwidth, and actuator bandwidth dictate the number of order of the design model. Therefore, the design

method must account for the additional states in the truth model. We will show that our distributed sensor and processing scheme theoretically allows us to use the orthogonality of the mode shapes to truncate the design to any even order without any interaction with the remaining states in the truth model.

To analyze the interaction between design model and truth model, we must formulate the closed-loop system in state space form. This will allow us to evaluate the effectiveness of the pole placement in the presence of the remaining dynamics [23]. The closed-loop system can be formulated by combining the systems (3.3.40) and (3.3.44) with the control law (3.3.6) and the observer (3.3.7). We begin by rewriting the observer.

Let

$$\begin{aligned}
\frac{d}{dt} \hat{\eta}_1(t) &= A_1 \hat{\eta}_1(t) + B_1 u(t) + \int_0^L K(x) (y(x,t) - C_1(x) \hat{\eta}_1(t)) dx \\
&= A_1 \hat{\eta}_1(t) + B_1 u(t) \\
&\quad + \int_0^L K(x) \left([C_1(x) \ C_2(x)] \begin{bmatrix} \eta_1(t) \\ \eta_2(t) \end{bmatrix} - C_1(x) \hat{\eta}_1(t) \right) dx \\
&= A_1 \hat{\eta}_1(t) + B_1 u(t) \\
&\quad + \int_0^L K(x) C_1(x) dx \eta_1(t) + \int_0^L K(x) C_2(x) dx \eta_2(t) - \int_0^L K(x) C_1(x) dx \hat{\eta}_1(t) \\
&= (A_1 - \tilde{K}_1) \hat{\eta}_1(t) + B_1 u(t) + \tilde{K}_1 \eta_1(t) + \tilde{K}_2 \eta_2(t),
\end{aligned} \tag{3.3.15}$$

where,

$$\tilde{K}_1 = \int_0^L K(x) C_1(x) dx, \tag{3.3.16}$$

and

$$\tilde{K}_2 = \int_0^L K(x)C_2(x)dx. \quad (3.3.17)$$

Then the closed-loop system is given by

$$\frac{d}{dt} \begin{bmatrix} \eta_1(t) \\ \hat{\eta}_1(t) \\ \eta_2(t) \end{bmatrix} = \begin{bmatrix} A_1 & B_1F & 0 \\ \tilde{K}_1 & A_1 - \tilde{K}_2 + B_1F & \tilde{K}_2 \\ 0 & B_2F & A_2 \end{bmatrix} \begin{bmatrix} \eta_1(t) \\ \hat{\eta}_1(t) \\ \eta_2(t) \end{bmatrix}. \quad (3.3.18)$$

The term \tilde{K}_2 causes the so-called observation spillover [3] because it allows the remaining states in the truth model to contaminate the estimate of the design states. However, for our distributed sensor

$$C_1(x) = [P_1 \ 0] \text{ and } C_2(x) = [P_2 \ 0], \quad (3.3.19)$$

so if we use (3.3.14) and the mode orthogonality property,

$$\tilde{K}_2 = \int_0^L \bar{S} C_1^T(x) C_2(x) dx = 0. \quad (3.3.20)$$

Hence, the observation spillover is zero. Therefore, the controller and observer poles for the design system may be placed independently, and the eigenvalues of the remaining system will be unaffected by the feedback. This decoupling of the design model and

remaining dynamics in the truth model is the principle performance advantage in the distributed sensor control system.

In point sensing systems,

$$C_{2p}(x) = [P_2(x)\delta(x - x_o) \ 0], \quad (3.3.21)$$

where $\delta(x)$ is the Dirac delta function. Therefore,

$$\begin{aligned} \tilde{K}_2 &= \int_0^L K(x)C_{2p}(x)dx \\ &= K(x_o)P_2(x_o), \end{aligned} \quad (3.3.22)$$

indicating that \tilde{K}_2 is nonzero for all x , where P_2 is nonzero. In other words, observation spillover is always present for point sensors. Hence, point sensing systems must evaluate the effects of the truth model on the control design explicitly. Since this is not always possible, as when the truth model is unknown, point sensor systems usually perform conservatively.

3.3.3 Simplification of the Continuous-Time Design

The estimator design may be separated further into spatial and temporal components while maintaining the modal filtering property, and the separate components may be condensed. First, we may divide equation (3.3.7) into temporal and spatial parts,

$$\begin{aligned} \frac{d}{dt} \hat{\eta}_1(t) &= A_1 \hat{\eta}_1(t) + B_1 u(t) + \int_0^L K(x)(y(x,t) - C_1(x)\hat{\eta}_1(t))dx \\ &= (A_1 - \tilde{K}_1)\hat{\eta}_1(t) + B_1 u(t) + \int_0^L K(x)y(x,t)dx. \end{aligned} \quad (3.3.23)$$

The integral in (3.3.23) is the spatial part. This separation allows us to directly implement the design, and most of the computation is performed by the temporal processor. However, the output of the spatial processor is $2N_1$ signals instead of the desired single signal; requiring $2N_1$ optical processors in parallel to process the measurement [24]. We proceed by first condensing the spatial component.

We condense the spatial processor by replacing the vector function $K(x)$ with a single valued function $g(x)$, where

$$g(x) = GP_1^T(x) \quad (3.3.24)$$

where $P_1(x)$ is the vector of the first N_1 modes shapes, and G is a vector of arbitrary weights. Then the signal

$$\begin{aligned} \varepsilon(t) &= \int_0^L g(x) y(x,t) dx \\ &= \int_0^L GP_1^T(x) p(x) \xi(t) dx \\ &= G\Xi_1(t) \\ &= \bar{G}\eta_1(t) \end{aligned} \quad (3.3.25)$$

where

$$\bar{G} = [G \ 0] \quad (3.3.26)$$

filters the remaining modes from the measurement, and results in a single valued signal for temporal processing. The observer can then be designed to estimate the modal amplitudes and velocities from $\varepsilon(t)$ as

$$\frac{d}{dt} \hat{\eta}_1(t) = (A_1 - H\bar{G})\hat{\eta}_1(t) + Bu(t) + H\epsilon(t), \quad (3.3.27)$$

where H is the new observer vector. The observer (3.3.27) combines the spatial filters in (3.3.23) into the single spatial filter (3.3.24). Next, we condense the temporal processor.

The temporal processor is still required to perform matrix-vector multiplications involving matrices and vectors of dimension $2N_1$. If N_1 is large, this may be difficult for a modest processor. To ease the computational burden, we could replace the state estimator with a functional estimator [25] [26]. A functional estimator can be used to calculate a linear combination of the states. The linear combination is arbitrary, and may be taken to yield the control signal.

The derivation of the functional estimator is given in Appendix A. The functional estimator that will implement the control design of Section 3.3 is summarized here. If the desired control signal is

$$\begin{aligned} u(t) &= F \eta_1(t) \\ &= [F_1 \ F_2] \begin{bmatrix} \xi_1(t) \\ \dot{\xi}_1(t) \end{bmatrix}, \end{aligned} \quad (3.3.28)$$

then the function $w(t)$ will converge to $u(t)$ as $t \rightarrow \infty$, where

$$\begin{aligned} w(t) &= z(t) + \epsilon_b(t) \\ \dot{z}(t) &= -\alpha z(t) + \epsilon_a(t) + \beta w(t). \end{aligned} \quad (3.3.29)$$

The functions $\epsilon_a(t)$ and $\epsilon_b(t)$ are given as in (3.3.25) by

$$\varepsilon_a(t) = \int_0^L g_a(x) y(x,t) dx \quad (3.3.30)$$

$$\varepsilon_b(t) = \int_0^L g_b(x) y(x,t) dx,$$

where

$$\begin{aligned} \beta &= [Z_1 \ Z_2] B \\ g_a(x) &= \Theta P_1^T(x) \\ g_b(x) &= \Omega P_1^T(x) \\ Z_1 &= F_2 \Lambda_{N_1} - \alpha F_2 \\ Z_2 &= F_2 \\ \Theta &= \alpha Z_1 - 2\zeta F_2 \Lambda_{N_1}^{1/2} \\ \Omega &= F_1 + F_2 \Lambda_{N_1} + \alpha F_2 \end{aligned} \quad (3.3.31)$$

where Λ_{N_1} and ζ are defined in Section 3.2, and α is chosen to place the single observer pole. The functional estimator allows us to condense the temporal processor into a single integrator regardless of the number of modes controlled. This reduced order-type observer is not expected to suffer from high frequency process noise, because the spatial filter removes all of the remaining modes including the high frequency modes.

3.3.4 The Discrete-Time Control System

We found that finite dimensional methods applied in the design of a control system utilizing a continuous time distributed sensor in the preceeding part. An observer was designed to extract N_1 of the modal amplitudes and the velocities from a distributed

measurement. Those modal amplitudes and velocities were then used to control N_1 modes of the beam. In the discrete-time case, the modes are not estimated and used in the control explicitly. Nevertheless, finite dimensional methods can be used in the design.

Instead of estimating the modal amplitudes explicitly, the states are maintained in their distributed form as position and velocity functions. The velocity function, as in continuous-time control design, is not measured and must therefore be estimated. The outputs of the estimator are a smoothed version of the position function and an estimate of the velocity function. The distributed observer output is then processed by a distributed controller to generate a single output signal for each actuator. The innovation of this method is that it combines the temporal and spatial processing which were separated in the continuous time design. This method is considered because it can be implemented using an all-optical processor which may offer performance and computational advantages.

The system (3.2.46) is used in the design of the control system. The design is similar to the design presented in Section 3.3.1., except the discrete-time Riccati equation is used. The control is to be of the form,

$$u(k) = F \hat{q}(k), \quad (3.3.32)$$

with the observer of the form

$$\hat{q}(k+1) = A \hat{q}(k) + B u(k) + \int_0^L K(x) (\tilde{y}(k) - \bar{C} \hat{q}(k)) dx, \quad (3.3.33)$$

where \bar{C} and \tilde{y} are defined as in (3.3.9).

In the discrete-time Linear Quadratic Gaussian design, we find F to minimize

$$J = \sum_{k=1}^{\infty} q^T(k) Q_c q(k) + u^T(k) R_c u(k), \quad (3.3.34)$$

where $Q_c \geq 0$ and $R_c > 0$ as in the continuous-time design. It has been shown [19] that (3.3.34) is minimized by

$$F = (R_c + B^T S B)^{-1} B^T S A, \quad (3.3.35)$$

where S is found by solving the discrete Riccati equation

$$0 = S - A^T S A + A^T S B (R + B^T S B)^{-1} B^T S A - Q. \quad (3.3.36)$$

Hence, F is based on the system doublet (A, B) , and the doublet of parameters (R_c, Q_c) . The observer function $K(x)$ is determined using the method developed in Section 3.3.1 for $K(x)$, except the discrete-time Riccati equation (3.3.36) is substituted for (3.3.4). Using the matrix inversion lemma [27], the solution can be put in the form

$$K(x) = \bar{S} C_1^T(x). \quad (3.3.37)$$

Define the distributed states at time $t = k = nT$, where $n \in \mathbb{N}$, as

$$\Phi(x, k) \equiv \begin{bmatrix} y(x, k) \\ \frac{\partial}{\partial t} y(x, k) \end{bmatrix}. \quad (3.3.38)$$

Using the integral inner product, the state feedback signal is given by

$$u(k) = \int_0^L f(x) \Phi(x, k) dx, \quad (3.3.39)$$

where $f(x)$ is a distributed control function. Similarly, the distributed estimator is defined by

$$\begin{aligned}\hat{\Phi}(x, k+1) = & \int_0^L a(x, \bar{x}) \hat{\Phi}(\bar{x}, k) d\bar{x} \\ & + b(x)u(k) + \int_0^L \ell(x, \bar{x})(y(\bar{x}, k) - \hat{y}(\bar{x}, k)) d\bar{x},\end{aligned}\quad (3.3.40)$$

where ℓ is the distributed observer function, a is the distributed system function, b is the distributed influence function, and

$$\hat{\Phi}(x, k) = \begin{bmatrix} \hat{y}(x, k) \\ \frac{\partial}{\partial t} \hat{y}(x, k) \end{bmatrix}. \quad (3.3.41)$$

Using (3.3.41), the control (3.3.39) can be rewritten as

$$u(k) = \int_0^L f(x) \hat{\Phi}(x, k) dx. \quad (3.3.42)$$

The design process for the distributed discrete time control system is to find a , b , f and ℓ given A , B , F , and $K(x)$.

We begin by defining the diagonal matrix function

$$\Pi(x) \equiv \begin{bmatrix} \text{diag}(P_1(x)) & 0 \\ 0 & \text{diag}(P_1(x)) \end{bmatrix}, \text{ such that } \int_0^L \Pi(x) \Pi^T(x) dx = I_{2N_1}. \quad (3.3.43)$$

Then

$$\begin{aligned}
u(k) &= F \hat{q}(k) \\
&= F \left(\int_0^L \Pi(x) \Pi^T(x) dx \right) \hat{q}(k) = \int_0^L F \Pi(x) \Pi^T(x) \hat{q}(k) dx.
\end{aligned} \tag{3.3.44}$$

Noting that

$$\Pi^T(x) \hat{q}(k) = \hat{\Phi}(x, k), \tag{3.3.45}$$

we can conclude

$$f(x) = F \Pi(x). \tag{3.3.46}$$

The observer in (3.3.33) estimates the modal amplitudes in discrete time. To transform the observer to estimate the distributed states, we must first multiply (3.3.33) by $\Pi(x)$. Since

$$\hat{\Phi}(x, k+1) = \Pi(x) \hat{q}(k+1), \tag{3.3.47}$$

the observer will now estimate distributed states. Immediately, we recognize the the system influence function is given by

$$b(x) = \Pi^T(x) B. \tag{3.3.48}$$

The system function is calculated by placing an identity matrix between A and $\hat{q}(k)$ as shown.

$$\begin{aligned}
\Pi(x) A q(k) &= \Pi(x) A \left[\int_0^L \Pi^T(\bar{x}) \Pi(\bar{x}) d\bar{x} \right] \hat{q}(k) \\
&= \int_0^L \Pi(x) A \Pi^T(\bar{x}) \Pi(\bar{x}) q(k) d\bar{x} \\
&= \int_0^L a(x, \bar{x}) \hat{\Phi}(\bar{x}, k) d\bar{x}.
\end{aligned} \tag{3.3.49}$$

Therefore, by matching coefficients,

$$a(x, \bar{x}) = \Pi^T(x) A \Pi(\bar{x}), \tag{3.3.50}$$

Similarly, using (3.3.37),

$$\begin{aligned}
&\Pi(x) \int_0^L K(\bar{x}) (\tilde{y}(k) - \bar{C} \hat{q}(k)) dx \\
&= \int_0^L \Pi(x) K(\bar{x}) (\tilde{y}(k) - \bar{C} \hat{q}(k)) dx \\
&= \int_0^L \Pi(x) \bar{S} C^T(\bar{x}) (\tilde{y}(k) - \bar{C} \hat{q}(k)) dx.
\end{aligned} \tag{3.3.51}$$

Therefore, matching coefficients with (3.3.40),

$$\ell(x, \bar{x}) = \Pi(x) \bar{S} C^T(\bar{x}). \tag{3.3.52}$$

The functions in equations (3.3.47,48,50,52) form the necessary set for the discrete-time control system of (3.3.39).

3.3.5 Extension to Plate Structures

In this part, the design methods are modified for two-dimensional structures such as plates. We begin by considering the design for the continuous sensor. The controller design proceeds as in the one-dimensional case using the pair (A_1, B_1) to calculate F such that

$$u(t) = F\eta_1(t), \quad (3.3.53)$$

where A_1 depends on the eigenvalues for the design modes of the plate, and B_1 depends on the position of the actuator. The state estimate $\hat{\eta}_1(t)$ is a $2N_1 \times 1$ vector. The estimator design uses the pair $(A_1, C_1(x))$, but the simple method of sampling $C_1(x)$ used in the one-dimensional case must be modified when $C_1(x)$ is sampled to maintain matrix compatibility. To understand the problem, consider first sampling the mode shapes in the x_1 and x_2 directions so that the mode shapes become matrices. That is, if

$$C_1(x_1, x_2) = [p_1(x_1, x_2) \ p_2(x_1, x_2) \ \dots \ p_{N_1}(x_1, x_2) \ 0 \ \dots \ 0] \quad (3.3.54)$$

is sampled at the points

$$x_{1i} = \frac{L_1(i-1)}{M_1} \quad i = 1, 2, \dots, M_1 \quad (3.3.55)$$

and

$$x_{2i} = \frac{L_2(i-1)}{M_2} \quad i = 1, 2, \dots, M_2, \quad (3.3.56)$$

where L_1 is the length of the plate in the x_1 direction, and L_2 is the length of the plate in the x_2 direction, then the vector function $C_1(x_1, x_2)$ becomes the matrix

$$\bar{C}_1 = [\bar{p}_1 \ \bar{p}_2 \ \dots \ \bar{p}_{N_1} \ 0 \ \dots \ 0], \quad (3.3.57)$$

where

$$\bar{p}_l = \begin{bmatrix} p_l(x_{11}, x_{21}) & p_l(x_{12}, x_{21}) & \dots & p_l(x_{1M_1}, x_{21}) \\ p_l(x_{11}, x_{22}) & p_l(x_{12}, x_{22}) & \dots & p_l(x_{1M_1}, x_{22}) \\ \dots & \dots & \dots & \dots \\ p_l(x_{11}, x_{2M_2}) & p_l(x_{12}, x_{2M_2}) & \dots & p_l(x_{1M_1}, x_{2M_2}) \end{bmatrix}. \quad (3.3.58)$$

While this matrix notation allows us to easily match elements of the matrix (3.3.57) with points in the function (3.3.54) (an important advantage in implementation), it is not compatible with the state vector η . The compatibility can be rectified by concatenating the columns of \bar{C}_1 such that

$$\hat{C}_1 = [p_1 \ p_2 \ \dots \ p_{N_1} \ 0 \ \dots \ 0], \quad (3.3.59)$$

where

$$\hat{p}_l = \begin{bmatrix} [p_l(x_{11}, x_{21}) \ p_l(x_{11}, x_{22}) \ \dots \ p_l(x_{11}, x_{2M_2})]^T \\ [p_l(x_{12}, x_{21}) \ p_l(x_{12}, x_{22}) \ \dots \ p_l(x_{12}, x_{2M_2})]^T \\ \dots \\ [p_l(x_{1M_1}, x_{21}) \ p_l(x_{1M_1}, x_{22}) \ \dots \ p_l(x_{1M_1}, x_{2M_2})]^T \end{bmatrix}. \quad (3.3.60)$$

We may now use the pair (A_1, \hat{C}_1) to calculate the observer matrix,

$$\hat{K} = \bar{S} \ \hat{C}_1^T, \quad (3.3.61)$$

where the product $\bar{S} \hat{C}_1^T$ is the result of solving a Riccati equation, as in Section 3.3.1. We may convert the observer matrix into a vector function by calculating the matrix \bar{S} explicitly, and interpolating between the elements in the columns of \hat{C}_1 . That is, if

$$\tilde{C}_1 = [\tilde{p}_1(x_2) \ \tilde{p}_2(x_2) \ \dots \ \tilde{p}_{N_1}(x_2) \ 0 \ \dots \ 0], \quad (3.3.62)$$

where

$$\tilde{p}_i(x_2) = \begin{bmatrix} p_i(x_{11}, x_2) \\ p_i(x_{12}, x_2) \\ \dots \\ p_i(x_{1M_1}, x_2) \end{bmatrix}, \quad (3.3.63)$$

then the observer function is given by

$$K(x_2) = \bar{S} \tilde{C}_1^T(x_2), \quad (3.3.64)$$

and the resulting observer is given by

$$\frac{d}{dt} \hat{\eta}_1(t) = A_1 \hat{\eta}_1(t) + B_1 u(t) + \int_0^{LM_1} K(x_2) (\tilde{y}(x_2) - \tilde{C}_1(x_2) \hat{\eta}_1(t)) dx_2. \quad (3.3.65)$$

This observer assumes the measurement can be expressed in a form $\tilde{y}(x_2)$ compatible with the estimate.

The two-dimensional discrete-time design is similar to that of the one-dimensional design. First we must calculate the control vector and observer matrix by sampling the two-dimensional structure as above, and applying the discrete-time Linear Quadratic Gaussian design method. Then we convert to distributed form. If F and $K(x_2)$ are the solutions from the Linear Quadratic Design, then let

$$\tilde{p}(x_2) = [\tilde{p}_1(x_2) \ \tilde{p}_2(x_2) \ \dots \ \tilde{p}_{N_1}(x_2) \ 0 \ \dots \ 0], \quad (3.3.66)$$

and

$$\Pi(x_2) = \begin{bmatrix} \text{diag}(\tilde{p}(x_2)) & 0 \\ 0 & \text{diag}(\tilde{p}(x_2)) \end{bmatrix}. \quad (3.3.67)$$

Then the control is given by

$$u(k) = \int_0^{LM_1} f(x_2) \hat{\Phi}(x_2) dx_2, \quad (3.3.68)$$

where

$$\begin{aligned} \hat{\Phi}(x_2, k+1) = & \int_0^{LM_1} a(x_2, \bar{x}_2) \hat{\Phi}(\bar{x}_2, k) d\bar{x}_2 + b(x_2) u(k) \\ & + \int_0^{LM_1} \ell(x_2, \bar{x}_2) (\tilde{y}(\bar{x}_2, k) - \hat{y}(\bar{x}_2, k)) d\bar{x}_2, \end{aligned} \quad (3.3.69)$$

and

$$\begin{aligned}
a(x_2, \bar{x}_2) &= \Pi(x_2)A\Pi^T(\bar{x}_2) \\
b(x_2) &= \Pi(x_2)B \\
\ell(x_2, \bar{x}_2) &= \Pi(x_2)K(\bar{x}_2) \\
f(x_2) &= F\Pi^T(x_2).
\end{aligned}
\tag{3.3.70}$$

3.3.6 Design Summary

We have presented a design method for using a distributed sensor to control the vibration in a set of selected modes in one-dimensional and two-dimensional flexible structures. The design method is a generalization of the usual Linear Quadratic Gaussian method to a single-input infinite-output system. The method applies equally well to the discrete-time system capable of distributed storage. The continuous design assumes only spatially distributed processing. Therefore, the continuous time processor must be supplemented with a temporal processor to complete the processing. In the discrete case, the sensor is also used in the processor to allow simultaneous temporal and spatial processing.

3.4 Summary

We modelled the structure using orthogonal mode shapes in the space domain, and the natural frequencies in the time domain. We calculated the mode shapes and natural frequencies from a partial differential equation. The control system design utilized the

infinite point (continuous) measurement of the holographic-type sensor, but is otherwise finite dimensional.

4.0 Example

4.1 *Introduction*

We have shown how to sense distributed functions, and presented a design method for processing the sensor measurements for control. The design was shown to solve the spillover problem. Now we will demonstrate the analytical results using a particular example.

The continuous system will be considered exclusively. Discrete implementations should anticipate aliasing problems if the sample rate is not sufficiently high. We use a cantilevered beam as our example structure. First, we illustrate the advantage of distributed sensing over point sensing. Next, since the analysis assumed exact knowledge of the design system, we use simulation to show that the design can tolerate some modelling error. Finally, the functional estimator design is compared to the full state estimator by pole placement and time response.

4.2 The Simulations

Our test structure is the uniform cantilevered beam of unit mass per unit length, and length L shown in Figure 4. We will consider a beam with length $L = 5$ in which the effects of the uncontrolled modes are significant. The open-loop system includes 0.5% proportional damping ($\zeta = 0.005$).

We consider two sensing methods. The first sensor is an ideal tip displacement sensor which senses the displacement of the free end. The second is an ideal distributed displacement sensor which senses the displacement of the beam along its entire length. The first four vibrational modes are selected for the design ($N_1 = 4$). A Linear Quadratic Gaussian design for the distributed sensor is performed to calculate F and $K(x)$ using the method described in Section 3.3.1 with $M = 128$,

$$Q_c = \frac{1}{2} \begin{bmatrix} \Lambda_{N_1} & 0 \\ 0 & I_{N_1} \end{bmatrix}, \quad R_c = .3, \quad Q_o = .0002 I_{2N_1}, \quad R_o = 2.5 \times 10^{-7} I_{2M}. \quad (4.2.1)$$

The closed-loop poles for this 4-mode design are shown in Figure 10. Using the pole locations in Figure 10, pole placement is used to place the poles of the point-sensor observer. The controller design for the distributed-sensor may be used directly for the point-sensor system. The resulting closed-loop pole locations for the point-sensor system are identical to those shown in Figure 10. Both designs are made without considering the uncontrolled modes.

The capability of the design in the control of the truth model may be tested by including some of the higher-order dynamics in the calculation of the closed-loop poles. If a 12-mode beam model is controlled by the distributed control system design based on the 4-mode model ($N_1 = 8$), the resulting pole locations are shown in Figure 11. If

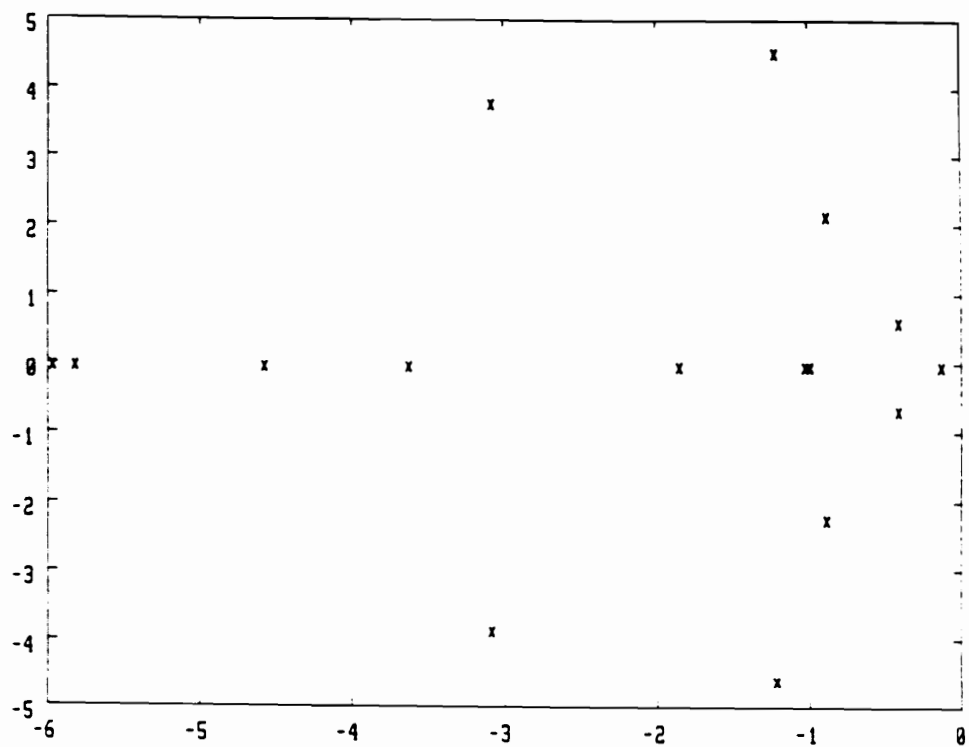


Figure 10. Closed-loop Poles for 4-mode Design: The Linear Quadratic Gaussian design method is used to place the poles assuming distributed sensing and only four vibrational modes exist. Pole placement is use to place the poles of the observer and controller in the same locations for the point sensor feedback.

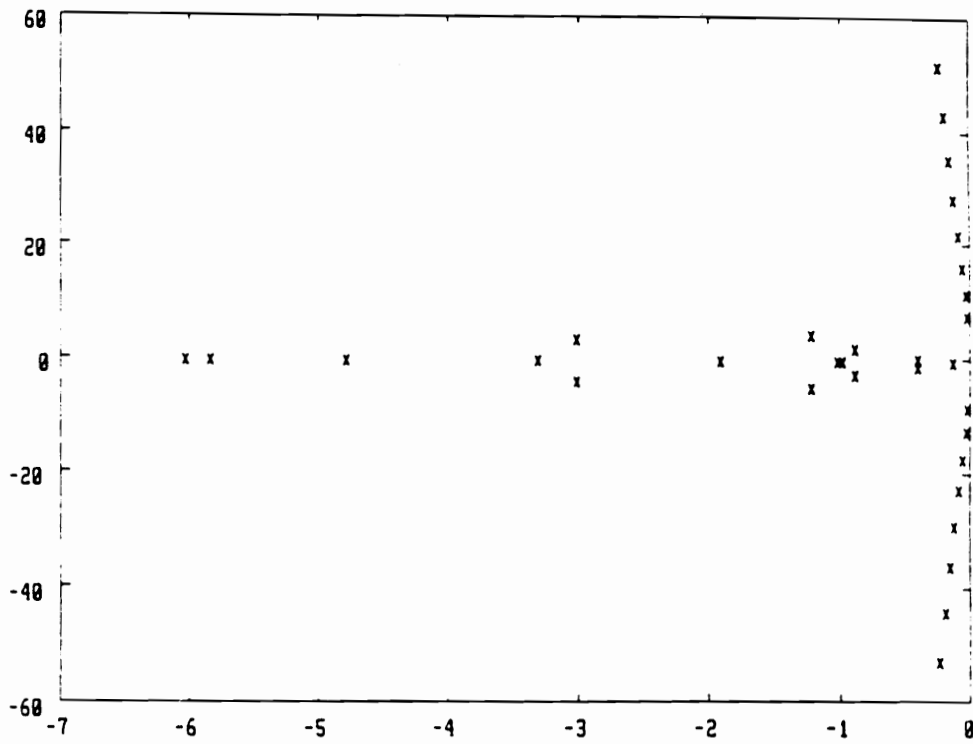


Figure 11. 4-mode Distributed Sensor Design Controlling a 12-mode Beam: The close-loop pole locations for a cantilevered beam with 12 vibrational modes controlled by the distributed sensor based control system designed to damp only four modes.

the same 12-mode model is controlled by the 4-mode point sensor based control system, the resulting pole locations are shown in Figure 12. Comparison of Figure 11 and Figure 12 shows that the higher-order dynamics have little effect in the distributed case, while the poles of the point system are greatly displaced from their nominal locations, and some of the poles corresponding to the uncontrolled modes are driven unstable. This is clearly a poor design for the point sensor based system, but it illustrates how the uncontrolled modes must be considered if distributed sensing is not used. The distributed sensor based control system is insensitive to the affects of the uncontrolled modes.

Our spillover result assumes exact knowledge of the mode shapes and modal frequencies. This is an unrealistic assumption in practice, because the modelling and system identification processes inevitably contain errors. We shall demonstrate, by example, that our design can tolerate significant errors in the parameters. We use the 4-mode design based on exact knowledge of the mode shapes and modal frequencies as our control system, and perturb the parameters of the 12-mode model in the simulation. The parameters of the 12-mode model are perturbed by altering the modal frequencies and mode shapes. The errors introduced are not related to any specific error in the modelling (such as non-uniformities). A uniformly distributed random number is added to the nominal modal frequencies to acheive a certain maximum percentage error. Another independent set of modal frequency perturbations are collected for use in the calculation of the mode shapes. Similar error might be expected if identification experiments are conducted to calculate the mode shapes and modal frequencies. For the given design, if errors up to 2% are introduced in the modal frequencies, then the simulations shown in Figure 13 demonstrate that the closed-loop system remains stable and the design modes remain well damped. If perturbations up to 5% are introduced, some of the systems are driven unstable under closed-loop control, as shown in

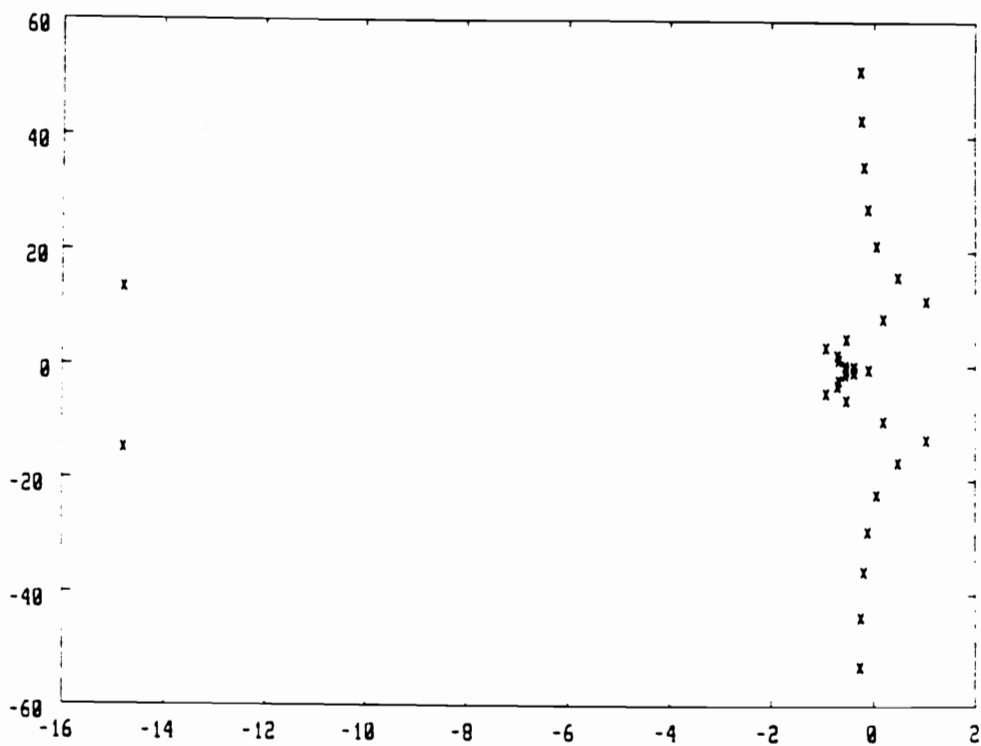


Figure 12. 4-mode Point Sensor Design Controlling a 12-mode Beam: The close-loop pole locations for a cantilevered beam with 12 vibrational modes controlled by the point sensor based control system designed to damp only four modes.

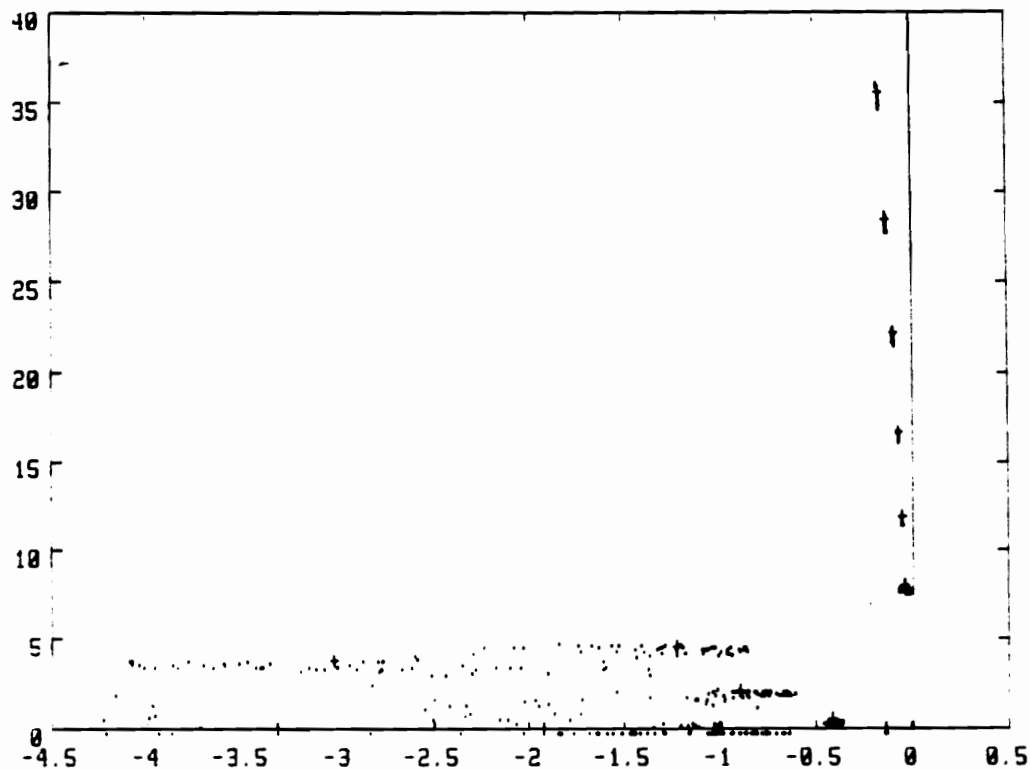


Figure 13. Closed-loop Poles with 2% Parameter Perturbations: The 4-mode design is used to control 50 different beams where the parameters have been perturbed by up to 2% from their nominal values. The design does not destabilizes any of the perturbed systems.

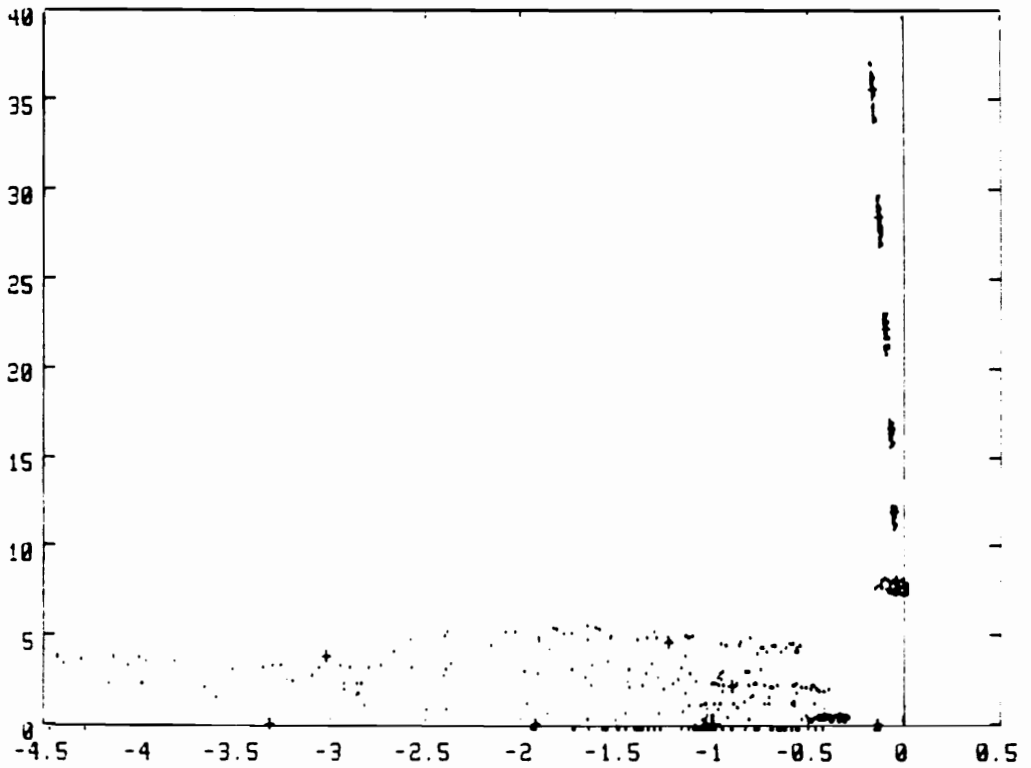


Figure 14. Closed-loop Poles with 5% Parameter Perturbations: The 4-mode design is used to control 50 different beams where the parameters have been perturbed by up to 5% from their nominal values. The design causes some of the systems to go unstable in the 5th mode.

Figure 14. Hence, the spatial filtering property is reduced in the presence of parameter errors, but exact knowledge of the parameters does not appear to be necessary. It should be noted that 2% errors in the natural frequencies used to calculate the mode shapes causes large errors in the mode shapes, as shown in Figure 15. Robust control design for the distributed sensor is an interesting topic for future research.

Instead of using the full state estimator, we could use the functional estimator. A functional estimator may be designed using the control vector F from the previous design. Since the estimator has only a single pole, it cannot be placed to perform exactly the same as the full state estimator. If we select $\alpha = 1$, the estimator pole will be placed at $s = -1$. The resulting integrating kernels $g_s(x)$ and $g_b(x)$ are shown in Figure 16.

We will compare the functional estimator to the full state estimator by pole placement and time response. The closed-loop pole locations for the functional estimator are shown in Figure 17. Comparison of Figure 17 and Figure 11 shows both methods place the controlled poles in the same locations. The only difference is in the observer poles, as expected. The performance of the designs may be compared by comparing the time responses to the same initial condition. The time response of beam under the control of the full state estimator based control system is shown in Figure 18. The time response of the beam under the control of the functional observer based control system is shown in Figure 19. The square error in the responses is shown in Figure 20. We can conclude from these simulations that the functional estimator design slightly out performs the full state estimator design, because the functional response has a smaller transient response and reduces the error to a lower level. However, this does not imply that the functional estimator design will always out perform the full state estimator design. It does show the performance of both designs is satisfactory.

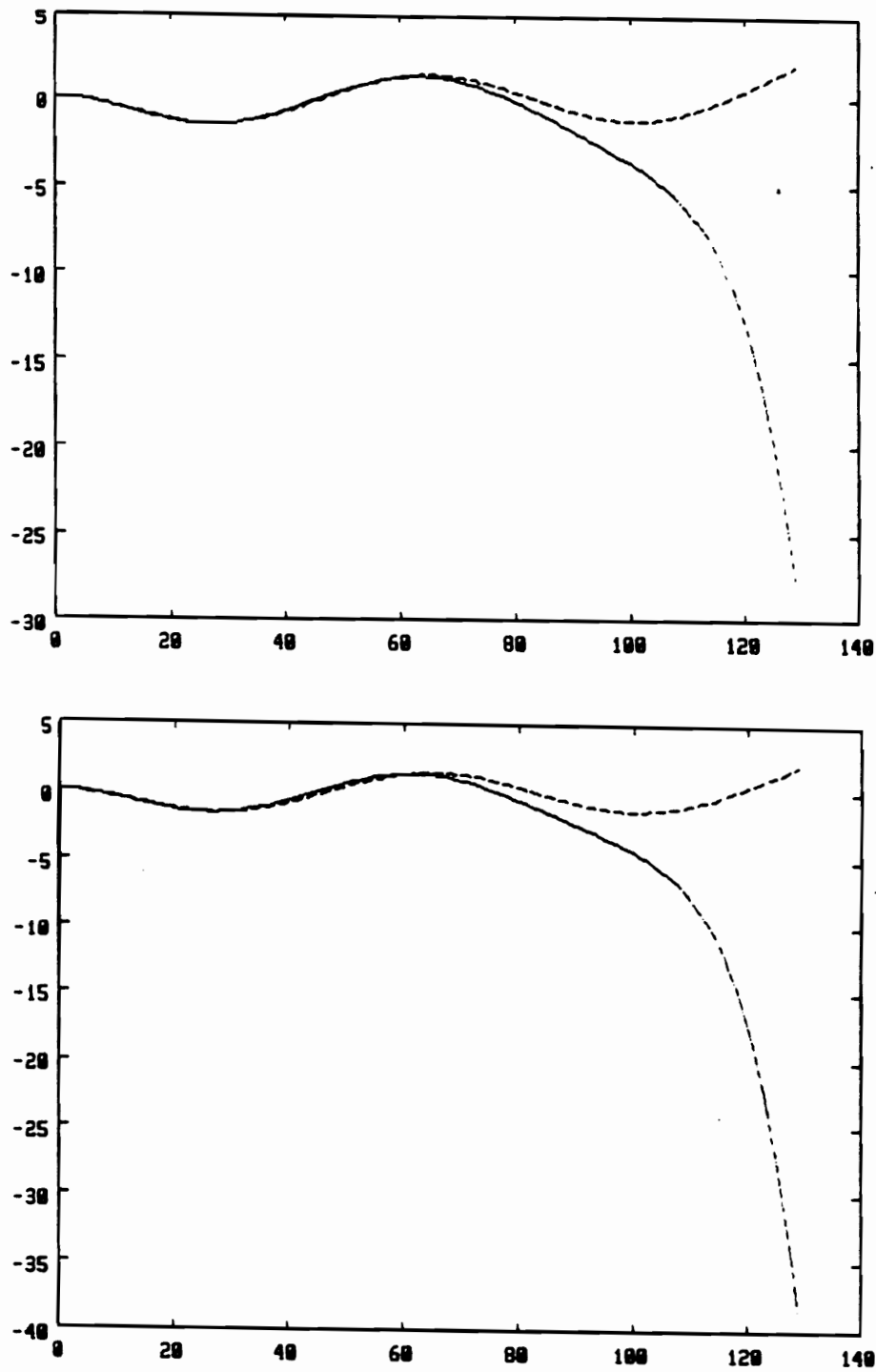


Figure 15. 2% and 5% Perturbations in 4th Mode Shape: The top figure shows the 4th mode shapes calculated with a 2% error in the natural frequency. The bottom figure shows the same mode calculated with a 5% error in the natural frequency.

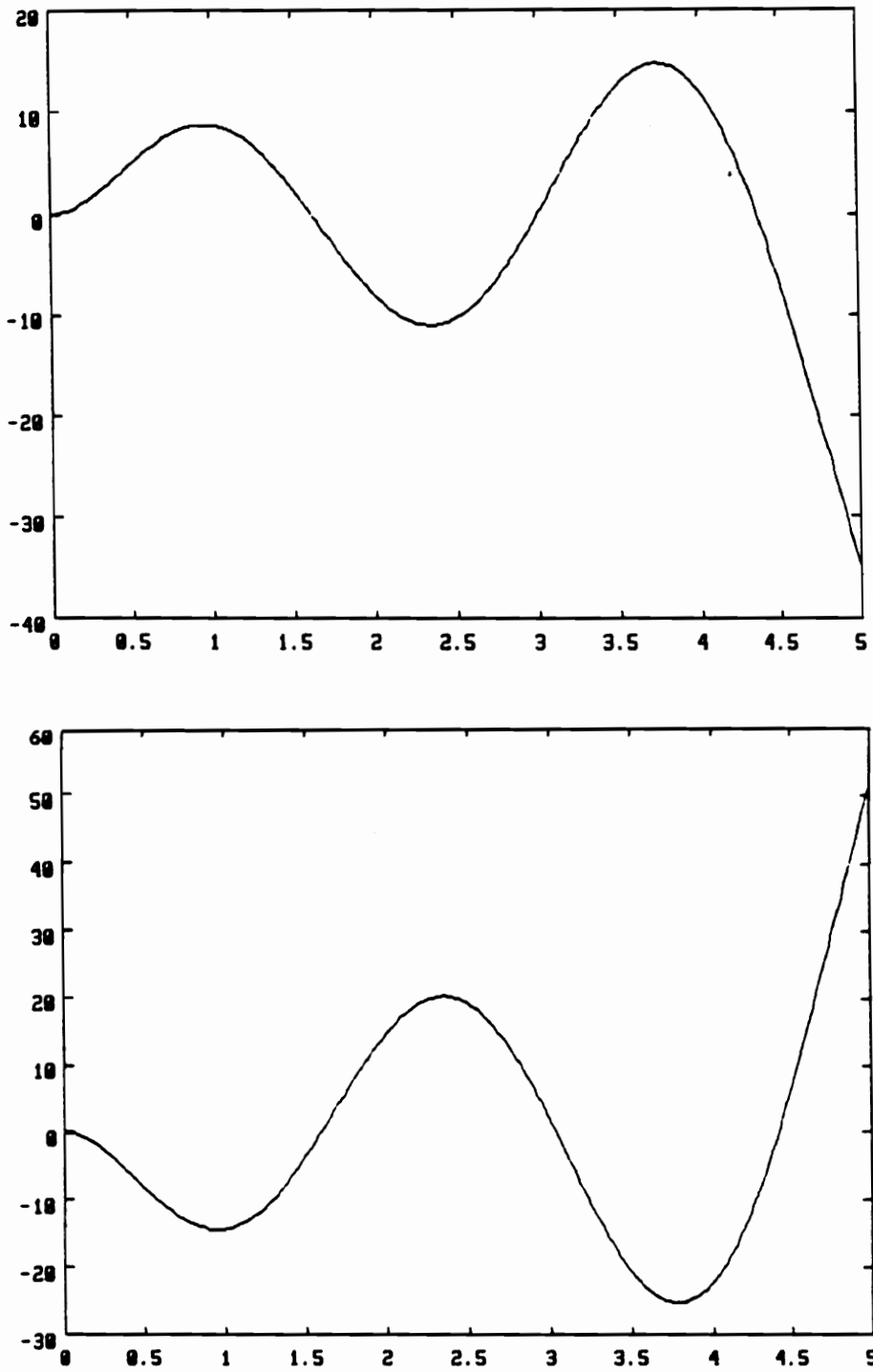


Figure 16. Integrating Kernels for Functional Estimator: The top figure is $g_a(x)$, and the bottom figure is $g_b(x)$

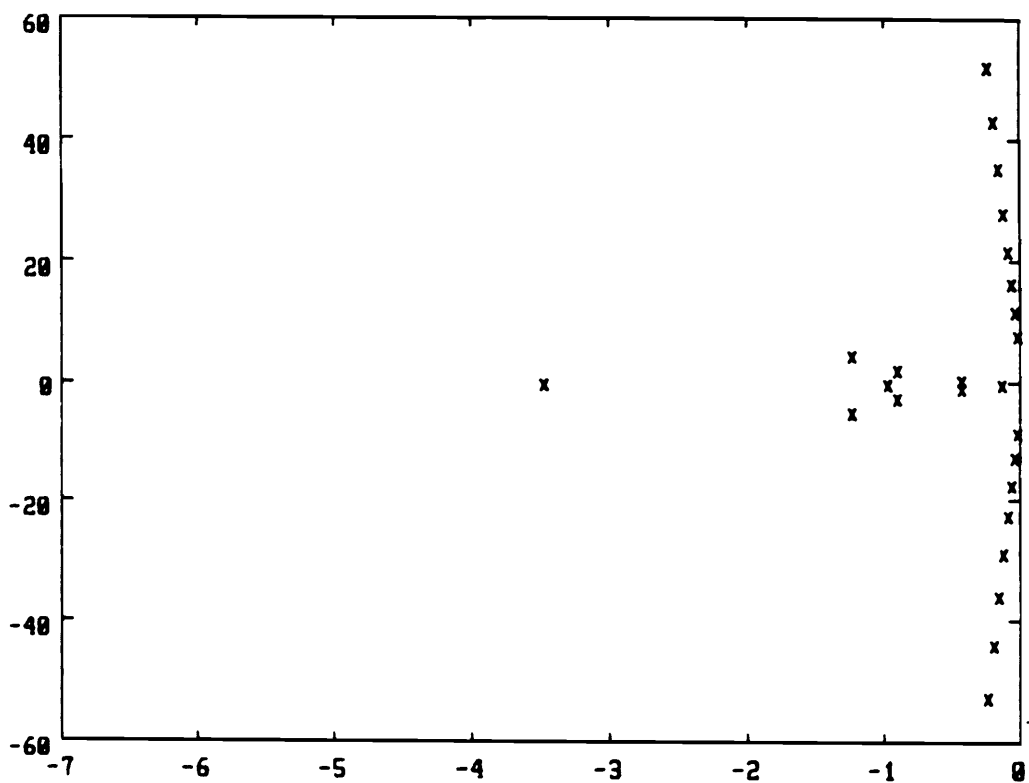


Figure 17. Closed-loop Poles for Functional Estimator: A 4-mode functional estimator is used to control a 12-mode cantilevered beam.

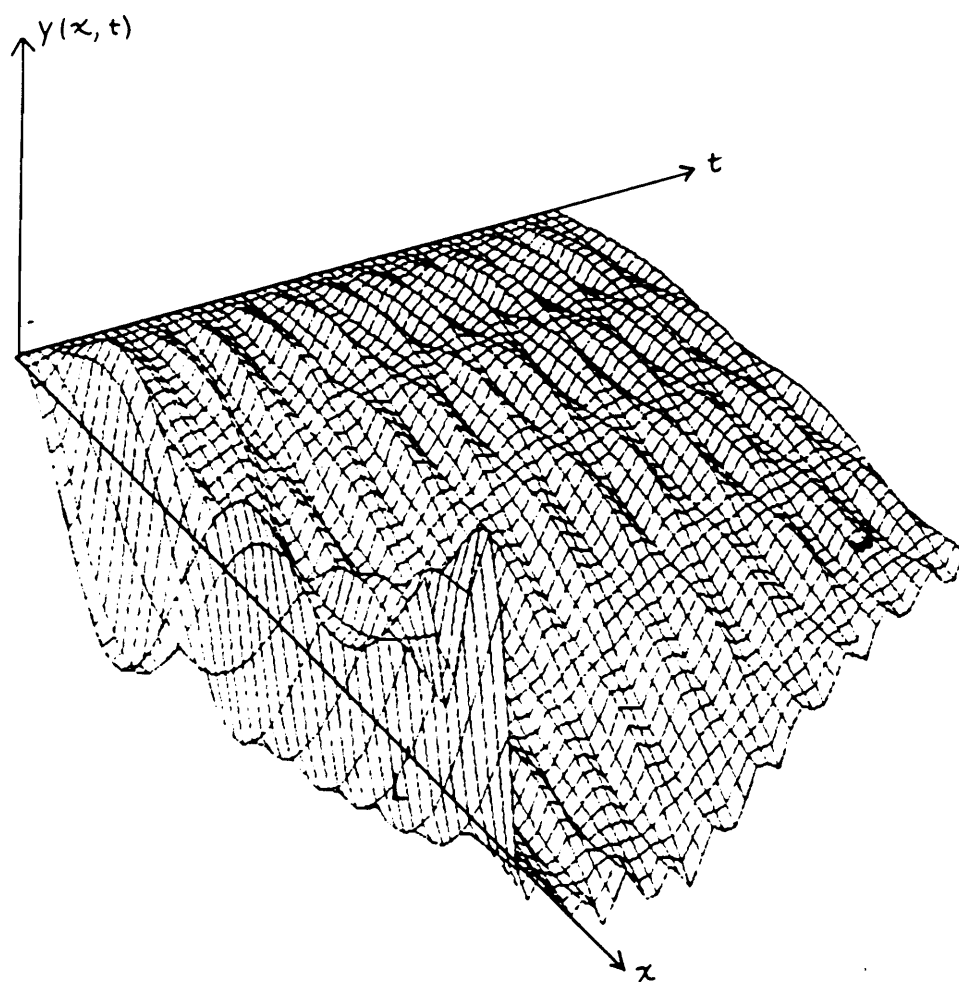


Figure 18. Time Response: The close-loop time response for a cantilevered beam with 12 vibrational modes controlled by the distributed sensor based control system designed to damp only four modes.

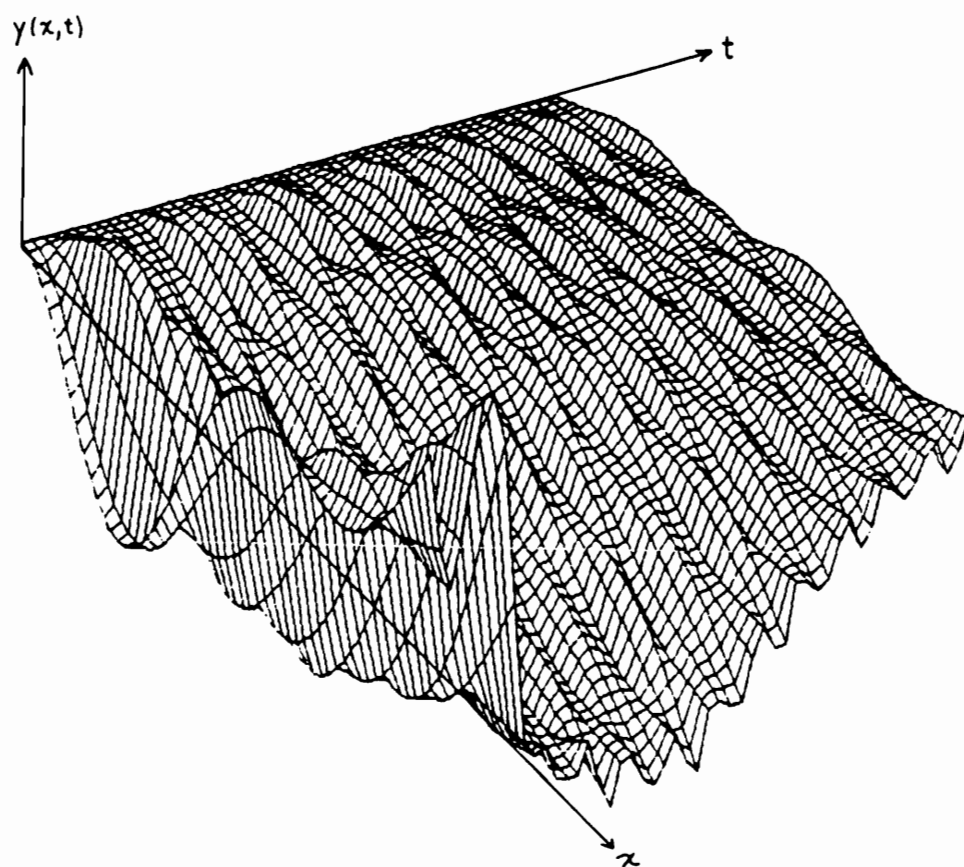


Figure 19. Time Response of Functional Observer: The time response of the 4-mode control system controlling the 12-mode cantilevered beam given a particular initial condition.

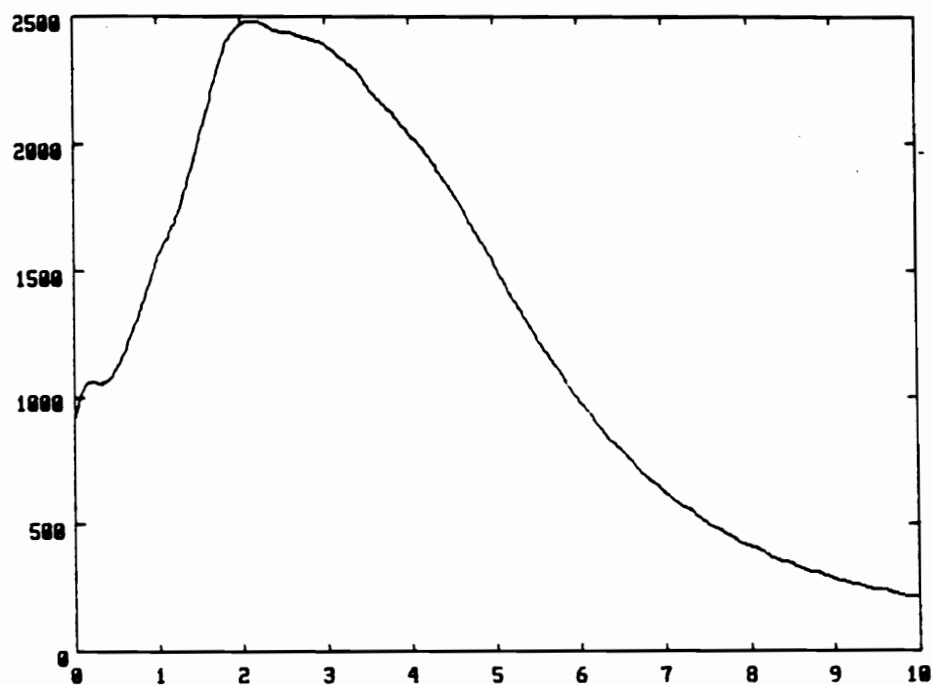
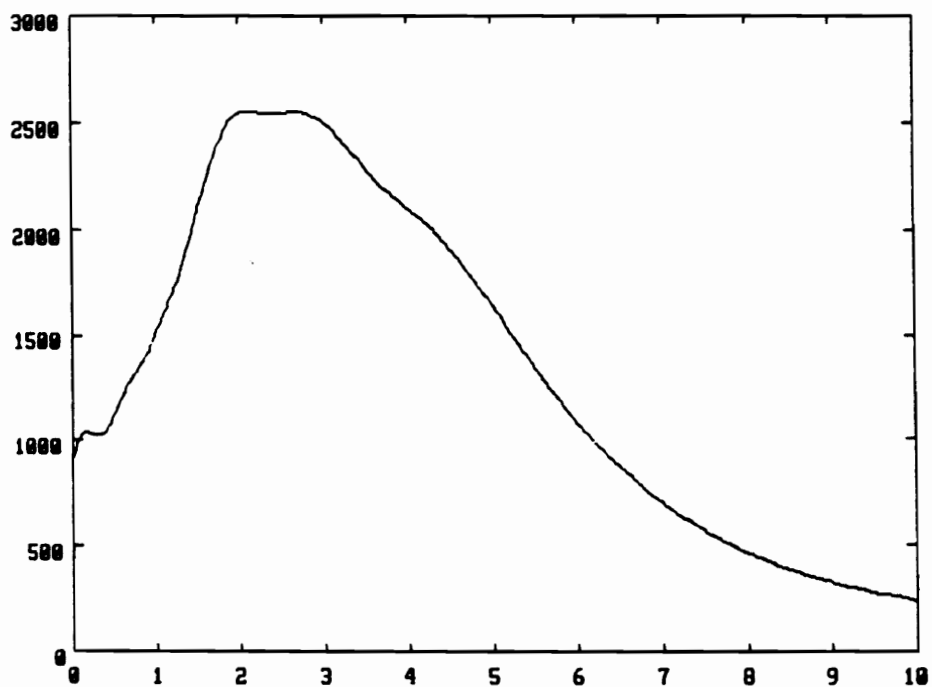


Figure 20. Squared Error in Time Responses: The top figure show the squared error from Figure 18. The bottom figure shows the squared error from Figure 19.

4.3 *Summary*

In this chapter, we demonstrated through simulation that our design is insensitive to the inclusion of uncontrolled dynamics. We considered an example where a 4-mode design was used to control a cantilevered beam with 12 vibrational modes. In the example, the distributed sensor design was found to decouple the design modes from the remaining modes, allowing the the 4 poles of the design to be placed arbitrarily. When the same design was attempted for a single point sensor colocated at the actuator, the result was an unstable system. Parameter perturbation simulations show that small errors in the modal frequencies and modes shapes do not destabilize the system. Finally, the full state estimator and functional estimator designs were compared. The functional estimator design was shown to effectively place the design poles and to out perform the full state estimator design in a time response simulation.

5.0 Implementation

5.1 Introduction

We have shown how to sense the distributed deflections of a flexible structure, how to design control systems to utilize the measurements, and how distributed sensing improves the resulting control system. Now we will consider the technology required to implement the control designs. We consider only the multifrequency continuous-time and discrete-time holographic sensors, but the processing methods apply equally well to any optical sensing method with an output given by

$$I_1(x,t) = I_\alpha + y(x,t) \quad (5.1.1)$$

where I_α is a bias intensity. For the holographic sensor, the bias is set by adjusting the difference in the path lengths of the object and reference beams. The bias I_α may also be a function of the x , but for simplicity, I_α is taken to be constant over the length of the beam. A typical intensity function is shown in Figure 4.

In the next section, implementations using mixed temporal-spatial processors are considered for the continuous time multifrequency holographic sensor. In Section 5.3 implementations of the all-optical processor are discussed for the discrete-time holographic sensor. In Section 5.4, the designs are extended to two-dimensional plate structures. The advantages and disadvantages of the all-optical and mixed implementations are summarized in the last section.

5.2 *Mixed Processor*

In this section, we present simple and effective implementations for the spatial part of the full state mixed processor and the entire functional estimator-type processor. In the Section 3.3.2, we demonstrated that the spatial processor must perform the spatial integral given in (3.3.25). The remaining of the processing may be performed by some temporal processor. In the case of full state estimation, the temporal processor is likely to be implemented using a microprocessor. However, in the functional estimator implementation, a single temporal analog integrator and a few analog adders should suffice.

The integral (3.3.25) is computed in two parts. First, the pointwise multiplication

$$\varepsilon_1(t) = g(x)y(x,t) \text{ for } 0 \leq x \leq L \quad (5.2.1)$$

is performed by focusing the beam $I_1(x,t)$ onto a gray scaled transparency with an absorption characteristic $d(x)$ as shown in Figure 21. When the beam $I_1(x,t)$ passes through the transparency $I_2(x)$, the absorption characteristic of the transparency absorbs the radiation in $I_1(x,t)$. Hence, a pointwise multiplication is performed. The

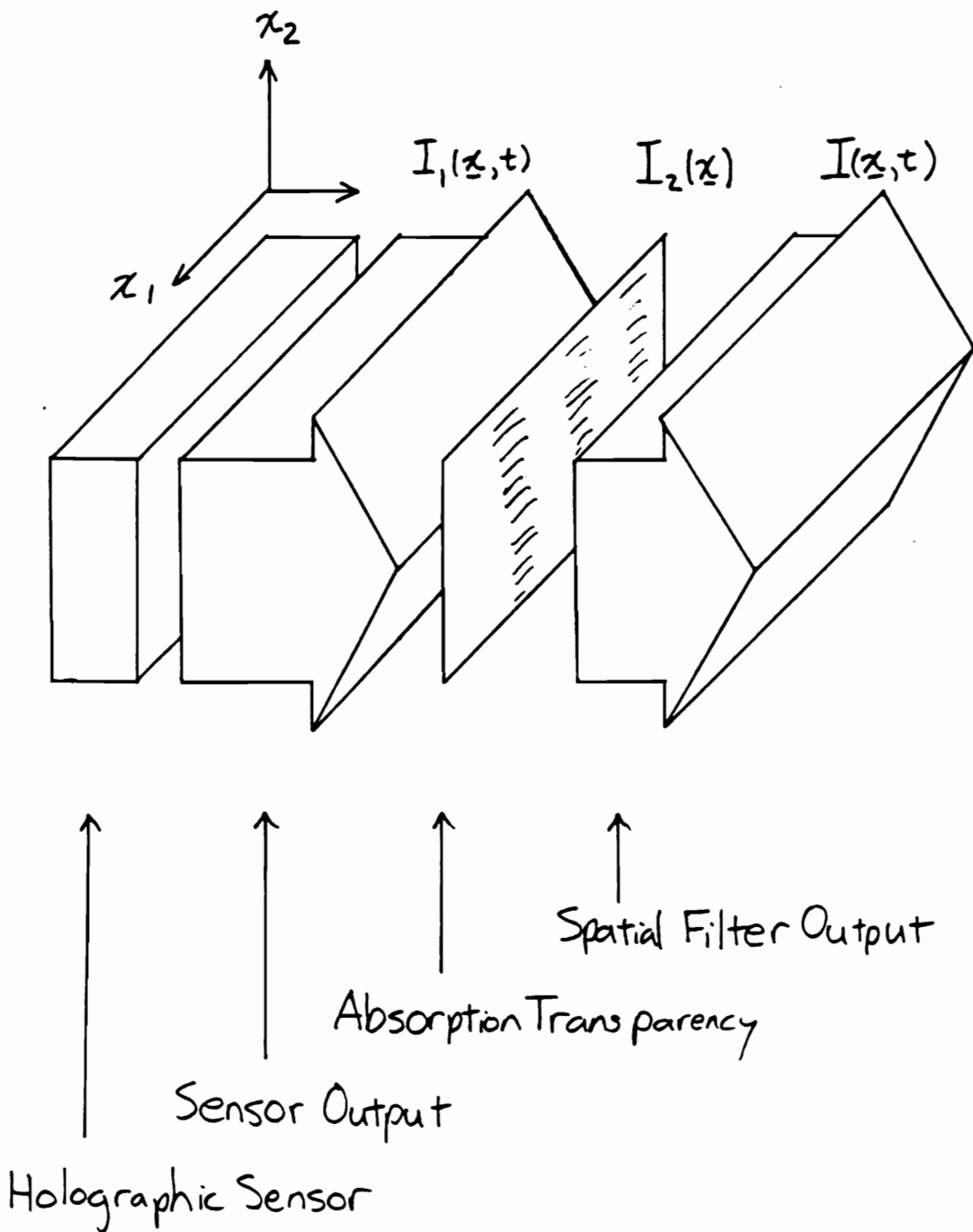


Figure 21. Pointwise Multiplication by Absorption Transparency: The output from the sensor is passed through an absorption transparency. The transparency scales the sensor signal as a function of x . The output is the function indicated in the figure.

transparency must be constructed to scale $I_1(x,t)$ as a function of x such that $0 \leq I_2(x) \leq 1$. Therefore, if $0 \leq g(x) \leq 1$, then we may take $I_2(x) = g(x)$. The second part of the processor consists of a photodetector. A photodetector is a transducer for converting the average incident intensity into a proportional electrical signal. We choose a photodetector with dimensions matching the area of the absorption transparency, as shown in Figure 22. The photodetector may be followed by an amplifier to set the proportionality constant of the conversion. The spatial average is performed continuously (we assume the temporal averaging is outside the control system bandwidth). Therefore, we can express the output from the photodetector as

$$\varepsilon_2(t) = \int_0^L I_2(x) I_1(x,t) dx. \quad (5.2.2)$$

Hence, the spatial processor consists of an absorption transparency mounted on the front of a photodetector. The output is an electrical signal to the temporal processor.

The output of the spatial processor (5.2.3) may be expanded as

$$\begin{aligned} \varepsilon_2(t) &= \int_0^L I_2(x) I_1(x,t) dx \\ &= \int_0^L g(x) (I_a + y(x,t)) dx \\ &= I_a + \int_0^L g(x) y(x,t) dx, \end{aligned} \quad (5.2.3)$$

where

$$I_a = \int_0^L I_a g(x) dx = \text{constant}. \quad (5.2.4)$$

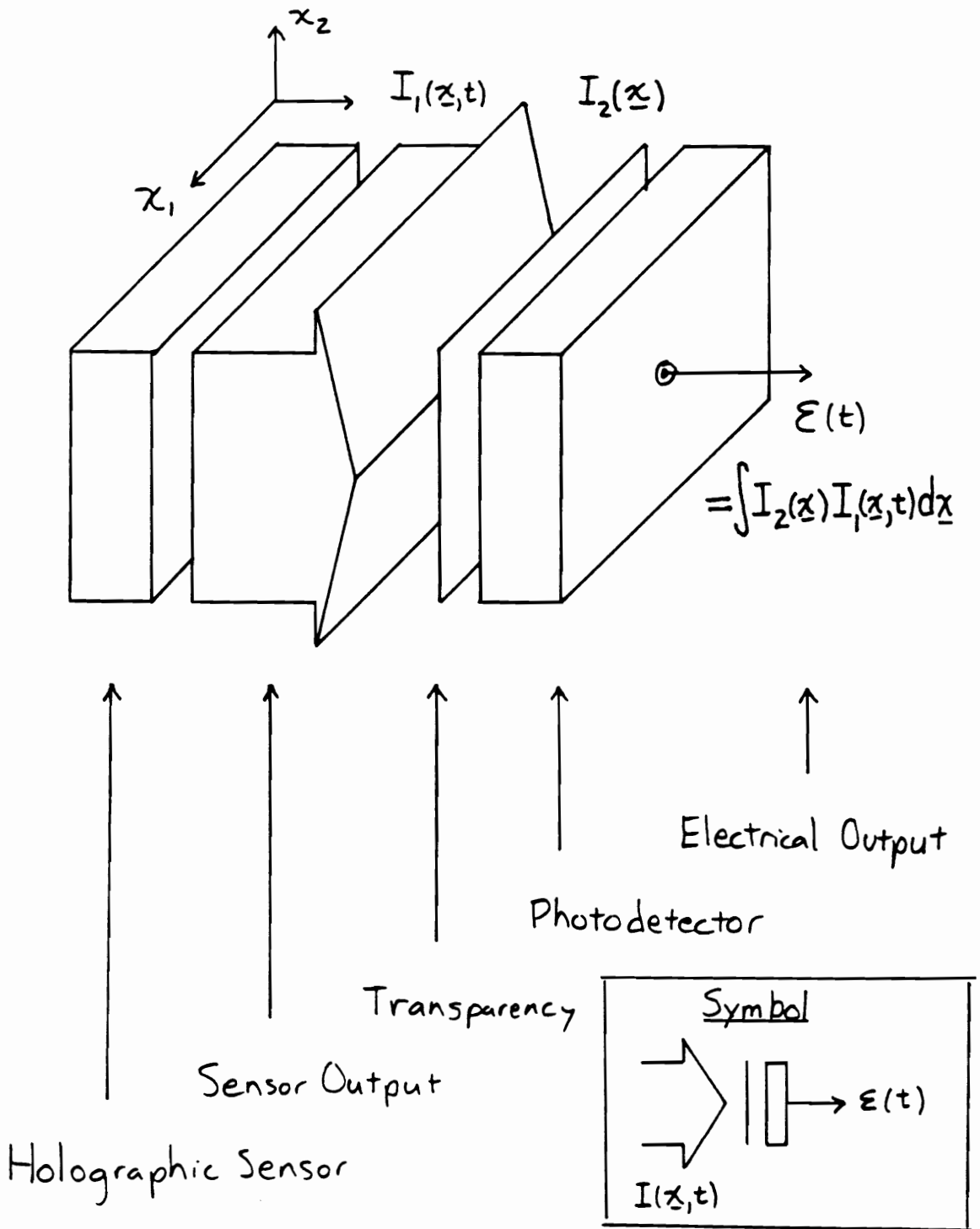


Figure 22. Full Spatial Processor: The photodetector averages the intensity over the area of the transparency to complete the implementation of the spatial integral.

Therefore, the implementation of Figure 22 produces the signal

$$\varepsilon(t) = \varepsilon_2(t) - I_a, \quad (5.2.5)$$

indicating that it should compute the desired integral.

The implementation of Figure 22 requires $g(x) \geq 0$ as presented. This is always possible because the deflection of the structure is merely the sum of mode shapes, and the structure can always be flexed so that its deflection is positive. For a cantilevered beam, the weighting of the modes is particularly simple. The sum of the first N modes will be positive if they are equally weighted, as shown in Figure 23. If the modes are summed using some other weighting, the resulting filter may be bipolar (positive for some x , negative for other x). Such a weighting scheme is necessary for the functional estimator implementation, as was shown in Figure 16 on page 82. However, care must be exercised in the implementation. For instance, consider the bipolar processor created by adding a bias to the bipolar function as in

$$\bar{g}(x) = I_\beta + g(x) \quad (5.2.6)$$

so that

$$0 \leq \bar{g}(x) \leq 1. \quad (5.2.7)$$

While this appears to allow bipolar $g(x)$ with positive $\bar{g}(x)$, we must take special measures to avoid losing the modal filtering property of the spatial filter. To see this, calculate $\varepsilon_2(t)$ with $g(x)$ replaced with $\bar{g}(x)$,

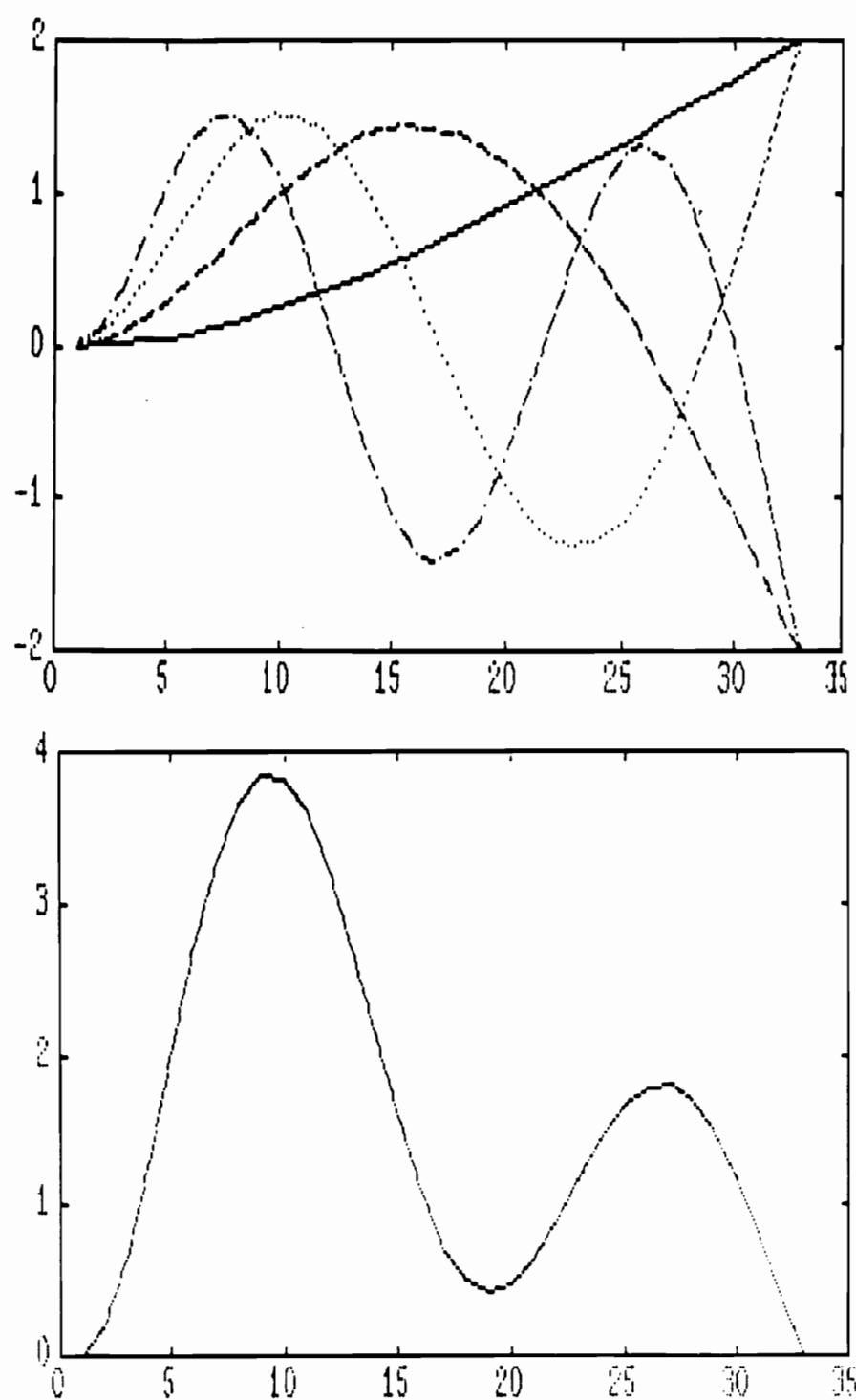


Figure 23. Sum of Modes for Cantilevered Beam: (a) First 4 modes for a cantilevered beam, equally weighted. (b) The sum of the first four modes.

$$\begin{aligned}
\varepsilon_2(t) &= \int_0^L (I_\alpha + y(x,t)) \bar{g}(x) dx \\
&= \int_0^L (I_\alpha + y(x,t))(I_\beta + g(x)) dx \\
&= I_b + \int_0^L I_\beta y(x,t) dx + \int_0^L g(x) y(x,t) dx.
\end{aligned} \tag{5.2.8}$$

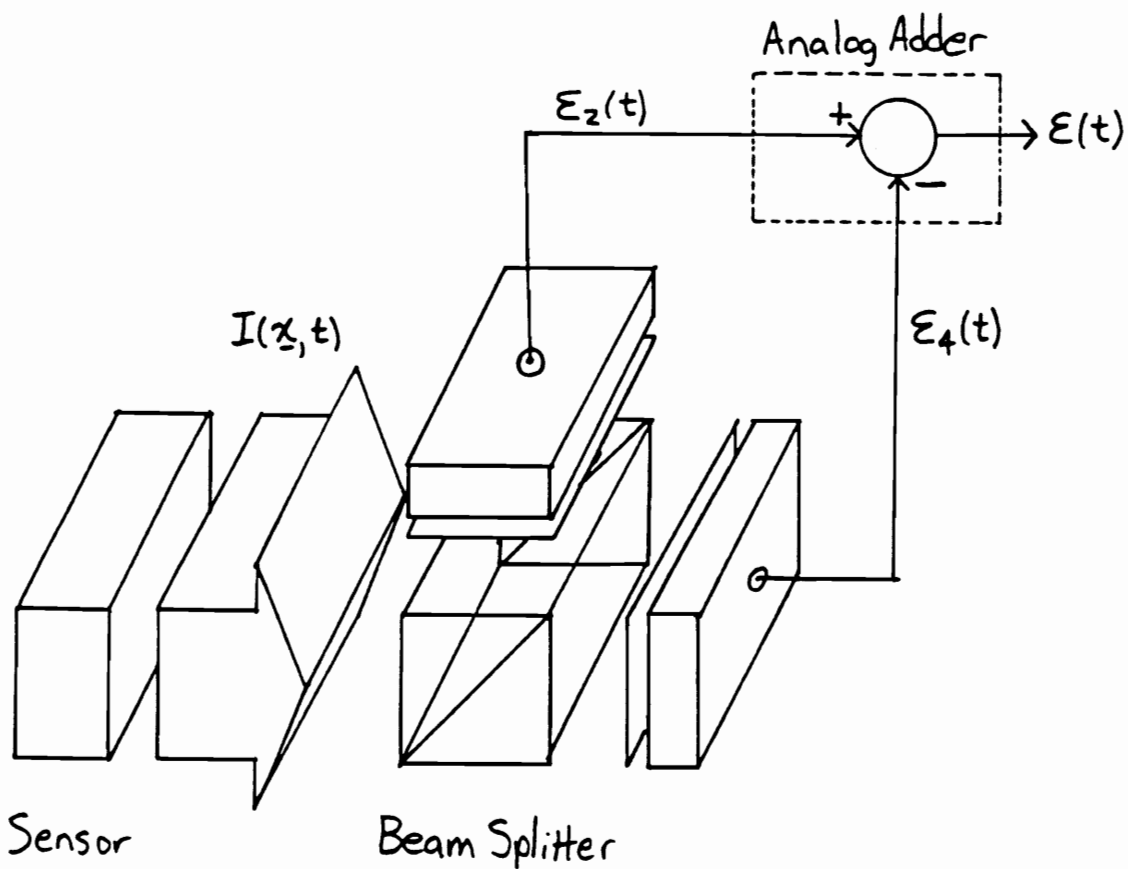
The term

$$\varepsilon_3(t) = \int_0^L I_\beta y(x,t) dx \tag{5.2.9}$$

contains both the effects of the design modes and the remaining modes. The observer is designed without knowledge of the remaining modes. Therefore, it cannot compensate for the created bias (5.2.9). However, we can measure the bias directly and subtract it from the result. A processor designed for bipolar operation is shown in Figure 24. The processor is essentially two spatial processors of the type shown in Figure 22, where the second processor removes the bias created by the first. The output of the second spatially integrating photodetector is given by

$$\varepsilon_4(t) = \int_0^L I_\beta I_\alpha + I_\beta y(x,t) dx. \tag{5.2.10}$$

Therefore, the processor output is



Schematic

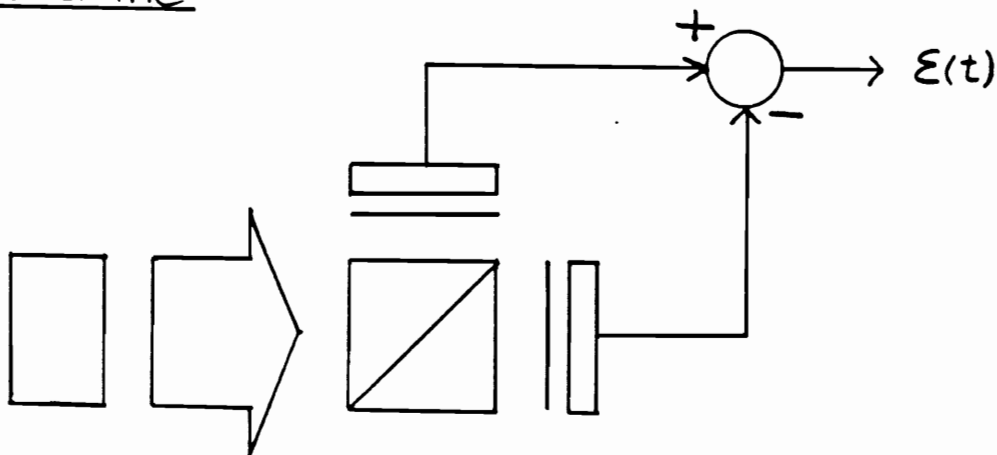


Figure 24. Bipolar Spatial Processor: The second absorption transparency and photodetector allow the bias of the first filter to be removed in the time domain, allowing bipolar spatial filtering.

$$\varepsilon(t) = \varepsilon_2 - \varepsilon_4$$

$$= \int_0^L I_a g(x) + g(x) y(x, t) dx \quad (5.2.11)$$

$$= I_a + \int_0^L g(x) y(x, t) dx,$$

as in (5.2.2).

A useful application of the bipolar processor is in the implementation of the functional estimator, where bipolar filters are required because the modal filtering, the control law, and the estimator are all combined. The output of the spatial processors is processed by a first order temporal processor to yield the control signal, as shown in Figure 25.

5.3 *The All-Optical Processor*

In this section, we consider an all-optical implementation of the distributed control system design [28]. The all-optical processor does not estimate the modal amplitudes explicitly. Instead, it estimates a shape by approximating the measurement with only the design modes. An optical inner product operation is then performed to create a control signal. We consider the discrete-time sensor only, because it does not require distributed integration. This implementation concept is still preliminary; many of the details remain.

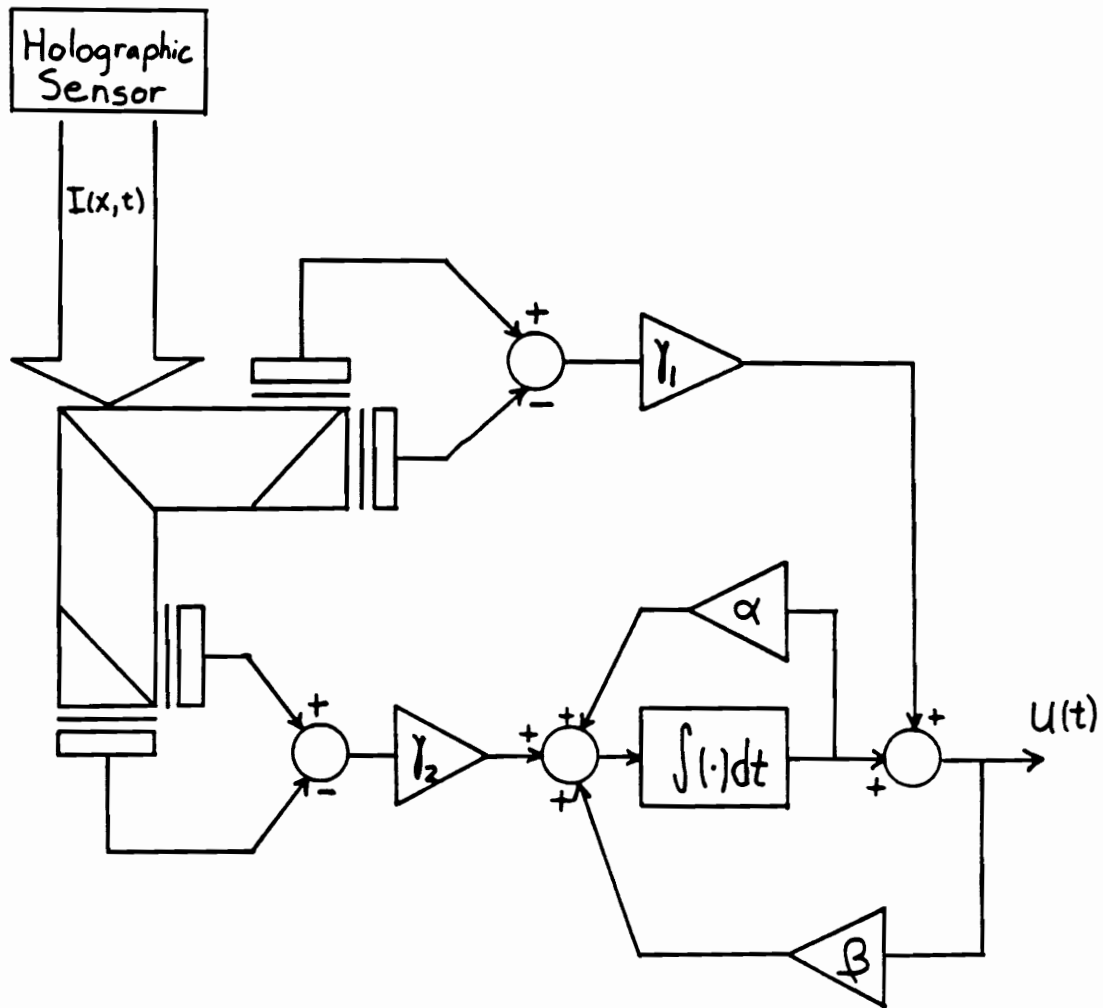


Figure 25. **Functional Estimator:** Two bipolar spatial processors are used to along with a single temporal integrator to compute the control signal. The gains γ_1 and γ_2 are chosen to scale the transparencies. No further processing is required.

We begin by simplifying the observer (3.3.40) to remove two summing operation as shown,

$$\begin{aligned}
\hat{\Phi}(x, k+1) &= \int_0^L a(x, \bar{x}) \hat{\Phi}(\bar{x}, k) d\bar{x} \\
&\quad + b(x)u(k) + \int_0^L \ell(x, \bar{x})(y(\bar{x}, k) - \hat{y}(\bar{x}, k)) d\bar{x} \\
&= \int_0^L (a(x, \bar{x}) - \ell(x, \bar{x})) \hat{\Phi}(\bar{x}, k) d\bar{x} \\
&\quad + b(x)u(k) + \int_0^L \ell(x, \bar{x})y(\bar{x}, k) d\bar{x}.
\end{aligned} \tag{5.3.1}$$

We expand (5.3.1) to show the actual operations required,

$$\begin{aligned}
&\begin{bmatrix} \hat{y}(x, k+1) \\ \frac{d}{dt} \hat{y}(x, k+1) \end{bmatrix} = \\
&\begin{bmatrix} \int_0^L (a_1(x, \bar{x}) - \ell_1(x, \bar{x})) (.) d\bar{x} & \int_0^L a_2(x, \bar{x}) (.) d\bar{x} \\ \int_0^L (a_3(x, \bar{x}) - \ell_2(x, \bar{x})) (.) d\bar{x} & \int_0^L a_4(x, \bar{x}) (.) d\bar{x} \end{bmatrix} \begin{bmatrix} \hat{y}(x, k) \\ \frac{d}{dt} \hat{y}(x, k) \end{bmatrix} \\
&\quad + \begin{bmatrix} b_1(x) \\ b_2(x) \end{bmatrix} u(k) + \begin{bmatrix} \int_0^L \ell_1(x, \bar{x}) (.) d\bar{x} \\ \int_0^L \ell_2(x, \bar{x}) (.) d\bar{x} \end{bmatrix} \begin{bmatrix} y(x, k) \\ 0 \end{bmatrix},
\end{aligned} \tag{5.3.2}$$

where

$$u(k) = \left[\int_0^L f_1(x) (.) dx \quad \int_0^L f_2(x) (.) dx \right] \begin{bmatrix} \hat{y}(x,k) \\ \frac{d}{dt} \hat{y}(x,k) \end{bmatrix}. \quad (5.3.3)$$

Equation (5.3.2) is shown graphically in Figure 26, where each block represents an optical operation. The integrals with one and two-dimensional kernels could be performed using Fourier optical computers (Figure 27 and Figure 28), while the summations could be performed using beam splitters (Figure 29), and the remaining operations could be performed using temporal light modulators (Figure 30). Imaging between the sensor and the various optical blocks requires careful attention to maintain the coherence of the distributed signal.

5.4 Extensions to Two-Dimensional Structures

It is a simple matter to extend the implementation of the mixed processor to two-dimensions. We must merely replace the absorption transparency in Figure 22 with a two-dimensional transparency $g(x_1, x_2)$ consisting of the sum of the two-dimensional modes. Since the integrator integrates in both directions, the output is given by

$$\varepsilon_2(t) = \int_0^{L_2} \int_0^{L_1} I_1(x_1, x_2, t) I_2(x_1, x_2) dx_1 dx_2 \quad (5.4.1)$$

where

$$I_1(x_1, x_2, t) = I_\alpha + y(x_1, x_2, t), \quad (5.4.2)$$

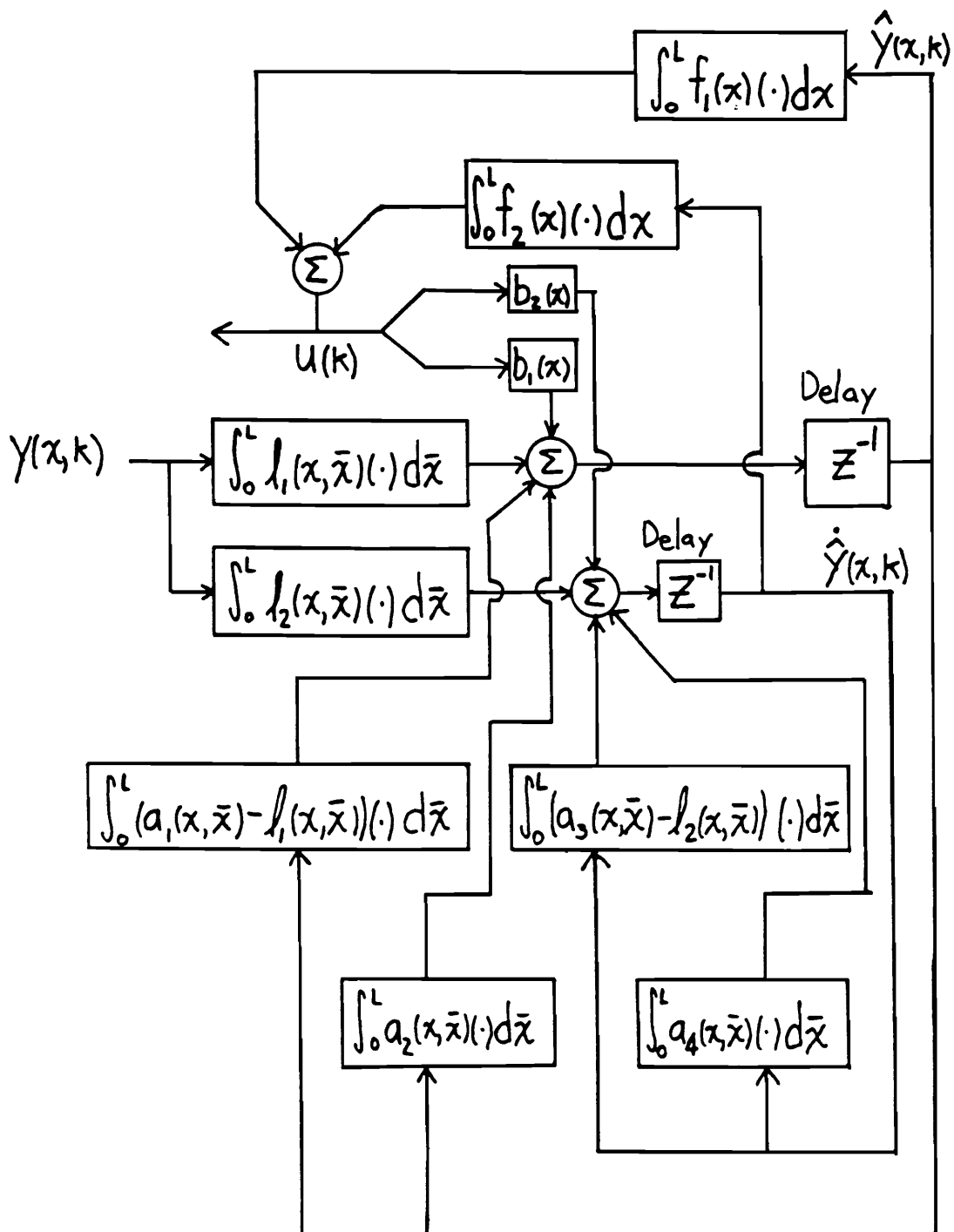


Figure 26. Block Diagram of an All-Optical Processor: This processor implements a functional state space control law with a functional observer.

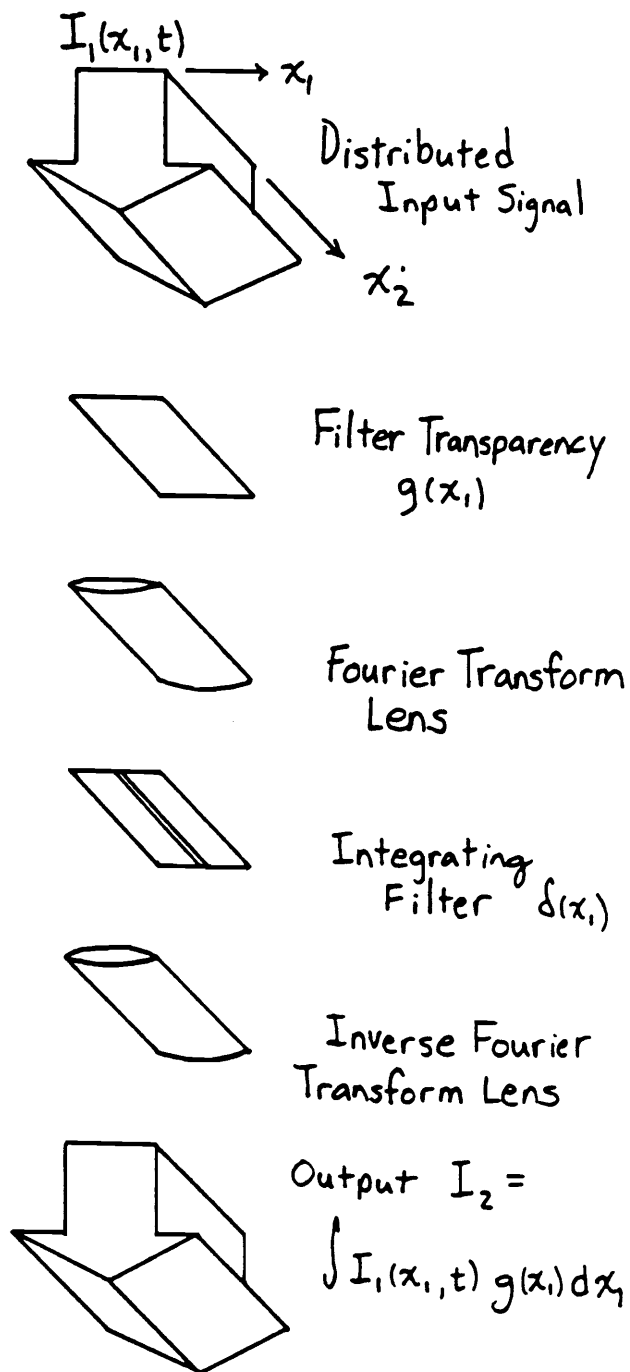


Figure 27. Integrator with one-dimensional kernel: This unit is used to compute the control signal given the estimate of the distributed states. The transparency scales the incoming signal as a function of x_1 . The first cylindrical lens transforms the product of the incoming signal and the transparency function into the spatial frequency domain. An filter approximating a Dirac delta function $\delta(x_1)$ filters the frequency domain signal. The second lens inverts the process of the first lens to yield the desired integral.

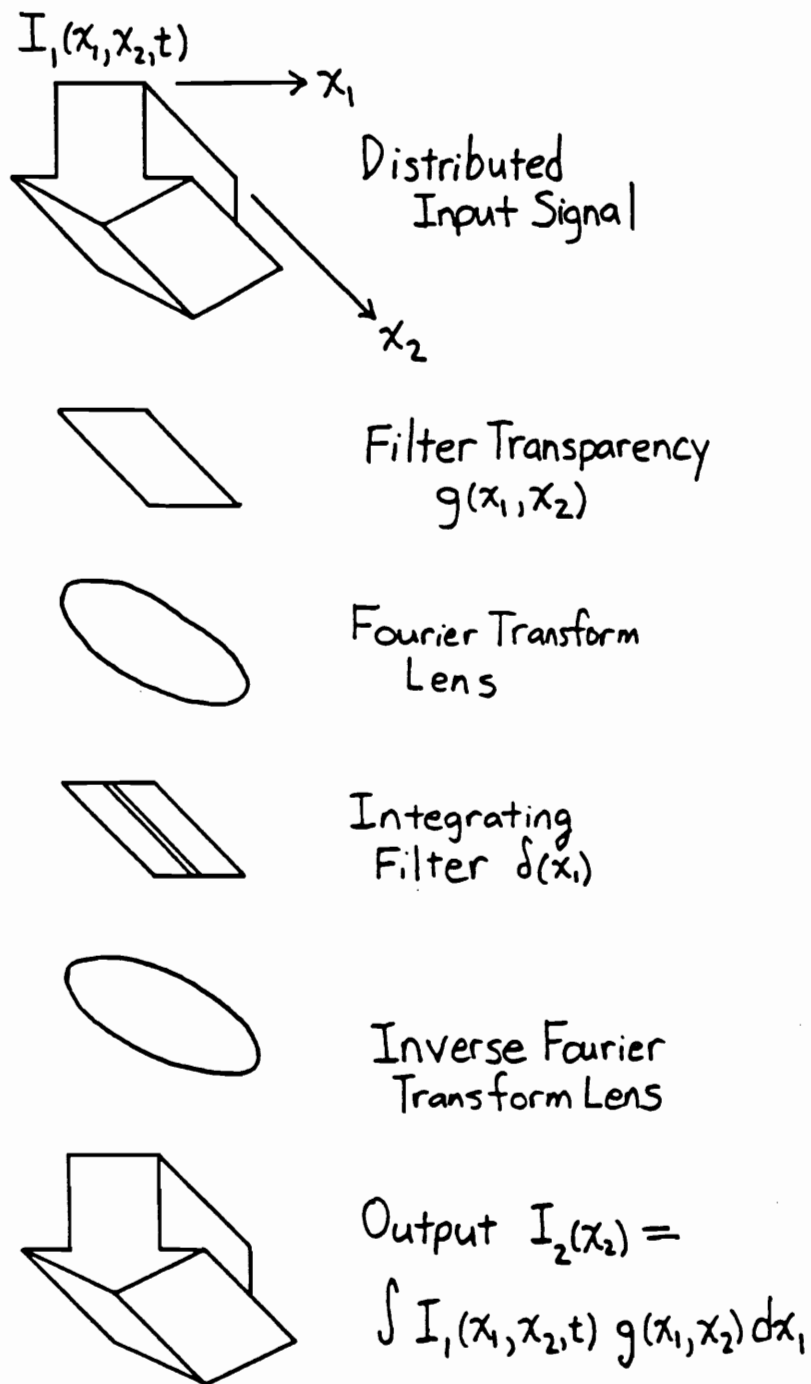


Figure 28. Integrator with two-dimensional kernel: All remaining integrals use this unit. The concept is the same as the integrator with a one-dimensional kernel. To allow two-dimensional kernel, make the incoming transparency a function of both x_1 and x_2 , replace the cylindrical lenses with spherical lenses, and approximate a two-dimensional delta function in the frequency domain.

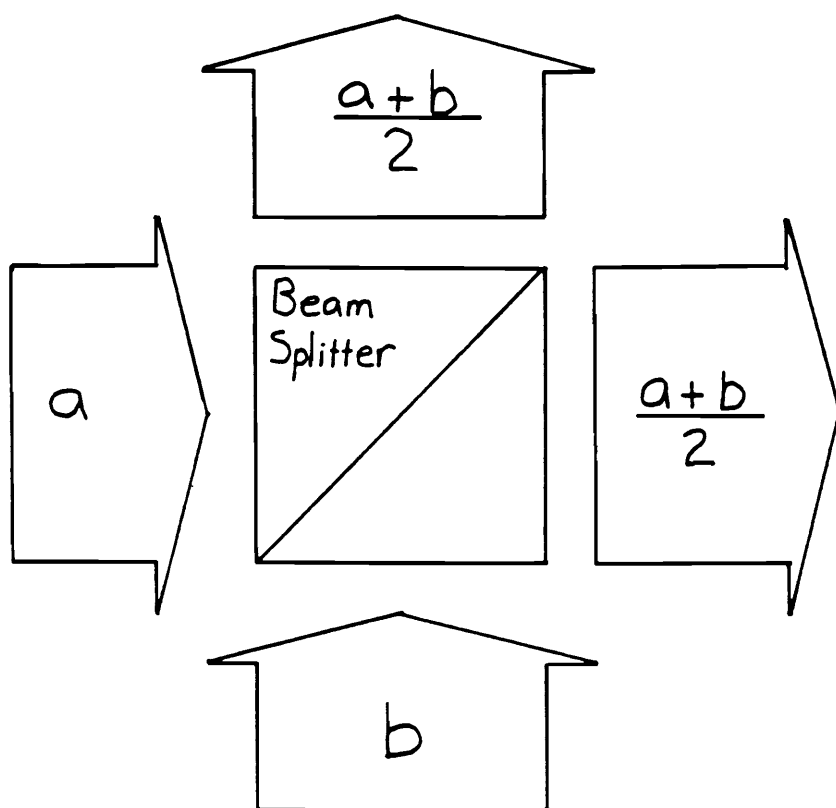


Figure 29. Beam Splitter for Addition: Beam splitter adds the amplitudes of two collimated beams. More than two beams by chaining additional beam splitters on the output.

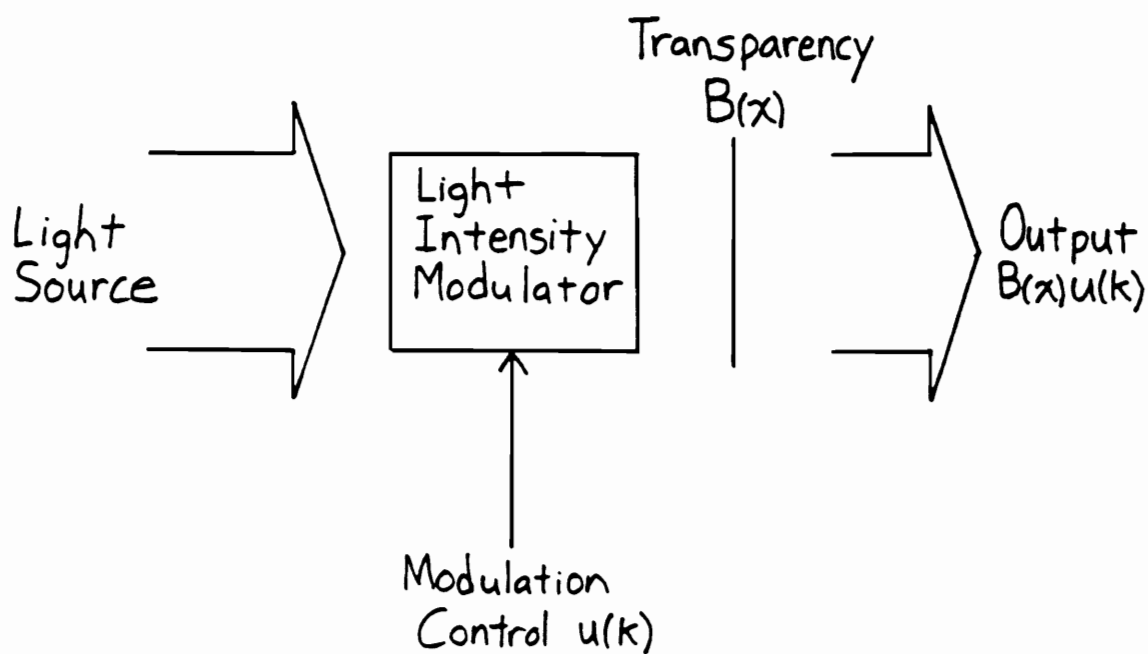


Figure 30. Control Modulator: A device such as a cross polarizer is modulated by the control signal and scaled by a transparency to feedback the control signal in the observer.

$$I_2(x_1, x_2) = g(x_1, x_2). \quad (5.4.3)$$

Of course, if $g(x_1, x_2)$ is bipolar, then a similar processor must be constructed using the bipolar design of Figure 24.

Extending the all-optical implementation to a second dimension appears to be awkward. The problem is that two-dimensional measurements require spatial integrators operating in four spatial dimensions. In Section 3.3.5, the discrete-time design is performed by assuming that the measurement is converted from two dimensions to a single dimension by scanning the structure. If the sensor were modified to scan the structure, then an implementation similar to that offered for one-dimensional sensing would be suitable. Another conceivable solution is to divide the processor into many parallel processors with interleaving optics, but such a system would be too complex and speculative to discuss at this level. We conclude that the extension of the all-optical implementation to a second dimension remains an open problem.

5.5 *Summary*

Full state estimator based and functional estimator based mixed processors were presented which divide the processing duties between an optical processor performing space domain operations only, and a temporal processor performing the remaining time domain operations. Very few optical operations are required, limiting the round-off error due to inaccuracies in the filters and error due to cumulative optical operations. The optical operations do not require coherent optics, further lessening the sensitivity of the computation to optical flaws. In both processors, the spatial processor performs

the modal filtering operation to generate a signal containing the modal amplitudes of only a finite number of modes, while a temporal processor performs the remaining computation. In the functional estimator based implementation, the spatial processor combines the measured modes in a linear combination which greatly simplifies the temporal processing. In the full state estimator based implementation, the spatial processor is simpler, but more temporal processing is required. The mixed processors apply equally well for both one and two dimensional structures.

The all-optical processor is considered for its potential performance advantages and the novelty of distributed computation. Temporal and spatial processing is combined and performed in a simultaneous process. The processing speed is limited by the sample rate of the discrete-time sensor. Hence, this implementation has the potential for controlling a large number of modes without a separate temporal processor. Presently, the all-optical implementation does not apply well to two-dimensional structures.

6.0 Summary and Recommendations

6.1 *Summary*

This dissertation has addressed the problem of developing a control system for flexible structures based on distributed optical sensing. Specifically, we have shown that holographic sensing methods can be used to sense the distributed shape of one and two dimensional flexible structures. Furthermore, the optical output of the sensor can be processed optically to generate a control signal to damp the vibrations in the structure using a point actuator. The combination of optical sensing and processing presented may solve both the spillover and implementation problems in the theory of the control of flexible structures.

First, the necessary sensing technology was presented in Chapter 2. It was shown that multifrequency real-time holography can generate an intensity function corresponding to the deflection of the flexible structure in space. Several other optical methods were also presented in the development including an intensity imaging method and interferometric methods.

In Chapter 3 we presented a design method based on a modal model from a partial differential equation. The control system design is based on standard deterministic Linear Quadratic Gaussian state feedback plus observer. The design is unusual in that it accommodates the continuous output function of the holographic sensor. The design controls (damps) a finite number of vibrational modes. Analysis was presented to show the design solves the spillover problem by eliminating the observation spillover.

In Chapter 4 simulation examples were given to compare the performance of the distributed sensor to a point sensor, and to test the sensitivity of the design to modelling errors. The simulations demonstrated that the distributed sensor provides clear performance advantages over point sensing, the modelling for the distributed sensor can tolerate small errors, and that the functional estimator based control system compares satisfactorily with the full state estimator based control system.

Finally, in Chapter 5 implementations for the control system were considered. Mixed processing implementations were considered which divide the processing into spatial and temporal parts, and all-optical implementations were considered which combined the temporal and spatial processing. Both approaches maintain the modal filtering aspect of the designs. Both mixed and all-optical implementations were considered which simplify temporal processing to eliminate the need for a microprocessor in the computation of the control signal.

6.2 Recommendations for Future Work

The theoretical analysis presented in this dissertation indicates that holographic sensing should be capable of performing the required measurement function, and that

optical methods can be used to efficiently process the measurement into a useful form. Thus, further research beyond this purely theoretical study appears to be justified. In this section, we divide the areas for further research into two parts. The first part is on proof of concept experiments. The technology cited in this dissertation has been largely established by others, but it has not been verified in the specific context of distributed sensing for control. The second part is on areas for further control theoretic study. Further control work includes analysis of the effects of numerical modelling on the spillover result, analysis with non-ideal processing elements, and development of control laws which further exploit the architecture of the processors. In summary, future work is required to verify and refine the results presented.

6.2.1 Experiments

The experiments presented in this section are designed to verify the sensing and processing concepts described in Chapters 2 and 5. The sensor is likely to be more difficult to build. Therefore, the experiments have been designed so that the sensor and processor may be tested independently. As the sensing and processing technologies become available, they may be combined to test the overall system. That is, the tests for the sensor and processor are separate, but compatible.

Sensing Experiments

In Chapter 2 we concluded that a multifrequency method of real-time holography would be required to fulfill our sensing needs. Several other methods were also presented. Rather than beginning with the multifrequency holographic method, it would

be useful to verify the operation of the other methods. This would allow us to gain experience with the optics. Furthermore, the additional insight may lead to new approaches to solving the sensing problem.

For example, we could verify the effectiveness of the imaging method presented in Section 2.3. The principle problem with this method is its lack of sensitivity at distances sufficient for effective focussing by the lens. Perhaps a coating could be developed to alter the reflective characteristics of the structure to improve the sensitivity. While any light source could be used for the imaging sensor, and the beam splitter are not required as shown in Figure 5, including these devices will allow us to easily modify the experiment to verify the Michelson interferometer.

The Michelson interferometer presented in Section 2.4 was deemed too sensitive. However, if fringe interpretation methods are developed, or if vibrations on the order of a fraction of the optical wave length are to be controlled, the interferometer could be a viable alternative. This experiment could be desensitized using a multifrequency laser. While demodulation problems exist in the multifrequency interferometer, the multifrequency laser is required in the holographic sensor, and it may be characterized in the interferometric setting. The sensor arrangement will also function as a testbed for other creative solutions to the demodulation problem described in Section 6.5.

Simultaneously, one may wish to develop experience in holography on film. Combining the multifrequency laser technology with the holographic process can be used to test how the real-time holographic sensor is likely to perform on static objects. Problems encountered on film are also likely to exist when the hologram is formed in a photorefractive crystal. As photorefractive crystals become available, the experience developed from working on film should be readily applicable. If only slow crystals are available, a small artificial flexible structure may be constructed to simulate the sluggish vibrations of large space structures.

The bandwidth of the real-time holographic sensor will depend on the type of crystal, whether the crystal is operated in the photoconductive or photovoltaic modes, and the intensity of the available light signals. The intensity of the light signals will depend on the size of the flexible structure, its reflective properties, and the output of the laser. Characterizing each of these quantities is important in the design of the control laws. Therefore, sensor characterization is necessary if the sensor is to be combined with the processor for closed-loop control.

Mixed Processor Experiments

The processing hardware and control theory can also be tested in stages, independent of the sensing hardware, by simulating the output of the sensor. The output of the sensor is simulated for static structures using the slide projector-type arrangement shown in Figure 31. The output of the simulator could be used to test the mixed processing systems shown in Figure 22 and Figure 24. At this stage, tests to verify the accuracy of the pointwise multiplication and the spatial filtering property are important. A narrow aperture or scanning photodetector (such as a CCD digitizing camera) may be used in the static simulations if a suitable integrating photodetector is not available.

To simulate the dynamic sensor output, the slide projector in the simulator could be replaced with a movie projector or a video monitor. A video monitor with high resolution under computer control would be ideal. The motions of the structure could be animated and programmed to react under closed-loop control. In this way, the closed-loop processor can be fully tested without the sensor. The concepts for two-dimensional processing may be confirmed in a similar manner.

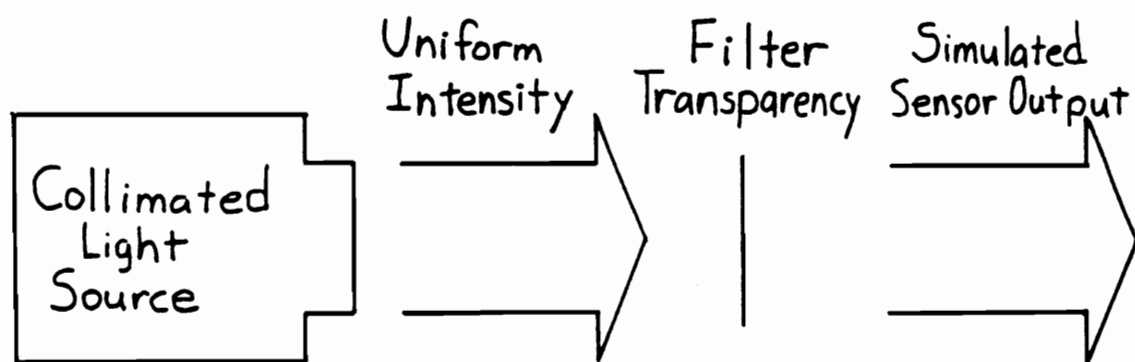


Figure 31. Slide Projector-type Sensor Output Simulator: A slide transparency attenuates the uniform intensity of the light source to produce a collimated light beam where the intensity represents a structure undergoing deflection from equilibrium.

All-Optical Processor Experiments

The concepts for the all-optical processor may also be verified and further developed through experiment in stages. First, the operation of the individual operational blocks in Figure 26 must be verified and characterized. In particular, a detailed evaluation of the limits of the computational accuracy must be conducted to determine an upper limit on the bandwidth of the control system, if one exists. Approximations made in the description of optical components may be more limiting than the tolerances of the components, in which case better approximation methods must be developed to describe higher order effects.

While the individual components are under development, we can develop the necessary interfacing optics to bring the output of one optical block to the next. Diffraction, for instance, can destroy the results at the output of the integrators unless the next component is placed precisely in the back focal plane of the inverse Fourier transform lens. In other cases the distributed signal must be converted from an incoherent form to a coherent form. This interfacing problem is likely to require additional optical technology such as optically addressed spatial light modulators [29].

The slide projector and video simulators can function in the all-optical processor as in the mixed processor to simulate the output of the sensor. These techniques may also be used in the processor itself to perform the distributed delay operation. As the discrete-time holographic delay becomes available, it may be inserted in the processor to replace the video simulated delay, or it may replace the simulated sensor output. In this way, the capabilities of the processor may be built and characterized in stages.

Verification of two-dimensional all-optical processors awaits the development of better two-dimensional optical implementations.

6.2.2 Control Theory

The future work in the control theory for holographic sensing and processing can be divided into two major areas, design and analysis. We have considered one approach to designing the control system for specific structures. Other existing approaches could be investigated, new approaches could be developed, and the methods could be generalized. Throughout, we have assumed ideal sensing and processing. Non-idealities could be identified and analyzed in both the sensor and processor. In summary, the future work in control theory deals with the control issues requiring resolution before actual construction begins.

Recommendations for Future Work in Design

In the area of design, we may generalize the method presented and consider new methods. The method presented is restrictive in several ways. First, the method presented requires us to sense the shape of the entire flexible structure. At this time, it is difficult to guess whether or not this assumption is reasonable. However, it probably would not be reasonable for a very large structure, a complicated structure, or a structure with three-dimensional vibrations. Therefore, one important generalization is to modify the design method to allow the sensing of only part of the structure. We call this the partial observation problem. The straightforward approach to solving the partial observation problem is to use the part of the mode shapes corresponding to the

part of the structure in view in the design. However, analysis show that parts of modes are not orthogonal. Therefore, if a new set of mode shapes that are orthogonal over the observed part of the structure could be found, the design method could be generalized intact.

The design could also be generalized in the modelling area. We assumed a partial differential equation exists to calculate the mode shapes and natural frequencies. Generally, numerical (non-analytical) methods must be used to calculate these parameters. Such methods are well-developed, but it remains to test their applicability to this sensor and processor. In particular, a thorough test of the spillover resulting from errors in numerical modelling is important.

In addition to generalizing the given method, we could consider developing new design methods. The all-optical processor might be particularly interesting for radical designs based on the control of distributed functions without resorting to variable separation. Control designs based on the estimation of distributed functions have been proposed [30]. Designs for the mixed processor which eliminate the temporal component would be useful in simplifying the implementation.

The forward looking designer should anticipate time-varying spatial filters [29] for adaptive control systems. Adaption could be useful both for self alignment of the system and to identify and track parameter variations.

Recommendations for Future Work in Analysis

At least half of the future work in analysis will be in the identification of problems requiring analysis. We mention a few here. First, it will be important to analyze the effects of non-ideal hardware on the performance. The sensor will have a finite bandwidth, and may have higher-order dynamics. The finite bandwidth is not expected

to be a problem provided the design modes are within the bandwidth of the sensor. The limited bandwidth of the sensor could possibly be beneficial in limiting the response due to the remaining modes. However, if the design does not include the sensor dynamics, the resulting system could lose performance. In addition to sensor dynamics, we can investigate the effects quantization and round-off in the processing filters. Other problems could be predicted such as misalignment and distortion in the optical processing. The analysis of all of these "secondary" effects can be incorporated into the designs and construction. In particular, element sensitivities could be calculated to specify tolerances for construction.

References

- [1] L. Mierovitch and H. Baruh, "Control of Self-Adjoint Distributed-Parameter Systems," *Journal of Guidance and Control*, Vol. 5, No. 1, pp. 60-66, Jan.-Feb. 1982.
- [2] R.A. Calico, Jr., and A.M. Janiszewski, "Control of a Flexible Satellite via Elimination of Observation Spillover," *Proceedings of the fourth VPI&SU/AIAA Symposium on Dynamics and Control of Large Flexible Spacecraft*, Blacksburg, VA, pp. 15-33, June, 1981.
- [3] M.J. Balas, "Feedback Control of Flexible Systems," *IEEE Transactions on Automatic Control*, Vol. 23, No. 4, pp. 673-679, Aug., 1978.
- [4] L. Mierovitch, **Analytical Methods in Vibrations**, Macmillan, New York, 1967.
- [5] Wen-Wei Chiang and Chih-Kung Lee, "Critical Damping of a Flexible Slender Plate Using a Distributed Modal Actuator and Sensor," *Proceedings of the Automatic Controls Conference*, pp. 700-705, Pittsburg, PA, 1989.
- [6] D.J. Ennis and D.A. Jared, "Optical Processing and Space Station Automation," *Optical Engineering*, Vol. 25, No. 7, pp. 808-820, July, 1986.
- [7] J. Feinberg, "Photorefractive Nonlinear Optics," *Physics Today*, pp. 46-52, October 1988.
- [8] S.S. Welch, R.C. Montgomery, M.F. Barsky, and I.T. Gallimore, "Optical Processing for Distributed Sensors in Control of Flexible Structures," *Proceedings of the Workshop on Computational Aspects in the Control of Flexible Systems*, NASA TM 101578, Williamsburg, VA, July, 1988.
- [9] S.G. Lipson and H. Lipson, **Optical Physics**, 2nd edition, Cambridge University Press, Cambridge, 1981.
- [10] M.V. Klein, **Optics**, John Wiley & Sons, New York, 1970.
- [11] D. Halliday and R. Resnick, **Fundamentals of Physics**, 2nd. Edition, John Wiley & Sons, New York, 1981.

- [12] J.W Foreman, Jr. "Optical Path-Length Difference Effects in Photomixing with Multimode Gas Laser Radiation," *Applied Optics*, Vol. 6, No. 5, May 1967.
- [13] H.M. Smith, **Principles of Holography**, 2nd edition, New York, John Wiley & Sons, 1975.
- [14] J. Goodman, **Introduction to Fourier Optics**, McGraw-Hill, New York, 1968.
- [15] L.O. Heflinger and R.F. Wuerker, "Coherence Length Measured Directly by Holography," *Applied Optics*, Vol. 28, No. 5, pp. 1015-1017, Mar. 1, 1989.
- [16] S.S. Welch, "Optical Distributed Sensing and Computation For A Proposed Flexible Beam Experiment," to appear in *Proceeding of the Seventh VPI&SU/AIAA Symposium on Dynamics and Control of Large Structures*, Blacksburg, VA, May 8-10, 1989.
- [17] M. Cronin-Golomb, B. Fischer, J.O. White, and A. Yariv, "Theory and Application of Four-Wave Mixing in Photorefractive Media," *IEEE Journal of Quantum Electronics*, Vol. 20, No. 1, Jan. 1984.
- [18] A. Yariv, "Four Wave Nonlinear Optical Mixing as Real-Time Holography," *Optics Communications*, Vol. 25, No. 1, April 1978.
- [19] H. Kwakernaak and R. Sivan, **Linear Optimal Control Systems**, Wiley-Interscience, New York, 1972.
- [20] J.S. Gibson and A. Adamian, "Approximation Theory for Optimal Control of Flexible Structures," ICASE Report No. 88-48, NASA Langley Research Center, August 1988.
- [21] J.S. Gibson and I.G. Rosen, "Numerical Approximation for the Infinite-Dimensional Discrete-Time Optimal Linear-Quadratic Regulator Problem," *SIAM J. Control and Optimization*, Vol. 26, No. 2, March 1988.
- [22] J.S. Gibson and A. Adamian, "A Comparison of Three Approximation Schemes for Optimal Control of a Flexible Structure," to appear in *SIAM Frontiers Edition on Control of Distributed Systems*, 1988.
- [23] M.F. Barsky and D.K. Lindner, "Distributed Sensing for Robust Control of Flexible Structures," to appear in the *Proceedings of the 27th Annual Allerton Conference on Communication, Control and Computing*, University of Illinois at Urbana-Champaign, September 27-29, 1989.
- [24] M.F. Barsky and D.K. Lindner, "Holographic Signal Processing for Control of a Flexible Beam," *Proceedings of the 28th IEEE Conference on Decision and Control*, pp. 2685-6, Tampa, Florida, December 13-15, 1989.
- [25] R.D. Gupta, F.W. Fairman, T. Hinamoto, "A Direct Procedure for the Design of Single Functional Observers," *IEEE Transactions on Circuits and Systems*, Vol. 28, No. 4, April 1981.
- [26] Chi-Tsong Chen, **Linear System Theory and Design**, CBS College Publishing, New York, 1984.

- [27] W.L. Brogan **Modern Control Theory**, second edition, Prentice Hall, New Jersey, 1985.
- [28] M.F. Barsky, K.M. Reichard, D.K. Lindner, and R.O. Claus, "Distributed Sensing Methods for Controlling Flexible Structures," *Proceedings of the VPI&SU/AIAA Symposium on Dynamics and Control of Large Structures*, May 8-10, 1989.
- [29] *Spatial Light Modulators and Applications Tech. Digest Series 1988*, Vol. 8, 1988.
- [30] D.B. Schaechter, "Estimation of Distributed Parameter Systems: Some Closed Form Solutions," *AIAA Journal of Guidance and Control*, Vol. 9, No. 4, pp. 408-412, July-Aug. 1986.

Appendix A. Functional Estimator

The functional estimator is designed to estimate the product $F\hat{\eta}_1(t)$ rather than $\hat{\eta}_1(t)$. This eliminates the need to form the product $\hat{\eta}_1(t)$ after the estimate, and reduces the computational burden in the estimator itself. The derivation closely follows a more general derivation given in [26]. We begin by defining a new estimator of the form

$$\dot{z}(t) = \Psi z(t) + \beta u(t) + \Theta \varepsilon(t), \quad (A.1.1)$$

where $z(t) = Z\hat{\eta}_1(t)$. If we multiply (3.3.27) by Z ,

$$Z \frac{d}{dt} \hat{\eta}_1(t) = Z(A_1 - H\bar{G})\hat{\eta}_1(t) + ZBu(t) + ZH\varepsilon(t), \quad (A.1.2)$$

and match coefficients with (A.1.1), we find

$$\begin{aligned} \Theta &= ZH \\ \beta &= ZB, \end{aligned} \quad (A.1.3)$$

and

$$ZA_1 + \Psi Z = \Theta \bar{G}. \quad (A.1.4)$$

Assume

$$\bar{G} = [I_{N_1} \ 0], \quad (A.1.5)$$

and let

$$w(t) = \Gamma z(t) + \Omega \varepsilon(t). \quad (A.1.6)$$

We want to choose Γ and Ω such that $w(t) \rightarrow F \hat{\eta}_1(t)$. Partition the design system (3.2.40) such that

$$\frac{d}{dt} \begin{bmatrix} \eta_{11}(t) \\ \eta_{12}(t) \end{bmatrix} = \begin{bmatrix} A_{11} & A_{12} \\ A_{13} & A_{14} \end{bmatrix} \begin{bmatrix} \eta_{11}(t) \\ \eta_{12}(t) \end{bmatrix} + \begin{bmatrix} B_{11} \\ B_{12} \end{bmatrix} u(t), \quad (A.1.7)$$

and partition Z and F such that

$$Z = [Z_1 \ Z_2] \text{ and } F = [F_1 \ F_2], \quad (A.1.8)$$

and (A.1.4) becomes

$$Z_1 A_{11} + Z_2 A_{13} - \Psi Z_1 = \Theta \quad (A.1.9)$$

$$Z_1 A_{12} + Z_2 A_{14} - \Psi Z_2 = 0.$$

Similarly, the partitioning causes (A.1.6) to become

$$\Gamma Z_1 + \Omega = F_1 \quad (A.1.10)$$

$$\Gamma Z_2 = F_2. \quad (A.1.11)$$

If we take $\Gamma = 1$ and $\Psi = -\alpha$, where alpha is an arbitrary constant, then $Z_2 = F_2$ and $Z_1 + \Omega = F_1$. From (3.2.28), we know $A_{11} = 0$ and $A_{12} = I_{N_1}$. Therefore, (A.1.9) simplifies to

$$F_2 A_{13} + \alpha Z_1 = \Theta \quad (A.1.12)$$

$$Z_1 + F_2 A_{14} + \alpha F_2 = 0,$$

implying

$$Z_1 = -(F_2 A_{14} + \alpha F_2). \quad (A.1.13)$$

Therefore, from (A.1.10),

$$\Omega = F_1 + F_2 A_{14} + \alpha F_2, \quad (A.1.14)$$

and from (A.1.9)

$$\Theta = -\alpha Z_1 + F_2 A_{13}. \quad (A.1.15)$$

Recalling the assumption (A.1.5), we see that

$$\varepsilon(t) = [I_{N_1} \ 0] \eta_1(t). \quad (A.1.16)$$

Therefore, in the estimator (A.1.1),

$$\Theta \varepsilon(t) = \Theta [I_{N_1} \ 0] \eta_1(t). \quad (A.1.17)$$

Using (3.3.25), we may define $\varepsilon_a(t)$ such that

$$\begin{aligned}
\varepsilon_a(t) &= \Theta \varepsilon(t) \\
&= [\Theta \ 0] \begin{bmatrix} \Xi_1(t) \\ \dot{\Xi}_1(t) \end{bmatrix} \\
&= \int_0^L \Theta P_1^T(x) P_1(x) \Xi_1(t) dx \\
&= \int_0^L \Theta P_1^T(x) y_1(x,t) dx \\
&= \int_0^L \Theta P_1^T(x) y(x,t) dx.
\end{aligned} \tag{A.1.18}$$

Therefore Θ is the weighting vector of the design modes in the spatial filter. Similarly,

$$\varepsilon_b(t) = \int_0^L \Omega P_1^T(x) y(x,t) dx, \tag{A.1.19}$$

so Ω is also a weighting vector of design modes in a spatial filter. The functional estimator design is summarized in Section 3.3.3.

Vita

Michael F. Barsky was born in Fredericksburg, Virginia, in 1962. He received his BSEE degree (Co-op) in 1984, and his MSEE degree in 1986, both from Virginia Polytechnic Institute and State University.

Since 1986 he has been pursuing a Ph. D. degree in Electrical Engineering at Virginia Polytechnic Institute under a NASA Graduate Student Training Grant. The NASA Grant included on-base work experience where he participated in the early development of control systems utilizing holographic sensing technology. His current research interests are in sensing and control systems.

Mr. Barsky has accepted a position as a member of the technical staff with the Space and Communications Group of the Hughes Aircraft Company in Los Angeles, California.

A handwritten signature in black ink, appearing to read "Michael Barsky", with a long horizontal flourish extending to the right.